

NPS ARCHIVE  
1969  
DAVIS, M.

AN ANALYTICAL STUDY OF SEPARATED  
FLOW ABOUT A CIRCULAR CYLINDER

by

Martin Dormer Davis



# United States Naval Postgraduate School



## THESIS

AN ANALYTICAL STUDY OF SEPARATED FLOW

ABOUT A CIRCULAR CYLINDER

by

Martin Dorner Davis

T132210

December 1969

*This document has been approved for public re-  
lease and sale; its distribution is unlimited.*

Library

U.S. Naval Postgraduate School

Monterey, California 93940

An Analytical Study of Separated Flow

About a Circular Cylinder

by

Martin Dörner/Davis

Lieutenant, United States Navy

BME, Speed Scientific School, University of Louisville, 1962

Submitted in partial fulfillment of the  
requirements for the degrees of

MECHANICAL ENGINEER

and

MASTER OF SCIENCE IN MECHANICAL ENGINEERING

from the

NAVAL POSTGRADUATE SCHOOL  
December 1969

# ABSTRACT

The problem of separated flow about a circular cylinder is studied analytically through the use of two potential flow models. Following a detailed review of the present state of knowledge, mathematical formulation of the models and appropriate computer programs are presented. These models are shown to be capable of simulating the asymmetric vortex shedding.

TABLE OF CONTENTS

I. INTRODUCTION - - - - - 9

II. REVIEW OF THE PRESENT STATE OF KNOWLEDGE - - - - - 16

    A. REYNOLDS NUMBER LESS THAN ONE - - - - - 16

    B. REYNOLDS NUMBER BETWEEN THREE AND FORTY - - - - - 21

    C. REYNOLDS NUMBER BETWEEN FORTY AND THREE  
        HUNDRED - - - - - 26

    D. REYNOLDS NUMBER BETWEEN THREE HUNDRED AND  
        CRITICAL - - - - - 34

III. TWO ANALYTIC MODELS - - - - - 41

    A. INTRODUCTION - - - - - 41

    B. BASIC POTENTIAL FLOW EQUATIONS - - - - - 42

    C. MODEL A - - - - - 48

    D. MODEL B - - - - - 62

IV. DISCUSSION OF RESULTS AND CONCLUSIONS - - - - - 74

APPENDIX A - - - - - 84

    A. DESCRIPTION OF COMPUTER PROGRAM, MODEL A - - - - - 84

    B. DEFINITION OF PARAMETERS - - - - - 85

APPENDIX B - - - - - 88

    A. DESCRIPTION OF COMPUTER PROGRAM, MODEL B - - - - - 88

    B. DEFINITION OF PARAMETERS - - - - - 88

COMPUTER OUTPUT - - - - - 91

    MODEL A - - - - - 91

    MODEL B - - - - - 95

COMPUTER PROGRAMS - - - - -	99
MODEL A - - - - -	99
MODEL B - - - - -	118
LIST OF REFERENCES - - - - -	128
INITIAL DISTRIBUTION LIST - - - - -	131
FORM DD 1473 - - - - -	133



# TABLES OF SYMBOLS AND ABBREVIATIONS

## ENGLISH

$C_D$	Drag coefficient; defined by equation (1)
$C_p$	Pressure coefficient; defined by equation (27)
$c$	Radius of circular cylinder or sphere
$D$	Differential operator
$\frac{dq_i}{dt}$	Cartesian tensor notation for Eulerian total derivative
$F_D$	Drag force on circular cylinder
$F_L$	Lift force on circular cylinder
$f_i$	Cartesian tensor notation for body forces
$g$	Acceleration of gravity
$i$	$\sqrt{-1}$
$K$	A free parameter in Free Streamline Theory
$M$	Mach number or number of free vortices
$N$	Total number of free and attached vortices in a flow field
$P$	Pressure
$q_i$	Cartesian tensor notation for the three axial velocities; $q_1 = u$ ; $q_2 = v$ , and $q_3 = w$
$Re$	Reynolds number; for circular cylinder, $Re = \frac{2 U_\infty c}{\nu}$
$S$	Strouhal number; for circular cylinder, $S = \frac{2 c}{U_\infty T}$
$T$	Strouhal period; $U_\infty T$ = length of wake generated in one period
$t$	Time
$U_\infty$	Velocity of the ambient flow; could be time dependent
$u$	Instantaneous velocity in x-direction of a two or three dimensional cartesian system

V	Instantaneous total velocity vector
v	Instantaneous velocity in y-direction of a two or three dimensional cartesian system
W(z)	A function of complex variables; defined by, $W(z) = \psi(x, y) + \phi(x, y)$
w	Instantaneous velocity in z-direction of a three dimensional cartesian system
Z	Complex variable; $z = x + iy$ , an undefined location; for example, $z_n = x_n + iy_n$ could be the location of the nth vortex

#### GREEK

$\Gamma$	Strength or circulation of a vortex; defined as the line integral of the tangential velocity component around a closed curve, or defined as the integral of vorticity over a surface bounded by a closed curve
$\gamma$	Specific weight; defined by, $\gamma = \rho g$
$\epsilon_{ijk}$	Cartesian tensor permutation symbol
$\zeta_i$	Cartesian tensor vorticity vector; defined by equation (20) in Section II
$\theta$	An angle measured from the positive x-axis
$\mu$	Absolute viscosity
$\nu$	Kinematic viscosity; defined by, $\nu = \frac{\mu}{\rho}$
$\rho$	Density
$\phi$	Velocity potential function
$\psi$	Stream function

#### SUBSCRIPTS

i	Cartesian tensor index; $i = 1, 2, 3$ ; or indicates quantity pertains to an image vortex
j	Cartesian tensor index; $j = 1, 2, 3$
k	Cartesian tensor index; $k = 1, 2, 3$
m	Vortex counter index; $m = 1, 2, \dots, M$
n	Vortex counter index; $n = 1, 2, \dots, N$

## ACKNOWLEDGEMENTS

To Professor T. Sarpkaya, I owe the greatest help and inspiration in theoretical and day to day guidance. Were it not for his original ideas, this thesis would not have been undertaken. To Professor G. Cantin, I express my special thanks for his help in numerical techniques.



## I. INTRODUCTION

The postulation of an analytic solution for a viscous fluid flow about a circular cylinder has perplexed hydrodynamic investigators for several centuries. Although notes left by Leonardo da Vinci (1452-1519) indicate more than a qualitative interest, it was not until the early seventeenth century, during the evolution of Potential Theory, that the first formal attempts were made at quantitative analysis. Though there was some understanding of viscous effects during this period, they were basically qualitative and were not taken into consideration when in 1750 D'Alembert found that:

The force on a body in steady motion relative to an otherwise undisturbed ideal fluid is zero. [1]<sup>1</sup>

This result, classically known as D'Alembert's Paradox, was of course unsatisfactory. Decades have elapsed since investigators found the qualitative reasons for the erroneous results given in this and other cases by Potential Theory.

Philosophically speaking, to the engineer the ultimate goal of any analytic procedure is to provide a power of prediction for design applications. As yet this capability is generally only realizable from experimental investigations and then only for certain flow characteristics. For a circular cylinder immersed in a steady cross-flow as shown in Figure 1, the drag force can be calculated from:

$$F_D = \rho c U_\infty^2 C_D \quad (1)$$

---

<sup>1</sup>The bracketed numbers refer to the item number in the List of References.

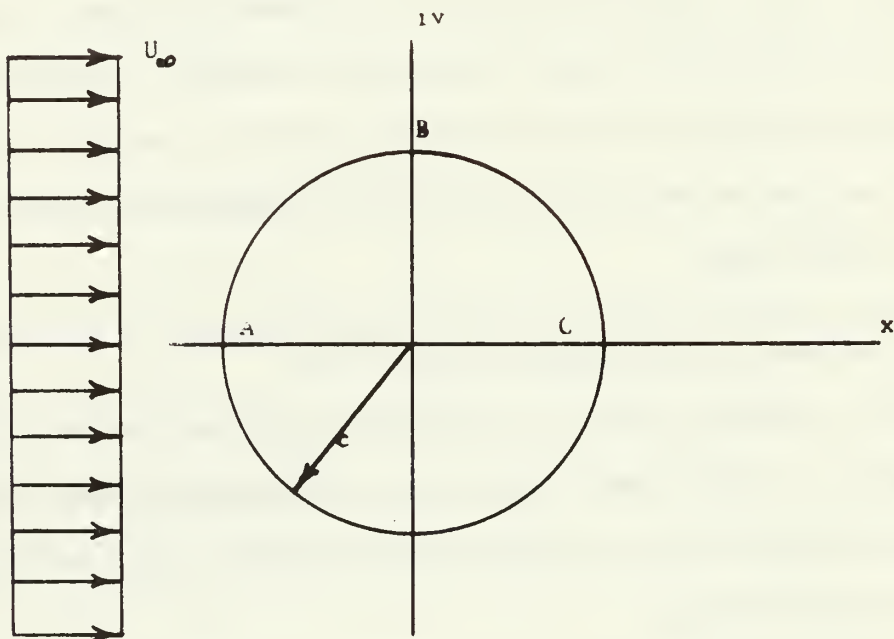


**Figure 1. Circular Cylinder Immersed in a Steady Fluid Cross-Flow and Indicating Relationship to a Complex Coordinate System.**

$C_D$  is determined experimentally as a function of the Reynolds number as shown in Figure 2. Except for  $Re < 1$ , there is presently no general analytical method available to generate these results. This exception will be discussed in more detail in Section II. The primary point involved here is that for each geometric shape, or group of geometric shapes immersed in a steady flow field, there would have to be an experimentally found  $C_D$  curve for each case. In fact, for an incompressible fluid, the form of equation (1) would have to be more general:

$$F_D = f(Re), \quad (2)$$

and for a compressible fluid:

$$F_D = f(Re, M). \quad (3)$$

For all but the simplest geometries, the definition of  $Re$  and  $M$  are in themselves difficult problems; not as to their general meanings, but as to specific combination of the physical parameters for a given application.

Though used only as an illustrative example above, the analytical determination of  $C_D$  has more subtle implications than those previously indicated. It requires a complete understanding of separated flow, particularly from the aspect of vorticity generation in the boundary layers before separation. It is this point that presents the greatest problem in the postulation of a mathematical model; for it is assumed that if a general analytical solution can be found for  $C_D$  in time-dependent flows, then analytic determination of all or most of the other flow characteristics will follow. Also, since a circular cylinder and its surrounding flow field can be easily represented in two dimensions

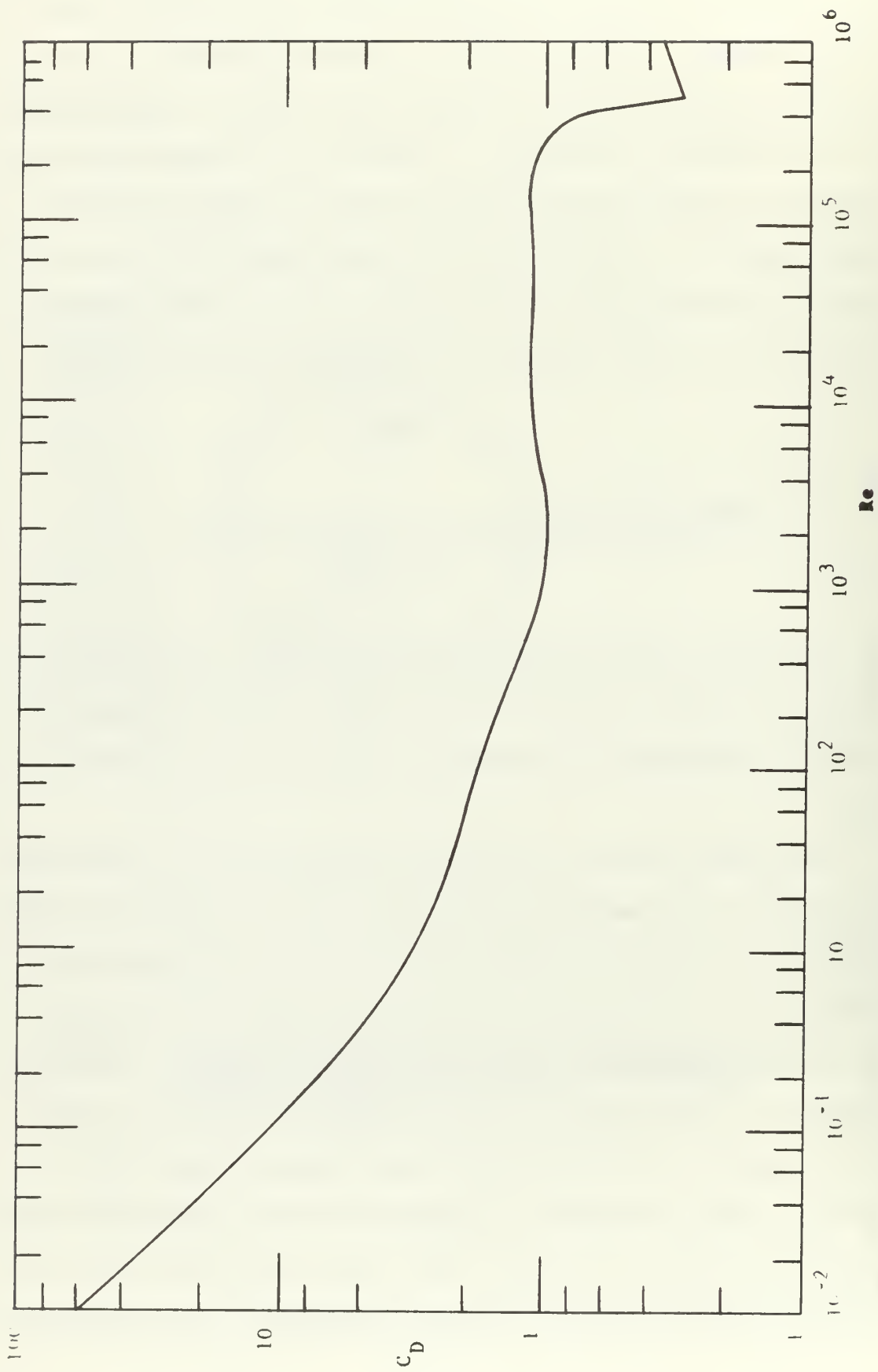


Figure 2. Log-log Plot of Drag Coefficient Versus Reynolds Number for a Circular Cylinder Immersed in a Steady Cross-Flow. [2]



by a function of complex variables, it is possible to easily transform the cylinder into other two-dimensional shapes using the technique of conformal mapping. For inviscid, incompressible fluids, this technique has been used to great advantage particularly in aerodynamics, however external knowledge of boundary layer effects was needed.

So far, the discussion has centered around total drag. For future analysis it is necessary to break this into its two classical components, skin friction and form drag. The skin friction is the integral of the shearing stresses over the surface of the body and is dependent on the action of the fluid in the boundary layer. The form drag is equal to the integral of the forces normal to the surface of the body and is assumed to be dependent only on the inviscid fluid action outside the boundary layer. This assumption is made since an order of magnitude analysis of the Navier-Stokes equations indicates that the pressure gradient through the boundary layer is negligible as compared to other effects. The practice of considering the fluid outside the boundary layer as inviscid is due again to an order of magnitude analysis of the Navier-Stokes equations. This time, when considering only the region outside the boundary layer, the equations reduce to the inviscid equations of motion and permit the application of Potential Theory to this region. Note that large Reynolds numbers have been assumed in both instances.

Following the above reasoning further, leads to the conclusion that if no separation of the boundary layer occurs, the form drag is essentially zero since there is no disturbance to the external inviscid flow. At very low Reynolds numbers, this conclusion is reasonable and can be considered a basis for the famous "creeping motion" solution of G. G. Stokes in 1851. In this case skin friction predominates. At larger

Reynolds numbers, however, there is boundary layer separation and form drag becomes important. The external flow field is disturbed by regions of intense vorticity which causes a decrease in pressure behind the body as compared to the undisturbed inviscid solution. It is evident then, that without considering the direct shear force effects of viscosity as represented by skin friction, and the indirect effects represented by vorticity regions, the qualitative concepts reduce such that D'Alembert's quantitative solution results.

Earlier in this discussion, mention was made concerning the practice of considering the undisturbed fluid outside the boundary layer as inviscid. This requires amplification and a word of caution. In 1908, H. Blasius presented a solution to the boundary layer on a circular cylinder. As far as his paper was concerned the method of solution, rather than the result, was the most important contribution. Briefly, it involves the use of a series expansion for the free stream velocity just external to the boundary layer.<sup>2</sup> If this velocity is taken as that found for incompressible, inviscid flows derived from Potential Theory on the surface of the cylinder, the angular distance between the upstream stagnation point, and the boundary layer separation point is found to be 108.8 degrees; the center of the cylinder is taken as the origin.<sup>3</sup> If experimental velocity determinations are used, the solution yields a separation point at about 82 degrees. The observed separation point is

---

<sup>2</sup>For a complete presentation of this method, see [2], pages 154-162.

<sup>3</sup>The boundary layer separation point is defined as:  $\partial u / \partial y |_{y=0}$  where  $u$  is the fluid velocity parallel to the body surface, and  $y$  is directed normal to the surface, with its origin at the surface.

at about 81 degrees. Herein then lies the problem with the above practice: even at high Reynolds numbers there is sufficient interaction between the boundary layer and the external "inviscid" flow to cause considerable error in the results of essentially exact methods of solution. As will be shown in Section III, the separation point is critical in any method that attempts to mathematically generate a reasonably correct drag coefficient curve.

In recent years, extensive experimental work with the flow past bluff bodies has provided researchers with a clearer understanding of the mechanism of boundary layer separation. As a result, several models have been devised to portray the overall fluid action. However, to date none has provided the sought-after general solution.<sup>4</sup> A survey of the literature indicates that there are two basically different analytical approaches being made. The first, and probably the most obvious, is the solution of the nonlinear Navier-Stokes equations using finite difference techniques. The second is a potential flow model in which the shear layers are represented as point concentrated vortices. Both these models, particularly the latter, will be described in greater detail in succeeding sections.

Since this thesis does not propose a general solution, it is hoped that the following sections will help to clarify the problem and to provide a basis from which future work can be done. Section II reviews the literature on separated flows; concentrating on those aspects that relate to incompressible flow about circular cylinders. Section III presents the two potential flow models that the author used in an attempt to generate the aforementioned drag curves.

---

<sup>4</sup>The development of the high speed, large storage capacity digital computer has also been extremely important to the study.

## II. REVIEW OF THE PRESENT STATE OF KNOWLEDGE

Because of the large number of references available on separated flows, the author has elected to limit this review through the use of the following guidelines. First, since there still exists a lack of basic understanding of the mechanism of separation only references to studies involving essentially incompressible fluid will be used. This enables the added complications of compressible phenomenon, both qualitative and mathematical, to be ignored. Secondly, a study of the literature reveals that several different geometries have been used both in experimental and analytical work; the results not always consistent nor related to each other. Therefore, the circular cylinder is taken as the basic geometry for this review. The use of a circular cylinder implies, to a large extent, two-dimensionality; which is another simplification. Though particularly helpful from a qualitative standpoint, this simplification is also useful mathematically. Thirdly, the information will not necessarily be presented in chronological order as is so often done in reviews of this nature. It is felt that a loose division by Reynolds number is more pertinent since the analytical solutions thus far derived are only applicable to given ranges of this "magic number," as von Kármán calls it. Lastly, the discussion will in general be limited to the laminar flow regime. As the Reynolds number increases above the critical value, increasing consideration must be given to compressibility and eventually to cavitation; two complicating subjects outside the scope of this thesis.

### A. REYNOLDS NUMBER LESS THAN ONE

In this Reynolds number range, the viscous forces acting on the



cylinder are considerably larger than the inertial forces. This leads to the conclusion that if the inertia terms are dropped from the Navier-Stokes equations, an approximate solution may result that would compare favorably with experimental data. Stokes, as previously indicated, did this in 1851 when he presented the first solution for the drag on any body. Though he used a sphere in his solution, it is still worthwhile presenting here. The mathematical details are not the same, but the basic steps are.

The complete Navier-Stokes equations for incompressible, constant temperature conditions are (expressed in three-dimensional Cartesian tensor notation [4]):

$$\frac{dq_i}{dt} = f_i - \frac{1}{\rho} P_{,i} + \nu q_{i,jj} \quad (4)$$

The incompressible continuity equation is:

$$q_{i,i} = 0 \quad (5)$$

By dropping the inertia and body force terms, then cancelling density from both sides of the rearranged equation, one has

$$P_{,i} = \mu q_{i,jj} \quad (6)$$

The four equations represented by (5) and (6) have the same usual boundary conditions used for any boundary layer problem of this nature when the body is immersed in an infinite fluid: the fluid velocities normal to and tangent to the body surface are equal to zero.

After taking the divergence of both sides of equation (6), it becomes:

$$P_{,ii} = \mu q_{i,i,jj} \quad (7)$$

But the right hand side of equation (7) can be written as  $\mu (\varphi_{i,i})_{,jj}$  which is the second derivative of the continuity equation and therefore equal to zero. This means that in creeping motion, the pressure field satisfies Laplace's equation and hence is a potential or harmonic function. Now, by introducing the two-dimensional stream function,

$$\varphi_{,i} = -\epsilon_{ij3} \psi_{,j} \quad , \quad (8)$$

into the right hand side of equation (7), dropping  $P_{,ii}$  and  $\mu$  the two-dimensional biharmonic equation results.

$$D^4 \psi = D^2 (D^2 \psi) \quad (9)$$

Without going into the mathematical details, it is sufficient to say that the pressure and velocity components reduce to:

$$u = U_{\infty} \left[ \frac{3}{4} \frac{c x^3}{r^3} \left( \frac{c^2}{r^2} - 1 \right) - \frac{1}{4} \frac{c}{r} \left( 3 + \frac{c^2}{r^2} \right) + 1 \right]$$

$$v = U_{\infty} \frac{3}{4} \frac{c x y}{r^3} \left( \frac{c^2}{r^2} - 1 \right)$$

$$w = U_{\infty} \frac{3}{4} \frac{c x z}{r^3} \left( \frac{c^2}{r^2} - 1 \right)$$

$$P - P_{\infty} = -\frac{3}{2} \frac{\mu U_{\infty} c x}{r^3}$$

$$r^2 = x^2 + y^2 + z^2$$

(10)

The geometric configuration is such that the center of the sphere is at

the origin of the coordinate system and is placed in a positive velocity field,  $U_{\infty}$ , which is parallel to the x-axis.

Next, by using the standard definitions of shear stress along with equation (10), the viscous and pressure forces can be found by integration over the sphere's surface. The total drag for the sphere then becomes,

$$F_D = 6 \pi \mu c U_{\infty} . \quad (11)$$

If a drag coefficient is formed in the normal manner (i.e., referring to the dynamic head and frontal area), then,

$$F_D = C_D \pi c^2 \left( \frac{1}{2} \rho U_{\infty}^2 \right) . \quad (12)$$

Equating (11) and (12), then,

$$C_D = \frac{24}{Re} \quad (13)$$

Comparison of this result with experimental data indicates that these equations are valid only for cases where  $Re < 1$ . A classic case of application is that of small, light particles, assumed spherical in shape, settling in a fluid. Assuming that the particle is at its terminal velocity, then summing the forces yields,

$$\frac{2}{9} c^2 g (\rho_{\text{sphere}} - \rho_{\text{fluid}}) = \mu U_{\infty} \quad (14)$$

Letting  $\Delta \gamma = g (\rho_{\text{sphere}} - \rho_{\text{fluid}})$  then equation (14) reduces to

$$\frac{c^2 \Delta \gamma}{\mu U_{\infty}} = \frac{9}{2} , \quad (15)$$

which is the famous Stokes' number.

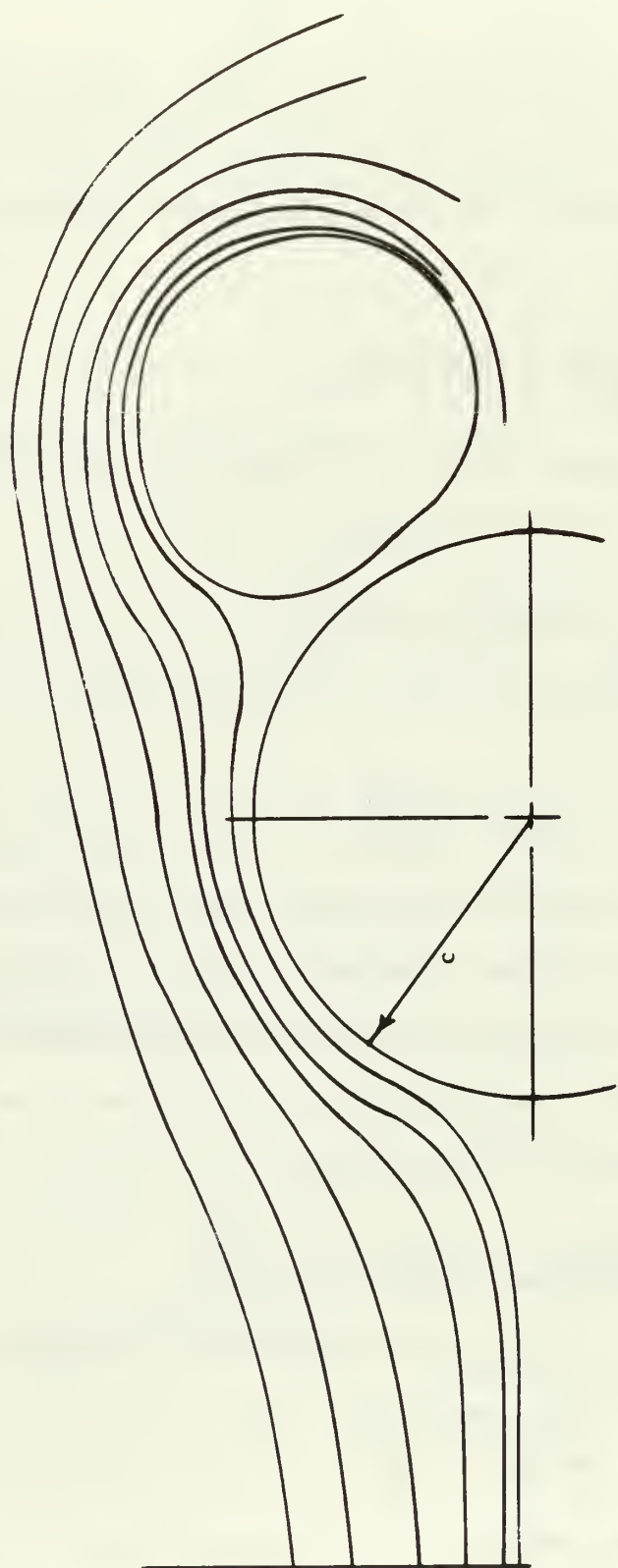


Figure 3. Flow Line Formation Around a Circular Cylinder for  $\beta < \text{Re} < 40$ . Bottom is mirror image of this.



C. W. Oseen, in a paper published in 1910, improved on the above by taking the inertia terms of the Navier-Stokes equations partly into account [2]. By doing so, the resultant drag coefficient became:

$$C_D = \frac{24}{Re} \left( 1 + \frac{3}{16} Re \right) . \quad (16)$$

Comparison of (16) with experimental data shows favorable correlation up to a Reynolds number of about 5.

In recent years, other investigators have formulated other solutions, however, their main contributions have not necessarily been to engineering but more to mathematical prowess. Kaplun [5] based his on an asymptotic solution of a series expansion of the Navier-Stokes equations. The results are generally restricted to two-dimensional bodies with equivalent Reynolds numbers less than one. Sir Horace Lamb [6] also presented a solution applicable to this range. He followed the basic ideas of Oseen, however, where Oseen used a sphere, Lamb used a circular cylinder.

#### B. REYNOLDS NUMBER BETWEEN THREE AND FORTY

In this Reynolds number region, the boundary layer is still laminar, however, separation occurs causing the formation of two vortex cores in the wake of the cylinder as indicated in Figure 3. This region is sometimes referred to as the "Twin-Vortex Stage." A great deal of experimental evidence indicates that the cores are generally stable in this region provided that no external excitation occurs. It is in this region also that the greatest successes have occurred with the "exact" solution of the Navier-Stokes equations. Remembering that, above a Reynolds number of about one, the inertia forces are too large to neglect, the phenomenon

requires the solution of the full Navier-Stokes equations.<sup>5</sup> This is most readily done through the use of either the forward or backward finite difference techniques. Until recently, without the advent of the digital computer, these methods have been difficult to employ. Thom [7] in 1933 used a relaxation method of hand calculation to produce the streamline pattern shown in Figure 4 at a Reynolds number of 20.

It is true that the relaxation method can be programmed for a digital computer and made to converge to any realistic degree of accuracy, however, it is also true that computation time increases rapidly for a slight increase in desired accuracy. Thus this method is not considered the most desirable. The Gauss-Siedel iteration method is somewhat different in procedure, but can require the same amount of computer time for solution. It should be noted that both of these methods can be modified if done by hand since one can make shortcuts that are difficult to program for the computer. Even so, the digital computer reduces the time required from ".....about one year and a half with twenty working hours every week, with a considerable amount of labour and endurance ....."[8] to a total computation time of about three to five hours. Even this could probably be reduced by streamlining the iterative procedures. Robertson [1, p. 366] summarizes these methods quite well.

Though these analytical methods produce interesting flow patterns, their primary reason for use is to give needed information about separated flow. Unfortunately, they do not appear to explain the mechanism of separation or more importantly the feedback aspects of the wake on

---

<sup>5</sup>Body forces,  $f_i$ , are usually neglected in these solutions since their presence adds nothing to the understanding of the problem and in general add unwanted complications to the mathematics.

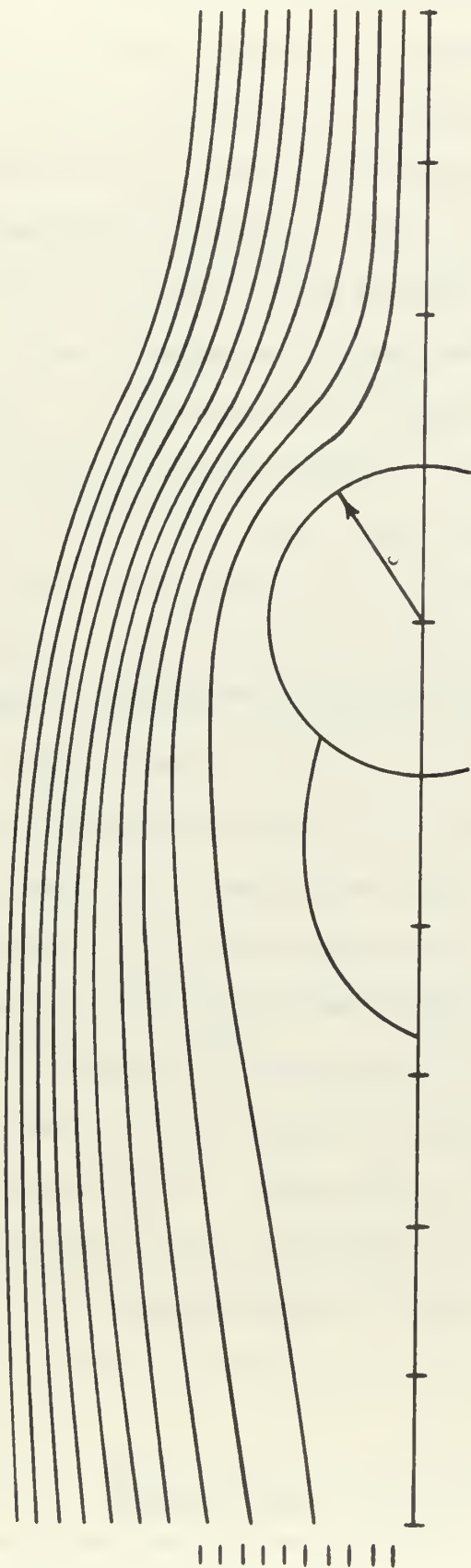


Figure 4 Calculated Streamlines past a Circular Cylinder at  $Re = 20$ , by Thom (1933) using Relaxation Method. The Undisturbed Flow Streamlines are Represented by the short lines at the end.

the vortex generation in the boundary layer. The experimental and analytical work does yield approximate Reynolds numbers for the beginnings of separation and the formation of the Kármán vortex street; about 5 and 40 respectively. From an analytical standpoint, the mesh size of the finite difference grid and the method of defining the conditions along the outside grid points<sup>6</sup> can affect the resultant separation and wake. Experimentally, just the placement of the confining walls of the apparatus used for testing can increase the Reynolds number, at which the wake becomes unstable, by more than 300 percent [9]. It should be noted here that although the wake is generally considered to be stable for steady flows in the Reynolds number range under discussion, it can be made unstable both theoretically and experimentally under artificial excitation. The ease with which this can be done, of course, increases as  $Re$  approaches the range of instability, making exact determination of the Reynolds number at which the vortex shedding begins very difficult. This same idea holds true for the determination of the separation Reynolds number. In both cases there appears to be some experimental evidence to indicate that the Reynolds number is not the exact similarity parameter that should be used in comparing results; the reasons for this are not entirely known. It is the belief of the author, however, that these disparities in results are probably due to variance in technique rather than to any fault of the parameter. It is recognized that in actuality there may be a three-dimensional effect that has not been taken into consideration theoretically or experimentally. Herein may be much of the reason for the differences in experimental results.

---

<sup>6</sup>Requiring that the velocity on the surface of the cylinder be zero provides the boundary condition for the grid points on the cylinder surface.

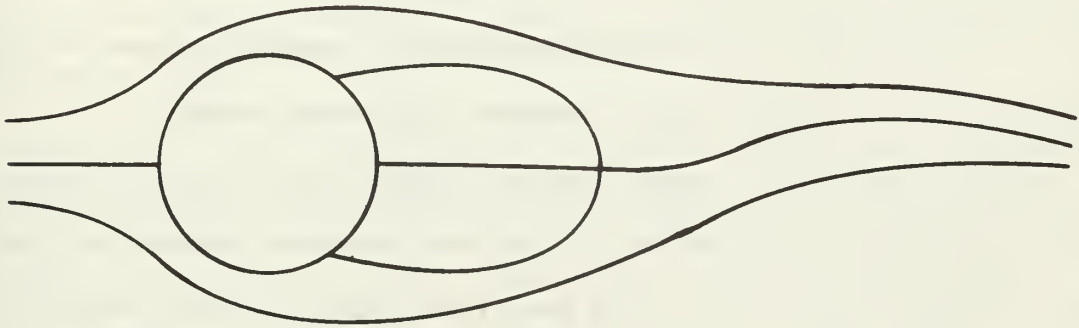


Figure 5. Beginnings of Vortex Street,  $Re \approx 40$ .

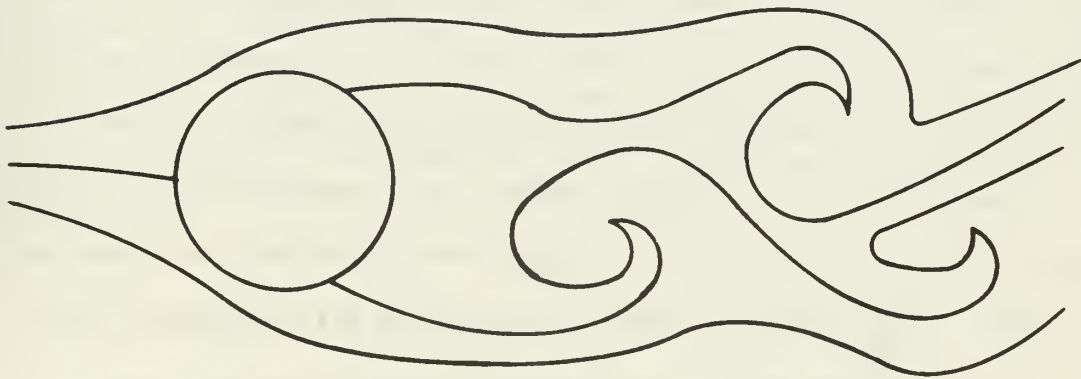


Figure 6. Kármán Vortex Street Indicating Cyclic Shedding Vortex Cores,  $80 < Re < 300$ .



### C. REYNOLDS NUMBER BETWEEN FORTY AND THREE HUNDRED

The primary phenomenon represented in this region is the Kármán vortex street; from the condition of an almost stable wake with slow viscous decay to the ultimate condition of cyclic detachment of vortex cores. Figures 5 and 6 indicate the flow patterns at these two "extremes." This region is also characterized by a smooth decrease in drag coefficient and an almost linear increase of Strouhal number,  $S$ .

Though study in this region has not produced any startling insight into the mechanism of separation, it has provided much information about vortex streets. Basically, it has been found that given two parallel vortex sheets separated by some initial distance, a solid body need not be present for a vortex street to develop [10]. The creation of these sheets is of course dependent on the viscous boundary layer effects caused by the presence of the solid body.

Due to the oscillatory nature of the vortex core separation into the wake, there is a cyclic shift in the separation points of the boundary layers on either side of the cylinder. This action is evidence of the strong "feedback" effect that the wake conditions have on the boundary layer in this Reynolds number region. This condition exists during the so-called steady state period after the various parameters such as drag coefficient, Strouhal number, etc., have settled to fairly constant values. In impulsively started flow situations, the flow patterns above and below the cylinder are basically mirror images of each other. The mechanism that causes eventual asymmetry is not clearly understood. In recent years, with the help of the digital computer, this asymmetry has been generated in finite difference solutions by the artificial insemination of small amounts of extra vorticity into one of the boundary layer separation regions, once the twin core pattern was

fairly well developed. Using this method, Fromm and Harlow [11] were able to duplicate the flow patterns around rectangular cylinders at these intermediate Reynolds numbers. At the lower numbers the system "absorbed" the extra vorticity with only minor disturbances to the wake, while at higher Reynolds numbers, the vortex cores separated cyclicly to form a vortex street.

Though the details of solution of the Navier-Stokes equations varies with the investigator, the same general procedures are used by all. The following is an attempt to clarify the salient points involved, but first, the reason for using these equations should be reiterated. Through this Reynolds number region, there appears to be a balance of sorts between the viscous and inertia forces, or effects, which implies that neither can be neglected or ignored. In the potential model that will be discussed later, the viscous forces are neglected from a drag standpoint. In the Stokes solution for  $Re < 1$ , the inertia forces were neglected with no apparent loss of practical accuracy. This region then appears to be nature's transition region from one extreme to the next, and therefore the complete governing equations must be used.

The method, in general, is as follows; dropping the body force term from equation (4), and expanding to the two-dimensional case, there results:

$$\frac{\partial u}{\partial t} + u \frac{\partial u}{\partial x} + v \frac{\partial u}{\partial y} + \frac{1}{\rho} \frac{\partial P}{\partial x} = \nu \left( \frac{\partial^2 u}{\partial x^2} + \frac{\partial^2 u}{\partial y^2} \right) \quad (17)$$

and,

$$\frac{\partial v}{\partial t} + u \frac{\partial v}{\partial x} + v \frac{\partial v}{\partial y} + \frac{1}{\rho} \frac{\partial P}{\partial y} = \nu \left( \frac{\partial^2 v}{\partial x^2} + \frac{\partial^2 v}{\partial y^2} \right). \quad (18)$$

Eliminating pressure by cross-differentiation and subtraction, one has:<sup>7</sup>

$$\begin{aligned}
 & \frac{\partial}{\partial t} \left[ \frac{\partial V}{\partial x} - \frac{\partial u}{\partial y} \right] + \frac{\partial u}{\partial x} \left[ \frac{\partial V}{\partial x} - \frac{\partial u}{\partial y} \right] + \frac{\partial V}{\partial y} \left[ \frac{\partial V}{\partial x} - \frac{\partial u}{\partial y} \right] \\
 & + u \frac{\partial}{\partial x} \left[ \frac{\partial V}{\partial x} - \frac{\partial u}{\partial y} \right] + v \frac{\partial}{\partial y} \left[ \frac{\partial V}{\partial x} - \frac{\partial u}{\partial y} \right] \\
 & = r \left\{ \frac{\partial^2}{\partial x^2} \left[ \frac{\partial V}{\partial x} - \frac{\partial u}{\partial y} \right] + \frac{\partial^2}{\partial y^2} \left[ \frac{\partial V}{\partial x} - \frac{\partial u}{\partial y} \right] \right\}
 \end{aligned} \tag{19}$$

The vorticity vector is defined as

$$\zeta = \epsilon_{ijk} f_{k,i} \tag{20}$$

which means that since only two dimensions are involved, vorticity exists only parallel to the Z-axis. Therefore, letting

$$\zeta = \zeta_3 = \frac{\partial V}{\partial x} - \frac{\partial u}{\partial y} \tag{21}$$

and substituting back into equation (19), one has

$$\frac{\partial \zeta}{\partial t} + \zeta \frac{\partial u}{\partial x} + \zeta \frac{\partial V}{\partial y} + u \frac{\partial \zeta}{\partial x} + v \frac{\partial \zeta}{\partial y} = r \left[ \frac{\partial^2 \zeta}{\partial x^2} + \frac{\partial^2 \zeta}{\partial y^2} \right],$$

or finally,

$$\frac{\partial \zeta}{\partial t} + \frac{\partial u \zeta}{\partial x} + \frac{\partial V \zeta}{\partial y} = r \left[ \frac{\partial^2 \zeta}{\partial x^2} + \frac{\partial^2 \zeta}{\partial y^2} \right]. \tag{22}$$

---

<sup>7</sup> u, v, and P must be assumed continuous functions of x, y, and t.



The system of equations needed becomes complete by introducing the stream function relationship,

$$q_i = -\epsilon_{ij3} \psi_{,j} \quad (8) \text{ Repeat}$$

into the continuity equation,  $q_{L,L} = 0$ . For the irrotational case, this would result with the Laplacian of the stream function equal to zero. However, there is rotation present and this introduction must be handled differently. By adding  $\zeta$  to both sides of the continuity equation, one obtains

$$\frac{\partial u}{\partial x} + \frac{\partial v}{\partial y} + \frac{\partial v}{\partial x} - \frac{\partial u}{\partial y} = \frac{\partial v}{\partial x} - \frac{\partial u}{\partial y} = \zeta. \quad (23)$$

The rearranging of the left side produces;

$$\frac{\partial}{\partial x} [u+v] + \frac{\partial}{\partial y} [v-u] = \zeta. \quad (24)$$

Now substituting for  $u$  and  $v$  the appropriate expanded relation from equation (8), i.e.,  $u = \frac{\partial \psi}{\partial y}$  and  $v = -\frac{\partial \psi}{\partial x}$ , and then performing the partial differentiation as indicated in front of each bracket, the equation becomes:

$$\frac{\partial^2 \psi}{\partial x \partial y} - \frac{\partial^2 \psi}{\partial x^2} - \frac{\partial^2 \psi}{\partial x \partial y} - \frac{\partial^2 \psi}{\partial y^2} = \zeta.$$

This of course reduces to a form of Poisson's equation,

$$\frac{\partial^2 \psi}{\partial x^2} + \frac{\partial^2 \psi}{\partial y^2} = -\zeta. \quad (25)$$

Equation (22), when written in terms of  $\psi$  and  $\zeta$  reduces to

$$\frac{\partial \zeta}{\partial t} + \left[ \frac{\partial \psi}{\partial y} \frac{\partial \zeta}{\partial x} - \frac{\partial \psi}{\partial x} \frac{\partial \zeta}{\partial y} \right] = r \left[ \frac{\partial^2 \zeta}{\partial x^2} + \frac{\partial^2 \zeta}{\partial y^2} \right], \quad (26)$$

which is somewhat easier to program since the necessity of finding the velocity gradients has been eliminated. If desired, these could be found from the other forms of the equations given above. As before, the assumption concerning continuous functions noted in footnote 7 still applies.

The specific finite difference formulas used to convert equations (25) and (26) into a numerically solvable system depends basically on the largest allowable truncation error and on the mesh size of the grid points. Crandall [12] discusses quite thoroughly all the aspects involved for both these considerations. It is sufficient to say that greater accuracy requires less truncation error and a finer mesh size. Generally, since finer mesh sizes require larger computer storage capabilities, they are used only in the areas of the flow field where large gradients are expected.

There are in general two basic methods of solving this system of equations. The one most widely used, until recently, has been of an iterative nature such as the relaxation or Gauss-Siedel methods; or modifications thereto. The primary concern here is that of convergence and stability of solution. The Gauss-Siedel method is adversely susceptible to both of these while the relaxation method generally does not have a stability problem, but can require an abnormally large number of iterations before some degree of convergence is attained. These methods are however, fairly simple to program. With the advent of the digital computer, more sophisticated numerical methods can be used to solve the system of equations explicitly using matrices. Methods such as Gaussian elimination with back substitution can produce a very accurate inverse for a matrix that is not singular, and a properly

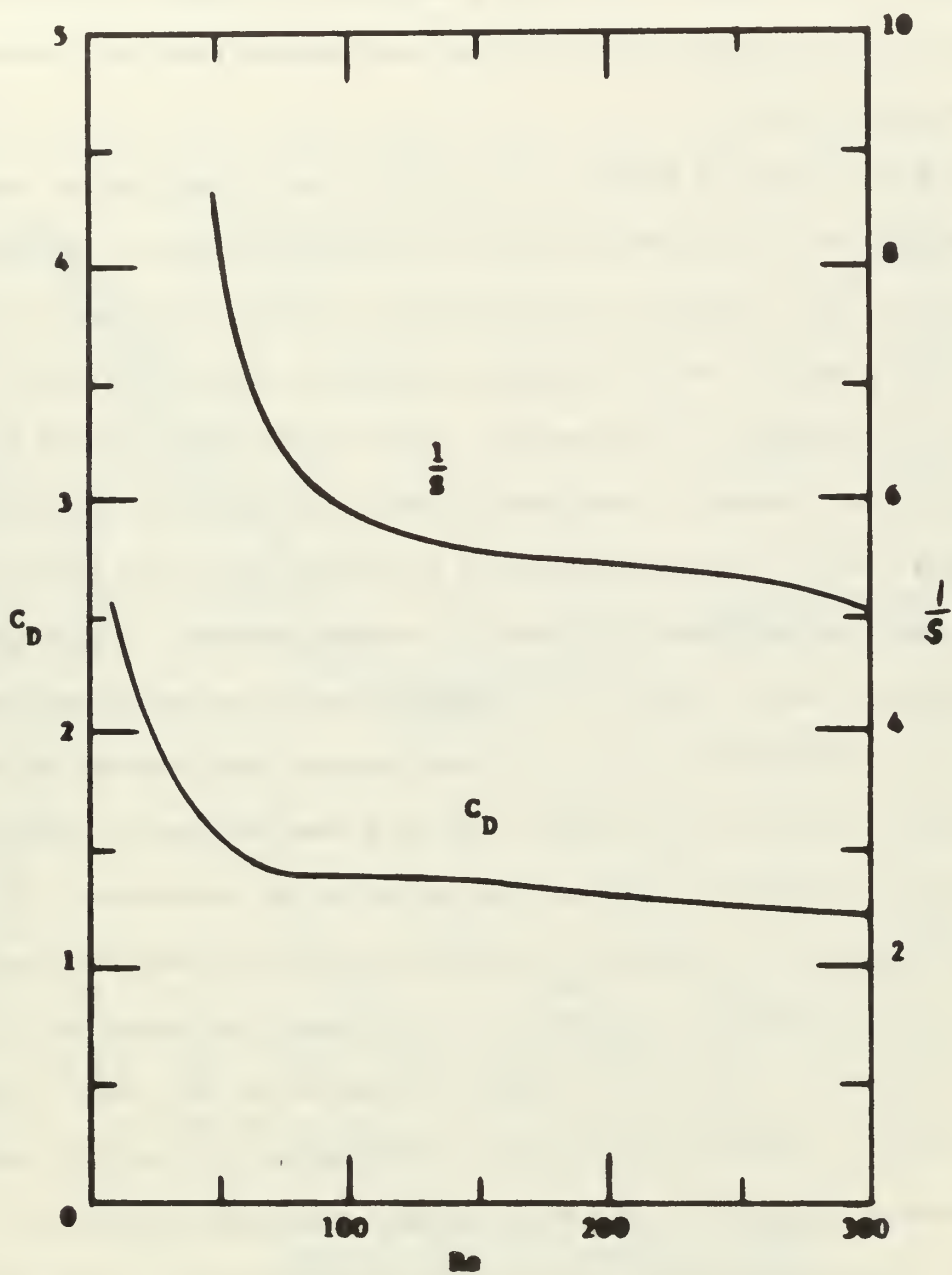


**Figure 7. Mean Drag Coefficient and Inverse of Strouhal Number Versus Reynolds Number**

constituted matrix representing a physical system should not be singular. For large systems of equations, the coefficient matrix can be reduced to a triangular form through the use of a sequence of linear operations. The inverse of this reduced matrix is then used rather than the inverse of the complete system.

Besides Fromm and Harlow [11] several other investigators have studied this Reynolds number region using modifications of the above procedures. Most numerical solutions have involved rectangular cylinders due to the ease with which Cartesian coordinate finite difference equations can be applied. Thompson [13] used a Gauss-Seidel method but appears to have assured convergence through the use of an "acceleration parameter" which is determined from a consideration of the eigenvalues of the matrices involved. His results compare favorably with experimental data, however, some of his computer runs required as much as nine hours on an IBM 360/40. This could have serious implications as far as accuracy is concerned, since each time step must adequately converge before the conditions for the next time step can be calculated. If convergence presents no problem, then there is another important result of his work that should be mentioned: no artificial introduction of vorticity is required to cause the eventual formation of the vortex street.

Wang [14] used cylindrical polar coordinates in a matched asymptotic expansion solution of the Navier-Stokes equations. Though the results offer no new insight, the method is indicative of the mathematical attempts being made. Ingham's paper [15] offers constructive criticism of Payne's method of finite difference solution [16], and is indicative of the pitfalls waiting for the unwary. Ingham's examples of variation of calculated  $C_D$  for different mesh sizes at the same Reynolds number is quite dramatic.

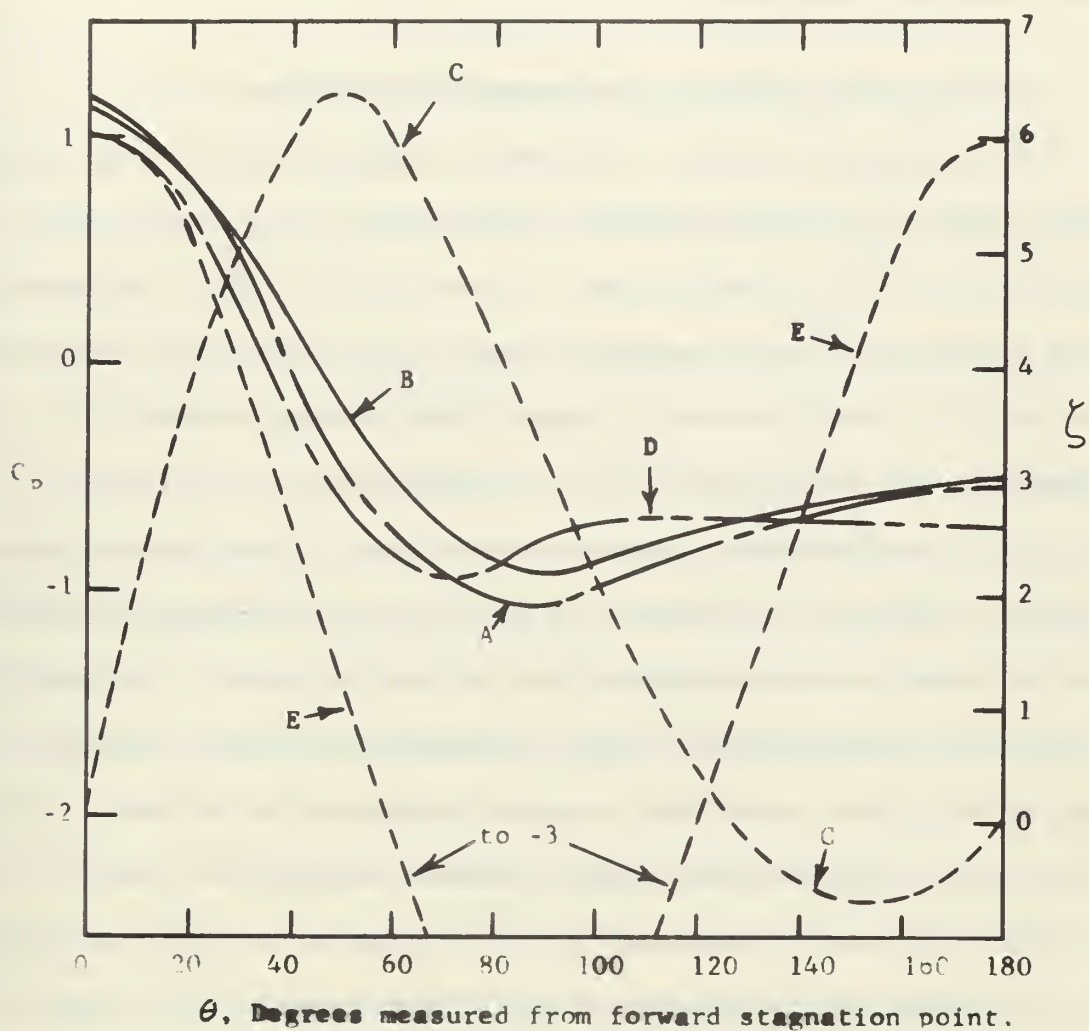


**Figure 8. Experimental and Computed Pressure Coefficient and Computed Surface Vorticity ( $\zeta$ ) at Low Reynolds Numbers.**

- A Computed  $C_p$ , Apelt,  $Re = 40$
- B Computed  $C_p$ , Kawaguti,  $Re = 40$
- C Computed  $\zeta$ , Apelt,  $Re = 40$
- D Experimental, Linke,  $Re = 2800$
- E Computed  $C_p$ , Potential Flow Theory



The pertinent experimental and analytical data derived by investigators in this Reynolds number range are shown in Figures 7 and 8. Important contributors of this information include Taneda [17], Tritton [18], Roshko [19], Rosenhead [20], Wille [21], and Apelt [22]; besides those previously mentioned.

#### D. REYNOLDS NUMBER BETWEEN THREE HUNDRED AND CRITICAL

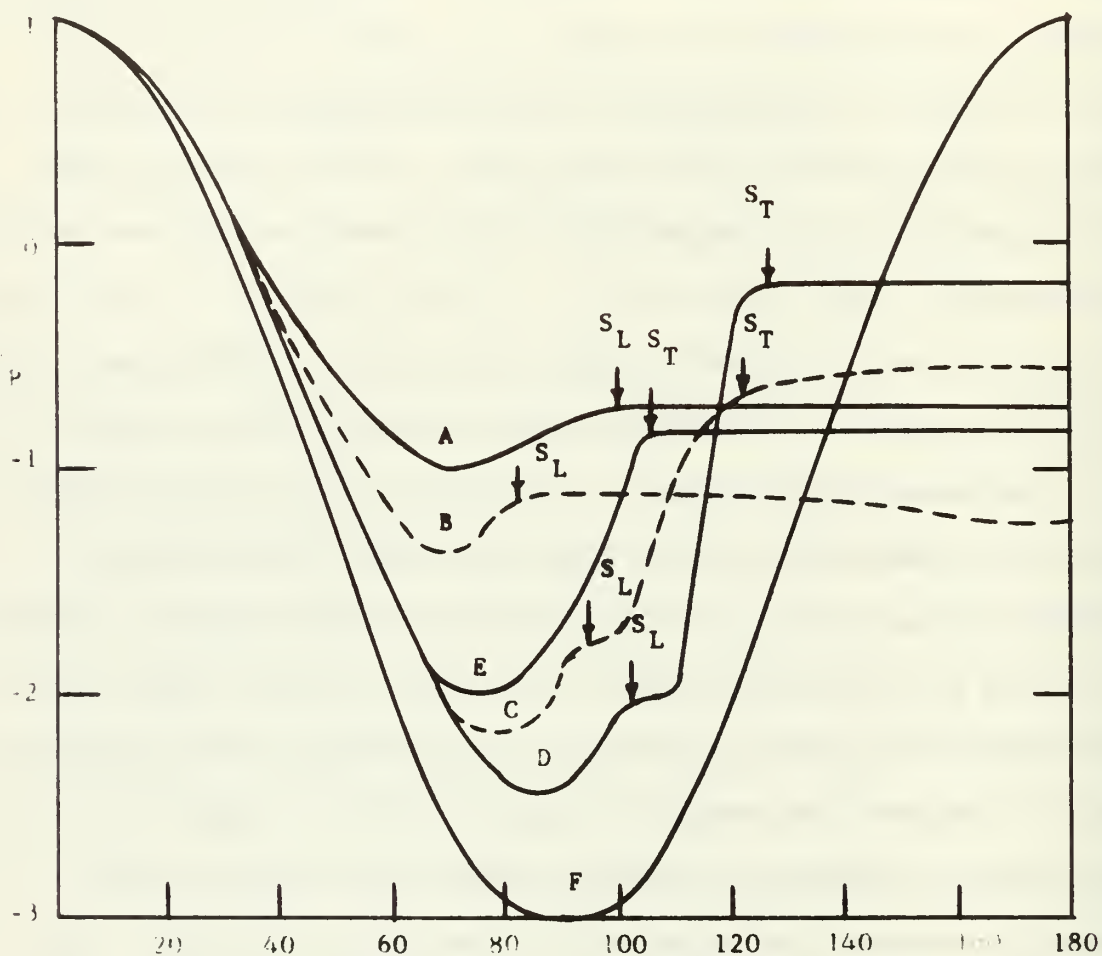
This subcritical region is in general characterized by a relatively constant mean drag coefficient and a progressive loss in the distinct visualization of the Kármán street. As the Reynolds number increases there appears to be less "feedback" effect of the wake on the separating boundary layers which are still laminar. The Strouhal number has a tendency to decrease slightly with an increase of  $Re$ . It is in this region that the potential flow point vortex model of the feeding sheet appears to have the best possibility of providing information since the inertia forces are so much larger than the viscous forces. The use of the finite difference Navier-Stokes equations to provide a solution seems to break down due to the increased turbulence in the wake. Although a much finer mesh size might alleviate this problem, the fact that the equations now being used do not provide for velocity perturbation is probably the more basic reason. There appears to be no argument that the equations are applicable for use in describing the boundary layer on the front part of the cylinder almost up to the critical  $Re$  of about  $5 \times 10^5$ . As the Reynolds number increases from the low end of this region, the boundary layer effects appear to feed vorticity into the wake at an ever increasing rate causing the wake to become extremely turbulent. As this occurs, the well ordered vortex core regions of the Kármán street essentially disappear. Although the Strouhal number can

still be measured, the dominant periodicity seen in the lower Reynolds number wake flows all but disappears. Experimental studies using turbulent flow measuring techniques have confirmed the increasing turbulence with increasing Reynolds number. Ironically, the feedback problem diminishes, but the problem of transition from laminar to turbulent flow conditions becomes more important. The understanding of the latter problem is even less than that of the former. The end result is that the applicability of the laminar Navier-Stokes equations decreases with increasing  $Re$ .

In the "critical" Reynolds number region, loosely defined as  $2 \times 10^5 < Re < 10^6$ , there is a sharp decrease in the mean  $C_D$  down to about 0.3.<sup>8</sup> According to Schlichting [2, p. 39], this is due to the following reason: when the total drag on any body is primarily form drag, the transition from a laminar to a turbulent boundary layer causes a decrease in the size of the wake and results in a decrease in drag. This can be interpreted as saying that the drop in  $C_D$  is a boundary layer phenomenon, though it does not quite explain the entire mechanism. After this transition occurs,  $C_D$  increases to a value slightly lower than that before transition. There is also a return of a distinct vortex street. This time however, the "vortex cores" are highly turbulent internally. As the Reynolds number increases beyond this region, compressibility effects become greater, further complicating the problem. Depending on the fluid, very high Reynolds numbers can bring on the added, sometimes predominant, problem of cavitation.

---

<sup>8</sup>This is true for a hydraulically smooth cylinder. The roughness of the cylinder surface can have a major effect on this minimum mean drag and the Reynolds number at which transition occurs. See [2, p. 621].



$\theta$ , Degrees measured from forward stagnation point.

Figure 9. Experimental Pressure Coefficients Found at Medium and High Reynolds Numbers Indicating Laminar ( $S_L$ ) and Turbulent ( $S_T$ ) Separation Points.

A Linke,  $Re = 2.8 \times 10^3$

D Flachabart,  $Re = 6.7 \times 10^5$

B {Fage and }  $Re = 1.1 \times 10^5$

E Roshko,  $Re = 8.4 \times 10^6$

C {Falkner }  $Re = 2.1 \times 10^5$

F Potential Flow Theory



Experimental studies of the pressure distribution on the cylinder's surface have yielded some valuable information necessary for future analytical postulation. The pressure coefficient, defined as

$$C_P = \frac{2 \Delta P}{\rho U_\infty^2} \quad (27)$$

is an excellent parameter for theoretical and experimental comparison particularly for creeping motions ( $Re < 1$ ), and at Reynolds numbers where the boundary layer separation points maintain fairly constant positions. At very low Reynolds numbers, the comparison is quite good especially on forward part of the cylinder, between points A and B in Figure 1. Between points B and C, the actual pressure decreases somewhat since energy is expended in the boundary layer; i.e., not all the kinetic energy acquired from A to B is recovered as potential energy as the fluid decelerates toward C. In Potential Flow Theory, points A and C are of course stagnation points, and whereas the pressure at A can be well approximated by this theory over the entire Reynolds number range, the pressure at point C cannot as indicated in Figure 9. Note how curve D, found for a Reynolds number above the critical, more nearly approximates curve F (potential flow). Photographs of the wake pattern produced for this post-critical Reynolds number shows a narrow wake with the rest of the flow field similar in appearance to that of an ideal fluid. Note also that after the boundary layer has separated,  $C_p$  assumes a nearly constant value, not the same for all Reynolds numbers however.

Though information about the Strouhal number is still incomplete above  $Re \approx 10^5$ , there is an interesting similarity between the inverse of this parameter and  $C_D$ . The curves for the two values, plotted over the whole range of  $Re$  from the beginning of core shedding through the

critical region, are very similar in shape. In fact, the similarity is so good that the drag coefficient could be written as

$$C_D = \frac{1}{S} - 1.4$$

with the resulting value having an accuracy within about 15 percent.

The explanation for this result is not complete, however, the point here is that there is apparently a strong conceptual connection between core shedding frequency and drag. It is interesting to also note that through the region of nearly constant drag, not only is  $1/S$  fairly constant, but that the oscillations of the boundary layer separation points are generally quite small in amplitude.

Investigators have attempted several approaches in the search for an analytic solution in this region and there have been some notable successes. Each approach, however, involves the use of at least one experimentally determined or arbitrarily selected parameter.

The free-streamline theory developed by Kirchhoff, idealizes the free shear layers that separate from the cylinder by considering them to be surfaces of velocity discontinuity; hence a free streamline. This supposition works quite well for liquid jets discharging into a gas, however, for cylinder wakes, because of the assumption that the pressure in the wake is the same as the free stream pressure, the resultant calculated drag coefficients are much lower than those experimentally observed. The agreement can be greatly enhanced by the introduction of an arbitrarily selected parameter usually symbolized by  $K$ . This parameter is concerned with the depth of discontinuity (notch) in the logarithmic hodograph plane,<sup>9</sup> and is therefore concerned with the ratio between the

---

<sup>9</sup>In this plane, the two-dimensional physical flow is represented by straight lines parallel to the two coordinate axes, and is the result of conformal mapping. See [1, p. 351].

free stream-line velocity and the free stream velocity. For very high Reynolds number flows, where cavitation exists,  $K$  is fixed by the cavitation index,  $\sigma$ . Fairly good agreement between experiment and theory exists in this case, particularly with respect to cavity flows.

Dennis and Shimshoni [26] have probably been two of the more successful investigators in analytically deriving the mean drag coefficient over the entire laminar boundary layer Reynolds number range. Their solution involves series expansions<sup>10</sup> of the Navier-Stokes equations, set up for finite difference evaluations. At slow, creeping motions, their solution converges to that of Stokes and Lamb, but at Reynolds numbers above about 1.5, the values of  $C_D$  are about 5 to 20 percent higher. They allow no asymmetry of vortex shedding. The mesh size they use appears to be much smaller than that of other attempts.

As noted earlier in the discussion, this Reynolds number region is characterized by the predominance of inertia forces over viscous forces. Also noted was that this leads to the possibility of using point concentrated, potential flow vortices to represent the shear layers or feeding sheets. Among those who have worked with this approach, Sarpkaya [35], Bryson [29], and Gerrard [25] have made some notable strides. The description of the work of the first two will be left to Section III, since it is basically with their ideas that the author worked. Gerrard's work, though similiar in mathematical approach to the others, appears to indicate a greater concern for wake characteristics than for finding solutions to the basic separation problem.

---

<sup>10</sup> Similar to Oseen and Lamb.

Besides the basic points covered here, there is a great wealth of experimental information on the more detailed aspects of the subject that should be covered by any reader desiring to proceed further with the investigation. Toward this end, the author has attempted to compile the more notable of these in the List of References. Although some references have not been mentioned specifically herein thus far, this is not intended to mean they are of lesser value.

### III. TWO ANALYTIC MODELS

#### A. INTRODUCTION

In the previous two sections, the discussion has centered on those few basic known facts and some of the many problems involved in this study. This section will present, in detail, two different analytic models, based on Potential Flow Theory, which are theoretically applicable to the relatively higher Reynolds region discussed in Section II (D).

The first model, called Model A hereafter, is conceptually more enlightening than the second; hence the reason for its presentation first. It is basically derived from Bryson's [29] model, but where his model was limited to the growth of axisymmetric vortex cores, the equations for Model A are recast to allow "forced" asymmetry to be included into the solution. To the author's knowledge, this is the first time this has been done. This method, like almost all the others, has no provision included in the governing equations for "natural" asymmetry. Thus if asymmetry is to be studied, its beginnings must be forced. In brief terms then, the basis of this model is that large vortex cores are fed vorticity through an infinitely narrow feeding sheet, or shear layer, connecting the center of the core with assumed stagnation points on the cylinder's surface.

In the second model, Model B, the shear layers are represented by a string of small strength vortices, called a vortex sheet; see [1, p. 111]. The equations for this model were also derived and programmed to allow forced asymmetry. Whereas Model A represents a continuously fed large vortex core, this one creates numerous small vortices which are



allowed to roll-up, coalesce and/or cancel at will. There are four birth areas in this model, two for the primary vortices, and two for the secondary vortices.<sup>11</sup> This arrangement is a modification of Sarpkaya's model [35] in which there are only two axisymmetric birth areas. Comparison between the two will be left until later in this section.

## B. BASIC POTENTIAL FLOW EQUATIONS

The basic general equations used in both models will be presented in this subsection. The actual application will be left to the discussion of that particular model. It is not felt that the history behind these equations is relevant to this thesis since the interested reader can refer to Sarpkaya [36] for this information.

As mentioned earlier, in Section I, a two-dimensional flow system can be represented mathematically by equations written in complex variables. Since the mathematical development of this representation is quite lengthy, the following is only a brief part of what can be found in many reference books and papers on hydrodynamics. To start with, it is well to review the basic assumptions. First, the fluid is considered inviscid. This implies that there are no viscous forces present and therefore that the models derived should be applicable to the higher laminar Reynolds number range. Secondly, since this aforementioned Reynolds number range is generally devoid of compressibility effects,  $\rho$  will be assumed constant. The usual "steady flow" assumption

---

<sup>11</sup>Vorticity is shed from the cylinder in the regions of boundary layer separation. These regions are associated with the "primary" boundary layers on the cylinder's upstream side and the "secondary" layers due to fluid back-flow on the downstream side. Since vorticity is created in these regions, they are called "birth" areas, and the small strength vortices created are called "nascent" vortices.



will not be made, because all the flow characteristics appear to be dependent on the manner in which the boundary layer generates vorticity and on the manner in which it diffuses into the wake. The key problem then is the formulation of a method by which vorticity can be generated in a supposedly inviscid fluid. This is in direct violation of Kelvin's theorem for inviscid fluids which says that vorticity once created, cannot be destroyed, and if not already existing, cannot be created. In order to overcome this, boundary layer information must be taken into consideration.

From basic considerations of hydrodynamics, an undefined number of vortices outside the boundaries of a circular cylinder, suspended in a uniform flow field as in Figure 10, can be represented by

$$W(z) = -U_{\infty} \left( z + \frac{c^2}{z} \right) + \frac{i}{2\pi} \left[ \sum_{n=1}^N \Gamma_n \mathcal{L}_n(z - z_n) - \sum_{n=1}^N \Gamma_n \mathcal{L}_n \left( z - \frac{c^2}{\bar{z}_n} \right) \right]. \quad (28)$$

There are no symmetry restrictions on this equation. The normally excluded terms have been left out.<sup>12</sup> Next it can be shown that for a general location  $z$ , on or outside the cylinder, the fluid velocity is given by:

$$\frac{dW(z)}{dz} = -u + iv = U_{\infty} \left( \frac{c^2}{z^2} - 1 \right) + \frac{i}{2\pi} \left[ \sum_{n=1}^N \frac{\Gamma_n}{z - z_n} - \sum_{n=1}^N \frac{\Gamma_n}{z - \frac{c^2}{\bar{z}_n}} \right]. \quad (29)$$

---

<sup>12</sup>These are the terms that are excluded by virtue of the condition that the vortices shed from the cylinder leave a circulation opposite to their own on the cylinder. See [38, p. 364].

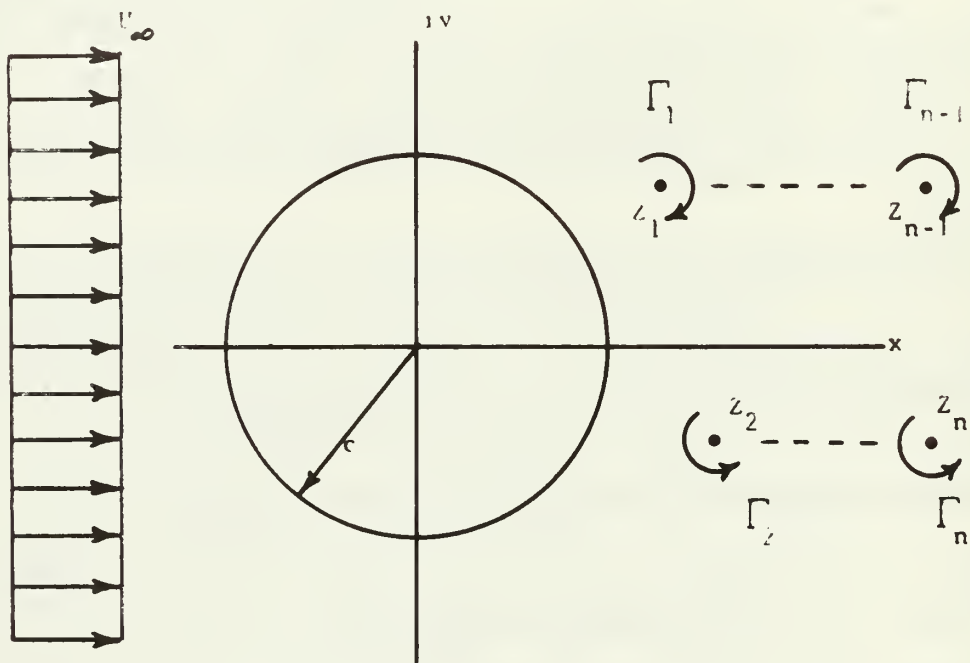


Figure 10. Circular Cylinder in the Presence of Numerous Vortices and a Uniform Flow Field.

Now that if  $Z=Z_n$ , the velocity goes to infinity. This is to be expected since the velocity at the center of an ideal, inviscid vortex is equal to infinity. This same equation can, however, be used to find the absolute velocity of the vortex with respect to cylinder, hereafter called the convective vortex velocity, by letting  $Z=Z_n$  and disregarding the term that goes to infinity. This is due to the fact that the motion of a vortex is governed not by its own internal velocity distribution, but by the forces induced upon it by other entities in the flow field. See [1, p. 124].

Next, the drag and lift forces on a body can be calculated from the generalized Blasius' theorem,

$$\overline{F_D + iF_L} = \frac{i\rho}{2} \oint \left( \frac{dW(z)}{dz} \right)^2 dz + i\rho \frac{\partial}{\partial t} \oint W(z) dz \quad (30)$$

Writing

$$\overline{F_D + iF_L} = (\overline{X_1 - iY_1}) + (X_2 + iY_2) \quad (31)$$

equation (30) can be broken down into its so called "steady state" part,

$$X_1 - iY_1 = \frac{i\rho}{2} \oint \left( \frac{dW(z)}{dz} \right)^2 dz \quad (32)$$

and the time dependent part,

$$X_2 + iY_2 = i\rho \frac{\partial}{\partial t} \oint W(z) dz \quad (33)$$

The steady part, using equation (29), can be evaluated [35] such that:

$$X_1 + iY_1 = i\rho \sum_{n=1}^N \Gamma_n (u_n + iV_n) \quad (34)$$

The evaluation of equation (33) must wait until the discussion of the individual models since it involves some assumptions as far as the method by which  $\Gamma$  is to vary over the feeding zones. To continue, non-dimensionalizing can easily be done by referring all the length, velocity and time quantities to  $U_\infty$  and  $c$ ; or for example,

$$\begin{aligned} Z &= c Z' , \\ u + i v &= U_\infty (u' + i v') , \\ \Gamma &= U_\infty c \Gamma' , \end{aligned} \quad (35)$$

and,

$$t = \frac{c t'}{U_\infty}$$

Substituting equations (35) into (29); letting  $U = 1.0$ ;  $c = 1.0$ , and dropping the primes for the sake of simplicity, this becomes;

$$-u + i v = \frac{1}{z^2} - 1 + \frac{i}{2\pi} \left[ \sum_{n=1}^N \frac{\Gamma_n}{z - z_n} - \sum_{n=1}^N \frac{\Gamma_n}{z - \frac{1}{\bar{z}_n}} \right] . \quad (36)$$

Up to this point a discussion of image vortices has not been necessary, however, certain relations will be needed for future development of equation (33) in succeeding subsections. It can be shown by interpretation of Milne-Thompson's circle theorem [38, p. 157], or by using the method of images [38, p. 220], that the second summation in equation (29) and consequently in (36), are in reality "image" vortices inside the cylinder. The location of the image vortex, corresponding to the real vortex at  $z_n$  is  $c^2/\bar{z}_n^2$ . Its circulation is in the opposite sense as compared to that of its corresponding real vortex. Positive numerical values for circulation indicate rotation in the counterclockwise direction, while negative numerical values indicate clockwise rotation. In the derivation of the equations, the

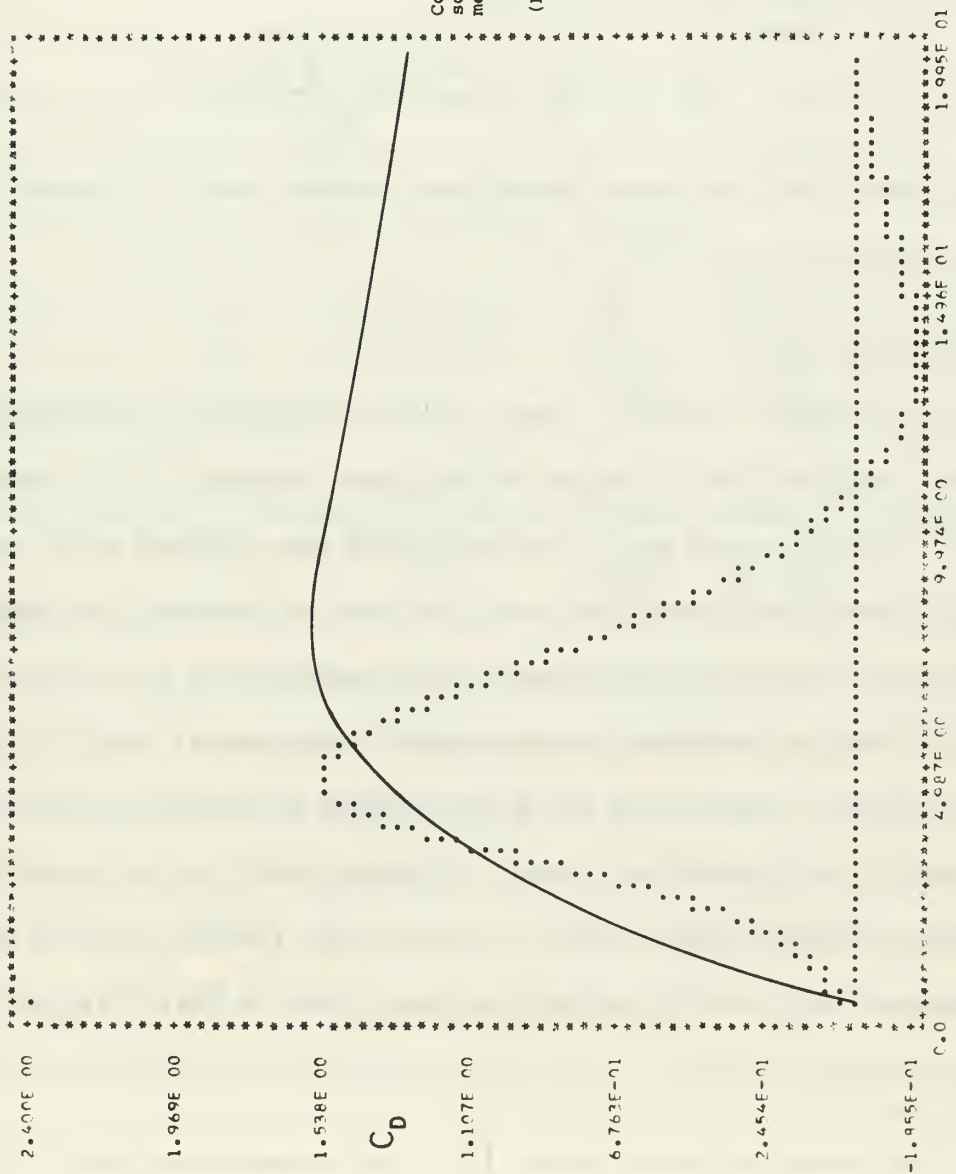


Figure 11  
 Comparison of Bryson's analytic  
 solution with Sarpkaya's experi-  
 mental results.  
 ....Bryson [29]  
 .....Sarpkaya [33]  
 (Re =  $1.5 \times 10^4$  to  
 $9.1 \times 10^4$ , experimental)

symbol  $\int$  has no inherent sign and can therefore take on positive or negative values as the situation warrants.

Since there are conditions well described in [38] that make equation (36) not applicable to the internal area of the cylinder, Sarpkaya [36] shows that the velocity of the image vortices are strictly a function of the position of the image vortex and the corresponding real vortex's velocity. By manipulating his expressions, the following equation for the image velocity results:

$$u_{in} + i v_{in} = \frac{-u_n + i v_n}{\bar{z}_n^2} \quad (37)$$

To reiterate, the term whose denominator equals zero is disregarded when solving for  $-u_n + i v_n$ .

#### C. MODEL A

As previously mentioned, this model is primarily a modification to Bryson's solution [29]. Though his solution appears to give reasonable drag coefficients during the beginning time periods of an impulsively started flow condition, once the peak is reached, the drag coefficient drops off to fluctuate about zero; Figure 11. This of course is not correct as Sarpkaya's superimposed experimental data [33] indicates. Though Bryson stops his solution when the vortices begin feeding circulation back to the cylinder,<sup>13</sup> this in itself is not enough to produce a reasonable drag curve. It was hoped that by studying his method, modified to allow asymmetry, more could be learned about the

---

<sup>13</sup>The condition occurs when  $\dot{\bar{z}}_n$  (to be developed later) for a given vortex changes sign. If the solution is not stopped at this point a negative drag coefficient results as shown in Figure 11.



effect of vortex core shedding on the drag coefficient. Before a discussion of those results is undertaken, the equations must be developed.

Using Figure 12 as the basis for nomenclature definition, the equation development starts with the necessary modifications to equation (36). Though these equations can be constructed to allow more than two vortices, this will not be done at this time in order to show a simplified version of the technique. As will be indicated later, the full equations are obtained by the simple addition of a summation term to each of the following equations. So, based on two vortices, the velocity of vortex 1, if it were free,<sup>14</sup> is given by

$$-u_1 + iV_1 = \frac{1}{Z_1^2} - 1 + \frac{i}{2\pi} \left[ \frac{\Gamma_2}{Z_1 - Z_2} - \frac{\Gamma_2}{Z_1 - \frac{1}{Z_2}} - \frac{\Gamma_1}{Z_1 - \frac{1}{Z_1}} \right]; \quad (38)$$

and likewise for vortex 2;

$$-u_2 + iV_2 = \frac{1}{Z_2^2} - 1 + \frac{i}{2\pi} \left[ \frac{\Gamma_1}{Z_2 - Z_1} - \frac{\Gamma_1}{Z_2 - \frac{1}{Z_1}} - \frac{\Gamma_2}{Z_2 - \frac{1}{Z_2}} \right]. \quad (39)$$

Next, the feeding aspect of the vortex cores is handled by considering the vortex sheet, or feeding layer, as the combination of a single concentrated vortex, situated at the center of vorticity, with a connecting sheet to the body of vanishingly small vorticity. This sheet can now be considered as a mathematical branch line between  $Z_T$  and  $Z_1$  for vortex 1, and  $Z_b$  and  $Z_2$  for vortex 2. Since there is a discontinuity, conceptually, in  $\phi$  across these branch lines, there is a velocity difference and therefore a pressure difference. This pressure difference

---

<sup>14</sup> A free vortex is one that is no longer being fed circulation.

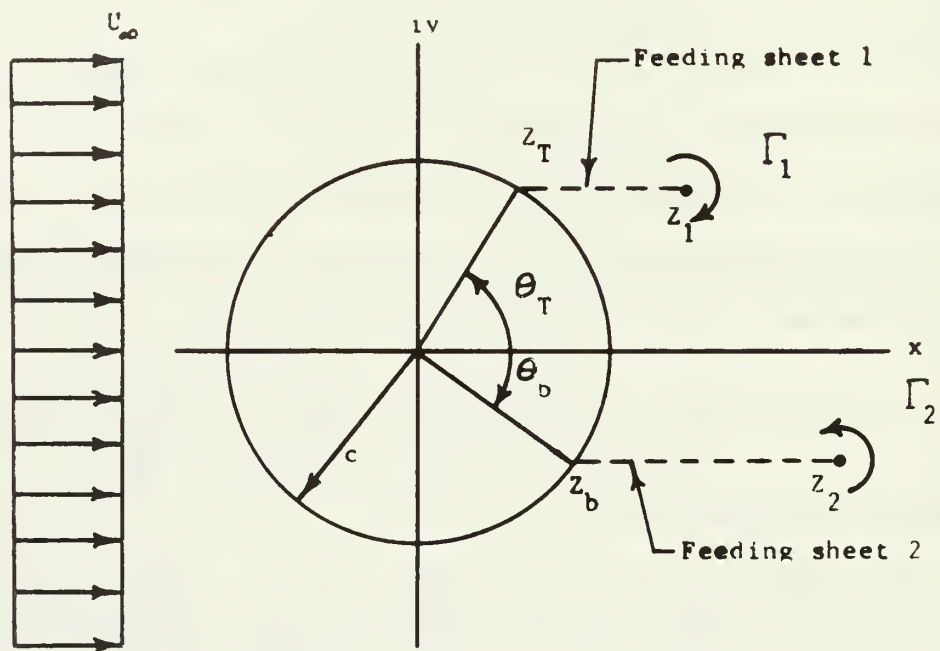


Figure 12. Model A, Indicating Capability for Asymmetry.

can be shown ([43] and [44]) to be equal to  $\rho \dot{\Gamma}_n$ . Since the distances over which the pressure differences act are  $(z_1 - z_T)$  and  $(z_2 - z_b)$  for vortices 1 and 2 respectively, the forces acting perpendicular to these sheets are given by  $i\rho \dot{\Gamma}_1 (z_1 - z_T)$  and  $i\rho \dot{\Gamma}_2 (z_2 - z_b)$ . The forces acting directly on the vortices is given, for vortex 1, by

$$i\rho \dot{\Gamma}_1 \left( \overline{\frac{dW(z)}{dz}} \right) \Big|_{z=z_1} + \dot{z}_1 ,$$

and for vortex 2, by

$$i\rho \dot{\Gamma}_2 \left( \overline{\frac{dW(z)}{dz}} \right) \Big|_{z=z_2} + \dot{z}_2 .$$

Thus to make the net forces on each sheet and its associated concentrated vortex vanish,<sup>15</sup> the sum of the respective forces must equal zero. Therefore, algebraically summing each pressure force with its proper vortex force, cancelling out  $i$  and  $\rho$ , and rearranging the terms, the two expressions formed become; for vortex 1:

$$\dot{z}_1 + (z_1 - z_T) \frac{\dot{\Gamma}_1}{\Gamma_1} = - \overline{\frac{dW(z)}{dz}} \Big|_{z=z_1} , \quad (40)$$

and for vortex 2;

$$\dot{z}_2 + (z_2 - z_b) \frac{\dot{\Gamma}_2}{\Gamma_2} = - \overline{\frac{dW(z)}{dz}} \Big|_{z=z_2} . \quad (41)$$

These equations indicate that unless  $\dot{\Gamma}_n$  is zero, the  $n$ th vortex does not move with the local fluid velocity,  $u_n + iv_n$ , but with an "attached" velocity of  $\dot{z}_n$ .

---

<sup>15</sup>The combination of vortex sheet and the concentrated vortex in a fluid medium has to be force free since no external force is exerted on the system.

$$\begin{aligned}
 \frac{\dot{\Gamma}_1}{2\pi} &= \dot{\Gamma}_2 \frac{K_1 K_2}{2\pi} + \dot{Z}_1 K_5 K_{12} + \bar{\dot{Z}}_1 K_6 K_{12} + \dot{Z}_2 \frac{\Gamma_1}{2\pi} K_1 K_2 \\
 &\quad + \bar{\dot{Z}}_2 \frac{\Gamma_2}{2\pi} K_1 K_{10} + K_1 (K_8 + \frac{K_T}{2\pi}) \\
 \frac{\dot{\Gamma}_2}{2\pi} &= \dot{\Gamma}_1 \frac{K_3 K_4}{2\pi} + \dot{Z}_1 \frac{\Gamma_1}{2\pi} K_3 K_{17} + \bar{\dot{Z}}_1 \frac{\Gamma_1}{2\pi} K_3 K_{18} + \dot{Z}_2 K_{13} K_{20} \\
 &\quad + \bar{\dot{Z}}_2 K_{14} K_{20} + K_3 (K_{16} + \frac{K_b}{2\pi})
 \end{aligned} \tag{43}$$

where the constants K are defined by:

$$K_1 = \frac{(Z_T - Z_1)(Z_T \bar{Z}_1 - 1)}{1 - Z_1 \bar{Z}_1}$$

$$K_5 = \left( \frac{Z_T \bar{Z}_1 - 1}{1 - Z_1 \bar{Z}_1} \right)^2$$

$$K_2 = \frac{Z_2 \bar{Z}_2 - 1}{(Z_T - Z_2)(Z_T \bar{Z}_2 - 1)}$$

$$K_6 = \left( \frac{Z_T - Z_1}{1 - Z_1 \bar{Z}_1} \right)^2$$

$$K_3 = \frac{Z_b - Z_2)(Z_b \bar{Z}_2 - 1)}{(1 - Z_2 \bar{Z}_2)}$$

$$K_7 = i U_\infty \left( 1 - \frac{1}{Z_T^2} \right)$$

$$K_4 = \frac{(Z_1 \bar{Z}_1 - 1)}{(Z_b - Z_1)(Z_b \bar{Z}_1 - 1)}$$

$$K_8 = i \dot{U}_\infty \left( 1 - \frac{1}{Z_T^2} \right)$$

$$K_9 = \frac{1}{(z_T - z_2)^2}$$

$$K_{16} = i \dot{U}_\infty \left(1 - \frac{1}{z_b^2}\right)$$

$$K_{10} = \frac{1}{(z_T \bar{z}_2 - 1)^2}$$

$$K_{17} = \frac{1}{(z_b - z_1)^2}$$

$$K_{11} = \sum_{m=1}^M \Gamma_m \left[ \frac{1}{z_T - z_m} - \frac{1}{z_T - \frac{1}{\bar{z}_m}} \right]$$

$$K_{18} = \frac{1}{(z_b \bar{z}_1 - 1)^2}$$

$$K_{12} = \frac{\Gamma_2}{2\pi} K_2 + \frac{K_{11}}{2\pi} + K_7$$

$$K_{19} = \sum_{m=1}^M \Gamma_m \left[ \frac{1}{z_b - z_m} - \frac{1}{z_b - \frac{1}{\bar{z}_m}} \right]$$

$$K_{13} = \left( \frac{z_b \bar{z}_2 - 1}{1 - z_2 \bar{z}_2} \right)^2$$

$$K_{20} = \frac{\Gamma_1}{2\pi} K_4 + \frac{K_{19}}{2\pi} + K_{15}$$

$$K_{14} = \left( \frac{z_b - z_2}{1 - z_2 \bar{z}_2} \right)^2$$

$$K_T = \sum_{m=1}^M \Gamma_m \left[ \frac{\dot{z}_m}{(z_T - z_m)^2} + \frac{\overline{\dot{z}_m}}{(z_T \bar{z}_m - 1)^2} \right]$$

$$K_{15} = i U_\infty \left(1 - \frac{1}{z_b^2}\right)$$

$$K_b = \sum_{m=1}^M \Gamma_m \left[ \frac{\dot{z}_m}{(z_b - z_m)^2} + \frac{\overline{\dot{z}_m}}{(z_b \bar{z}_m - 1)^2} \right]$$

NOTE: Since the M vortices are unattached,  $\dot{z}_m$  and  $\overline{\dot{z}_m}$  are calculated from equation (29).

Since there are more unknowns than there are equations, the system is still ill-defined. Four more equations can be gotten by imposing the Kutta condition at the point from which the vortex cores are fed. This is done by assuming that the fluid velocity relative to the cylinder at these points is zero, i.e.,  $Z_T$  and  $Z_b$  are stagnation points. By solving equation (36) for  $-u_T + iv_T$  and for  $-u_b + iv_b$ , then setting these equations equal to zero and rearranging in matrix form, the two new equations become;

$$\frac{1}{2\pi} \begin{bmatrix} 1 & -K_1 K_2 \\ -K_4 K_3 & 1 \end{bmatrix} \begin{Bmatrix} \Gamma_1 \\ \Gamma_2 \end{Bmatrix} = \begin{Bmatrix} K_1 (K_7 + \frac{K_{11}}{2\pi}) \\ K_3 (K_{15} + \frac{K_{19}}{2\pi}) \end{Bmatrix} \quad (42)$$

The  $K$ s are the same ones associated with equation (43). Though not included in equations (38) and (39) for the sake of simplicity, the above equations include the extra summation terms,  $K_{11}$  and  $K_{19}$ , necessary for the calculation if more than two vortex cores are present. To give the velocity equations (38) and (39) the same versatility, all that is necessary is to multiply these terms by  $i/2\pi$ , adding the first one to right hand side of (38) and the second one to (39). This has been done in the computer program for this model.

The next two equations are gotten by solving the first equation of (42) for  $\Gamma_1$  and the second one for  $\Gamma_2$ . Then the time derivatives,  $\dot{\Gamma}_1$  and  $\dot{\Gamma}_2$ , are taken, assuming that  $Z_T$  and  $Z_b$  are constants. Since the procedure is long and involved, but quite straight forward, only the results will be presented; see equations (43). These equations also include the terms necessary for more than two vortex cores. There is also a provision made in these equations for  $\dot{U}_\infty$  to be taken into consideration. This quantity was set to zero for the study undertaken in this



thesis, but could be utilized in future work. Note that the equations have been non-dimensionalized. This means that  $\dot{U}_\infty$  is also a non-dimensionalized quantity.

This now leaves three six unknowns,  $Z_b$ ,  $Z_T$ ,  $Z_1$ ,  $Z_2$ ,  $\bar{Z}_1$ , and  $\bar{Z}_2$  in the system of equations without a corresponding number of defining equations. The latter two unknowns can be easily handled by forming the conjugates of both sides of (40) and (41) to yield,

$$\begin{aligned} \bar{Z}_1 + (\bar{Z}_1 - \bar{Z}_T) \frac{\dot{\Gamma}_1}{\Gamma_1} &= - \frac{dW(z)}{dz} \Big|_{z=Z_1}, \\ \bar{Z}_2 + (\bar{Z}_2 - \bar{Z}_b) \frac{\dot{\Gamma}_1}{\Gamma_1} &= - \frac{dW(z)}{dz} \Big|_{z=Z_2}. \end{aligned} \quad (44)$$

as mentioned earlier,  $Z_b$  and  $Z_T$  are considered constants. This is an assumption based on experimental observations at higher laminar Reynolds numbers. The origins of these feeding sheets are in reality functions of time, but their motions are so small that the assumption seems justified. Besides, to consider  $\dot{Z}_b$  and  $\dot{Z}_T$  anything but zero, would have made the derivation of (43) at least another order of magnitude more tedious. This may, however, prove to be a necessary future sophistication of the model. As a result, these two locations are taken from experimental data to be about 50 degrees either side of the cylinder's downstream axis; i.e.,  $\theta_T = 50$  and  $\theta_b = -50$  degrees.

No mention thus far has been made concerning the propagation aspects of this solution, however since time dependent solutions generally imply that starting and ending conditions are necessary, it is well to discuss these now with respect to  $Z_1$  and  $Z_2$ . With the assignment of any values to these two parameters, there have been enough equations derived and assumptions made to have the proper balance between unknowns

and defining equations to describe the system at any given instant. Not just any value of  $Z_1$  and  $Z_2$  is desirable however, since this will not give even an approximate picture of core growth and drag buildup. Bryson [29], through certain mathematical considerations, found that the path line of the vortex cores, as they grow and move away from the cylinder, is unique in the sense that for any given feeding sheet origin,  $Z_T$  or  $Z_b$ , there can be only one path, per vortex, followed as time progresses. Without going into the details of his work, he also found that the feeding points, like the Föppl curve points,<sup>16</sup> are mathematical equilibrium positions for symmetric vortex pairs. On the basis of these findings, it is also determined that cores can leave the cylinder's surface only in a direction 30 degrees downstream from the tangent to the cylinder at the sheet origin. Bryson arbitrarily selected the starting values for  $Z_1$  and  $Z_2$  as a distance of  $0.05c$  away from the origins along these respective preferred lines of departure. This practice was continued in this study even though the model can handle asymmetry and more than two vortex cores. It was felt that these are good assumptions for an initial study of asymmetry.

Except for determining when and how the vortex sheets are cut, there are no more assumptions to be made in completing the solution. The procedure for solving the previously developed equations and the development of the  $(F_D + iF_L)$  equation are not complicated and follow next.

---

<sup>16</sup>The Föppl curve is a symmetric curve about the downstream X-axis originating at the rear stagnation point, on which a vortex pair can be symmetrically located such that they will maintain their positions. This is much the condition that exists at Reynolds numbers below about 50. See [6, p. 223].

$$\begin{bmatrix}
 \frac{1}{2\pi} & -\frac{K_1 K_2}{2\pi} & -K_5 K_{12} & -K_6 K_{12} & -\frac{\Gamma_2}{2\pi} K_1 K_9 & -\frac{\Gamma_2}{2\pi} K_1 K_{10} \\
 -\frac{K_3 K_4}{2\pi} & \frac{1}{2\pi} & -\frac{\Gamma_1}{2\pi} K_3 K_{17} & -\frac{\Gamma_1}{2\pi} K_3 K_{18} & -K_{13} K_{20} & -K_{14} K_{20} \\
 \frac{z_1 - \bar{z}_1}{\Gamma_1} & 0 & 1 & 0 & 0 & 0 \\
 \frac{\bar{z}_1 - z_1}{\Gamma_1} & 0 & 0 & 1 & 0 & 0 \\
 0 & \frac{z_2 - \bar{z}_2}{\Gamma_2} & 0 & 0 & 1 & 0 \\
 0 & \frac{\bar{z}_2 - z_2}{\Gamma_2} & 0 & 0 & 0 & 1
 \end{bmatrix}
 =
 \begin{bmatrix}
 \dot{\Gamma}_1 & \dot{\Gamma}_2 & \dot{z}_1 & \dot{\bar{z}}_1 & \dot{z}_2 & \dot{\bar{z}}_2
 \end{bmatrix}
 =
 \begin{bmatrix}
 K_1 \left( K_8 + \frac{K_7}{2\pi} \right) & K_3 \left( K_{16} + \frac{K_6}{2\pi} \right) & u_1 + i v_1 & u_1 - i v_1 & u_2 + i v_2 & u_2 - i v_2
 \end{bmatrix}
 \quad (45)$$

Equations (40), (41), (43), and (44) can be rearranged and combined in a straight forward manner for the matrix equation (45). Both this matrix equation and equation (42) are solved using the partitioned matrix technique as given in Fox [39, p. 121]. Briefly, this involves breaking up the basic matrix equation into its real and imaginary parts and forming a new equation whose matrices are twice the order of the original. To describe the technique, suppose the original equation is;

$$[A] \{B\} = \{C\},$$

where  $[A]$  is a square matrix of order  $j$ , while  $\{B\}$ , and  $\{C\}$  are column matrices with  $j$  elements each. Since all the elements of  $A$ ,  $B$ , and  $C$  are assumed to be complex, the matrices can be written as;

$$\begin{aligned} [A] &= [A_R] + i [A_I], \\ \{B\} &= \{B_R\} + i \{B_I\}, \\ \{C\} &= \{C_R\} + i \{C_I\}. \end{aligned}$$

Substituting these expressions back into the original equation, results in

$$([A_R] + i [A_I]) (\{B_R\} + i \{B_I\}) = (\{C_R\} + i \{C_I\}).$$

Carrying out the indicated multiplication, and separating the real and the imaginary parts of both sides, yields

$$[A_R] \{B_R\} - [A_I] \{B_I\} = \{C_R\},$$

and,

$$[A_I] \{B_R\} + [A_R] \{B_I\} = \{C_I\}.$$

These two equations are combined to form the new matrix equation:

$$\begin{bmatrix} [A_R] & -[A_I] \\ [A_I] & [A_R] \end{bmatrix} \begin{Bmatrix} \{B_R\} \\ \{B_I\} \end{Bmatrix} = \begin{Bmatrix} \{C_R\} \\ \{C_I\} \end{Bmatrix}. \quad (46)$$

Since there are no imaginary numbers involved, this equation is solved by existing numerical methods, i.e., the inverse of the coefficient matrix premultiplies the constant matrix to yield the unknown values of  $\{B\}$ . In the computer program for this model, the inverse is found using a standard inversion subroutine with row pivoting.

The propagation aspect of the solution is handled in the program through the use of a simple Runge-Kutta integration technique [40, p. 232] by finding the subsequent vortex positions, after a  $\Delta t$  time step, from equations (40) and (41). There are, of course, more sophisticated techniques, but in view of the parameters assumed, it is felt that the increased accuracy is not necessary at this point. In fact, there is not really that much difference in results if a straight Eulerian approximation is used.

The final relation to be developed is that for  $C_D + iC_L$ . This is done by completing the derivation of equation (30), or more specifically by finding the appropriate solution for equation (33). For this case, in which the cores are fed by a single feeding sheet originating at a point, Sarpkaya, [33], and [35], has previously derived the necessary equation, so the details will not be given here. The result, in non-dimensional form and adapted to this model is:

$$\begin{aligned}
 C_D + iC_L = & 2\pi \dot{U}_\infty + i \left[ \dot{\Gamma}_1 \left( z_1 - \frac{1}{z_1} \right) + \dot{\Gamma}_2 \left( z_2 - \frac{1}{z_2} \right) \right] \\
 & + i \left[ \dot{\Gamma}_1 (\dot{z}_1 - \dot{z}_{i1}) + \dot{\Gamma}_2 (\dot{z}_2 - \dot{z}_{i2}) \right] \\
 & + i \sum_{m=1}^M \dot{\Gamma}_m \left[ u_m + i v_m - (u_{im} + i v_{im}) \right] .
 \end{aligned} \tag{47}$$



The image velocities for the free and attached vortices are both calculated, in a sense, using equation (37). However, where the results of equation (29) are used directly for the vortices, the results of solving matrix equation (45) must be used for the attached vortices. The modification to equation (37), used for this purpose is; for the image of vortex 1,

$$\dot{Z}_{i1} = - \frac{\dot{\bar{Z}}_1}{\bar{Z}_1^2}$$

and for that of vortex 2,

$$\dot{Z}_{i2} = - \frac{\dot{\bar{Z}}_2}{\bar{Z}_2^2} . \quad (48)$$

The computer program written for this model is listed in its entirety in the last portion of this thesis. It is written in FORTRAN IV as applied to the IBM 360/67 digital computer at the Naval Postgraduate School. In general, the calculations are carried out using sixteen digit numbers. The typical run, describing the impulsively started flow up to  $\frac{U_\infty t}{c} \approx 15.0$ , requires less than three minutes of computer execution time. Provided that the initial starting points,  $Z_1$  and  $Z_2$ , are accurately defined, the solution appears to be stable and well behaved. The stability problem was previously discussed in connection with the vortex path line being unique. If the initial estimate for  $Z_1$  and  $Z_2$  are even slightly off, the solution technique attempts to return to the path, but as a consequence there may be some abnormally large absolute values for  $\dot{\Gamma}_1$ ,  $\dot{\Gamma}_2$ ,  $\dot{Z}_1$ , and  $\dot{Z}_2$ . To increase the stability, smaller time steps are taken at the start and just after a vortex has been shed and a new vortex starts to grow. The normal time step is 0.05, while this reduced time step is 0.02. The program will accept as many as twenty vortices before it terminates execution.



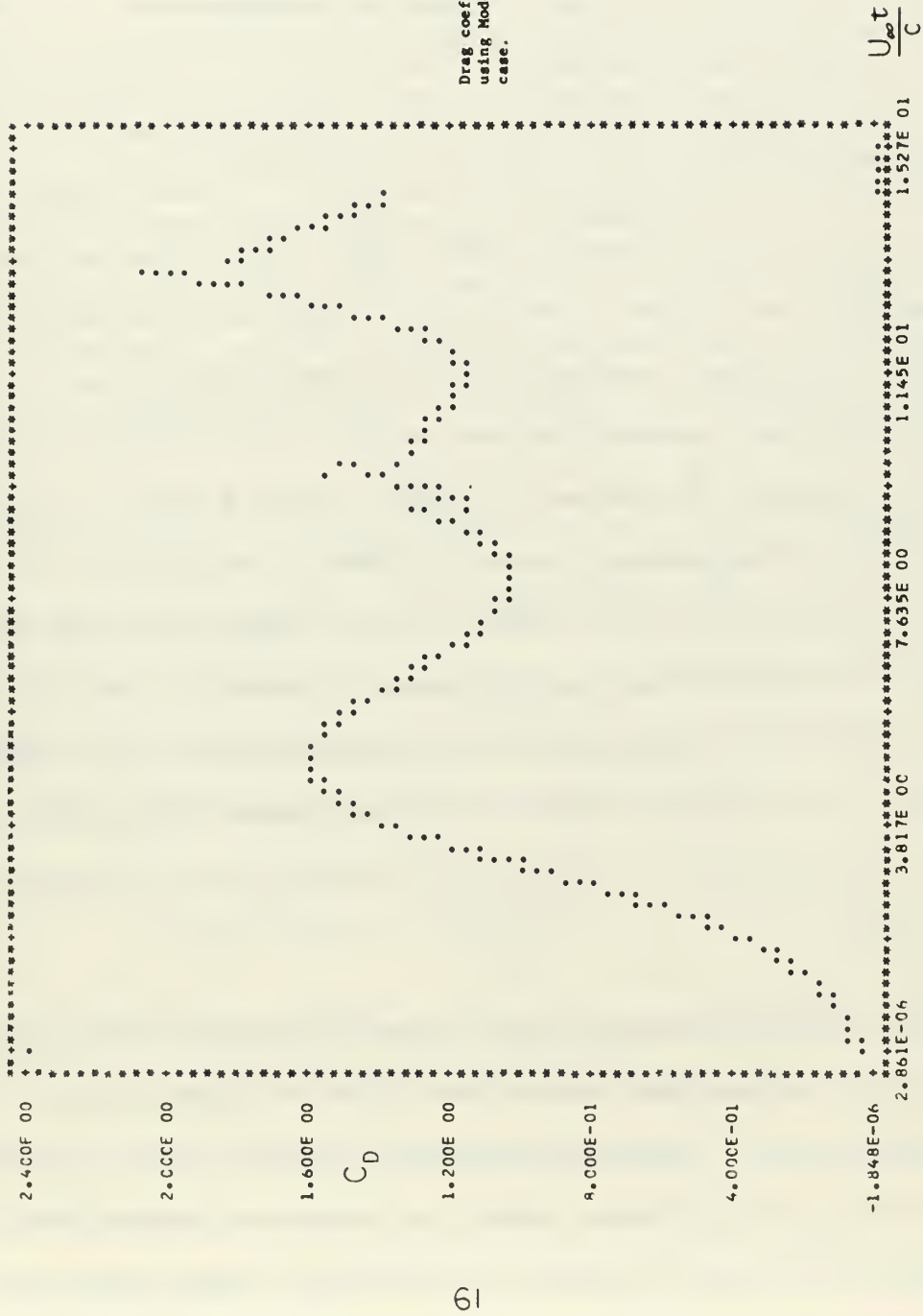


Figure 13  
 Drag coefficient curve calculated  
 using Model A for an asymmetric  
 case.

Since anyone desiring to utilize this program must become intimately familiar with its internal workings, it is felt that any further discussion is unnecessary here. There is a brief, but more detailed description in Appendix A.

It was possible, through the use of this program, to generate a reasonably good drag curve using asymmetric considerations. To start with, if no shedding was allowed, it was found that by multiplying the value of  $\int_1$ , during each time step, from equation (42) by 1.05, prior to its use in equation (45), that the value of  $\dot{\int}_1$  never changed sign. It did however, peak at about the same  $\frac{U_\infty t}{c}$  that it had previously (no asymmetry), but instead of decreasing to zero and subsequently changing sign; it decreased somewhat and then increased beyond bound. The drag curve followed somewhat the same pattern. By arbitrarily cutting the vortex sheet at the minimum  $\dot{\int}_n$  values, the drag curve in Figure 13 was generated. The computer listing for Model A, though meant to be modified for other uses, is in fact, the same program that produced this curve. It is realized that the amount of asymmetry imposed is much too large, but is an illustration of the possibilities. A good beginning point for future work, would be with von Kármán's stability conditions or to investigate the works done by Roshko [19] and Bearman [27].

#### D. MODEL B

Since this model is an attempt to approximate the vortex sheets generated by boundary layer separations, it is much more sensitive to the placement of the nascent vortices than is Model A to the location of the feeding sheet origins. Hence, the problem of mathematically describing vortex sheet formation is more obvious. This model has a distinct advantage over the other, in that it is not necessary to

incorporate any assumptions into the derivation of the basic equations of motion that take the place of matrix equation (45). The assumptions are present, however, in the determination of the strength and initial nascent vortex positions. Probably the most important single advantage of this model, is that in general, once the separation points and vortex strengths have been determined, the vortex sheets will roll up to form vortex cores, taking care of the vorticity transport and diffusion automatically. To discuss these aspects further will require the development of the applicable equations, so this follows next.

Since the nascent vortex is assumed to gain its total strength during the time step in which it is born, equation (29) can be used to determine its convective velocity. It is repeated here for convenience.

$$-u + iV = U_{\infty} \left( \frac{c^2}{Z^2} - 1 \right) + \frac{i}{2\pi} \left[ \sum_{n=1}^N \frac{\Gamma_n}{Z - Z_n} - \sum_{n=1}^N \frac{\Gamma_n}{Z - \frac{c^2}{\bar{Z}_n}} \right] \quad (29) \text{ Repeat}$$

The vortex convective velocity, as indicated in the initial discussion of equation (29), is calculated by setting  $Z = Z_n$  and ignoring the term in the first summation that has the denominator equal to zero. The velocity of the image vortex can still be calculated from

$$u_{in} + iV_{in} = \frac{-u_n + iV_n}{\bar{Z}_n^2} \quad (37) \text{ Repeat}$$

The drag and lift coefficients are again calculated from equation (30), however, this time, some liberties can be taken with its use. Again, since the nascent vortex is born during one time step, a part of the effect of the unsteady portion of (30), more specifically parts of equation (33), can be assumed negligible. In fact, a study of the results of [41] indicates that the algebraic sum of the values of the terms concerned with feeding and growth of the vortices actually only account

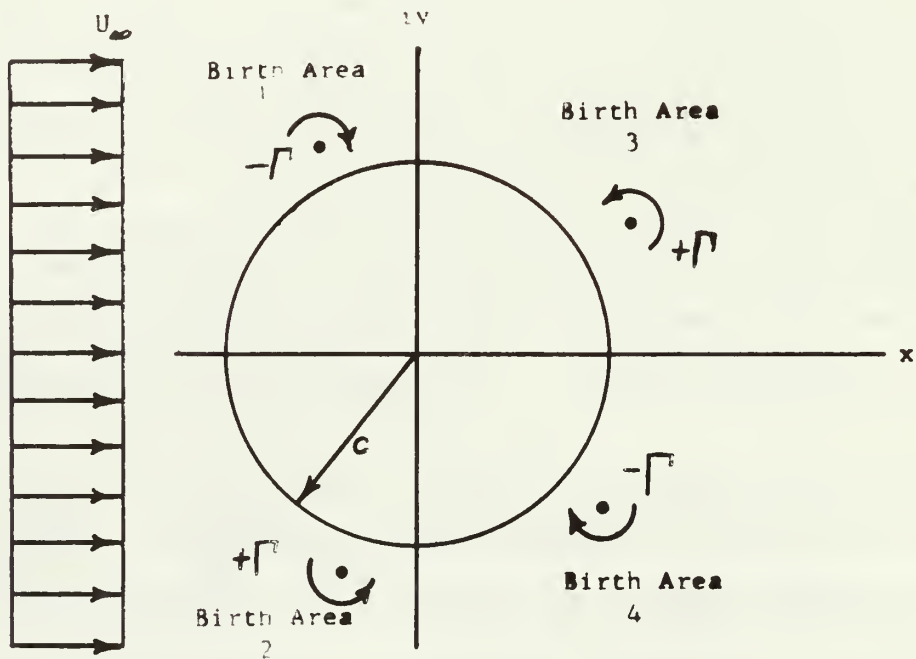


Figure 14 Configuration of Model B Showing the Birth Areas and the Rotation Direction of the Vortices Born Therein.

for about three percent of the drag. The two terms being discussed are equivalent to the terms inside the first and second sets of brackets on the right hand side of equation (47). Since in this case  $M = N$ , the rest of the terms become applicable to this model. Therefore,

$$C_D + iC_L = 2\pi \dot{U}_\infty + i \sum_{n=1}^N \Gamma_n \left[ u_n + i v_n - (u_{in} + i v_{in}) \right] \cdot \quad (49)$$

The system of basic equations is now complete, and like Model A, it has been programmed to allow asymmetry. The programming of equation (49) does not include the  $\dot{U}_\infty$  term since during the study conducted for this thesis, only a uniform, steady cross-flow of  $U_\infty = 1$  was considered. It is simple enough to include this term, but then the deleted terms may become more important such that some kind of determination might have to be made for them. It would be hoped that by the time these terms would be needed, the uniform flow problem would be solved and its results would be used to make this determination.

This program is also written in FORTRAN IV, but unlike that of Model A, its calculation is carried out in only seven digits. The program, as written, will allow as many as one hundred nascent vortices to be born in any of the four birth areas during any given run. A run, which goes through the complete 100 time steps allowed, requires approximately 30 minutes of computer execution time. Since the propagation aspects of the model are handled by Eulerian approximations, this could have serious error implications. However, since an approximate solution is all that is presently desired, it is felt that these errors are acceptable. The large execution time is due primarily to the large number of vortices involved in the evaluation of (29), particularly at high  $\frac{U_\infty t}{c}$ .



This must be done for each vortex, during each time step. The model also has the option of considering only the primary birth areas, 1 and 2, rather than all four.

Before discussing some of the output from this model, the general method of determining vortex strengths must be considered. It has been shown by Fage and Johansen [42] that in the absence of back-flow and in a steady flow situation, the amount of vorticity leaving a separation zone can be accurately approximated by

$$\left| \frac{\partial \Gamma}{\partial t} \right| = |0.5 V^2| , \quad (50)$$

where  $V$  is the fluid velocity just outside the boundary layer at the point of separation. Thus, making the time steps,  $\Delta t$ , small enough, the nascent vortex strength can be given by

$$|\Gamma_n| = |0.5 V^2 \Delta t| \quad . \quad (51)$$

The key problem now is to decide where and how to measure  $V$  and where the nascent vortex of this strength is placed. The four birth area model purports to take care of back-flow through the use of the secondary birth areas, 3 and 4. Now since the maximum velocities on or near the cylinder's surface in these regions are very small as compared to the velocities in the primary regions, the effect of making some assumptions here is not too critical. The assumption made in most of the computer runs was that the maximum back-flow velocity on the cylinder's surface in that birth area was used in equation (51). From experimental studies, these back-flow vortices appear to separate at points located



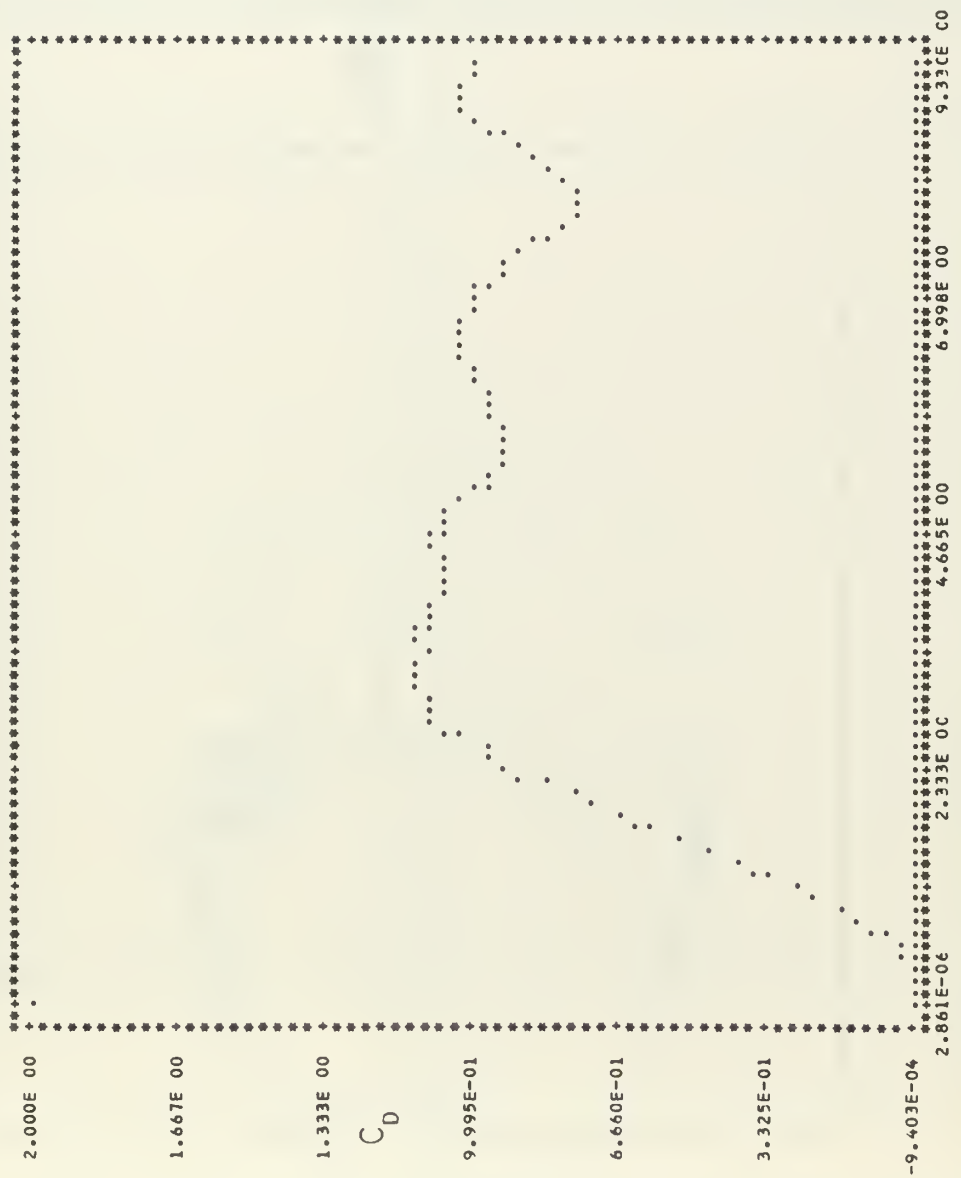


Figure 15

Drag coefficient curve generated  
by Model B for an asymmetric case.

Figure 16  
Wake development corresponding  
to  $\frac{V_{\text{tot}}}{U} = 1.8$  in Figure 15.

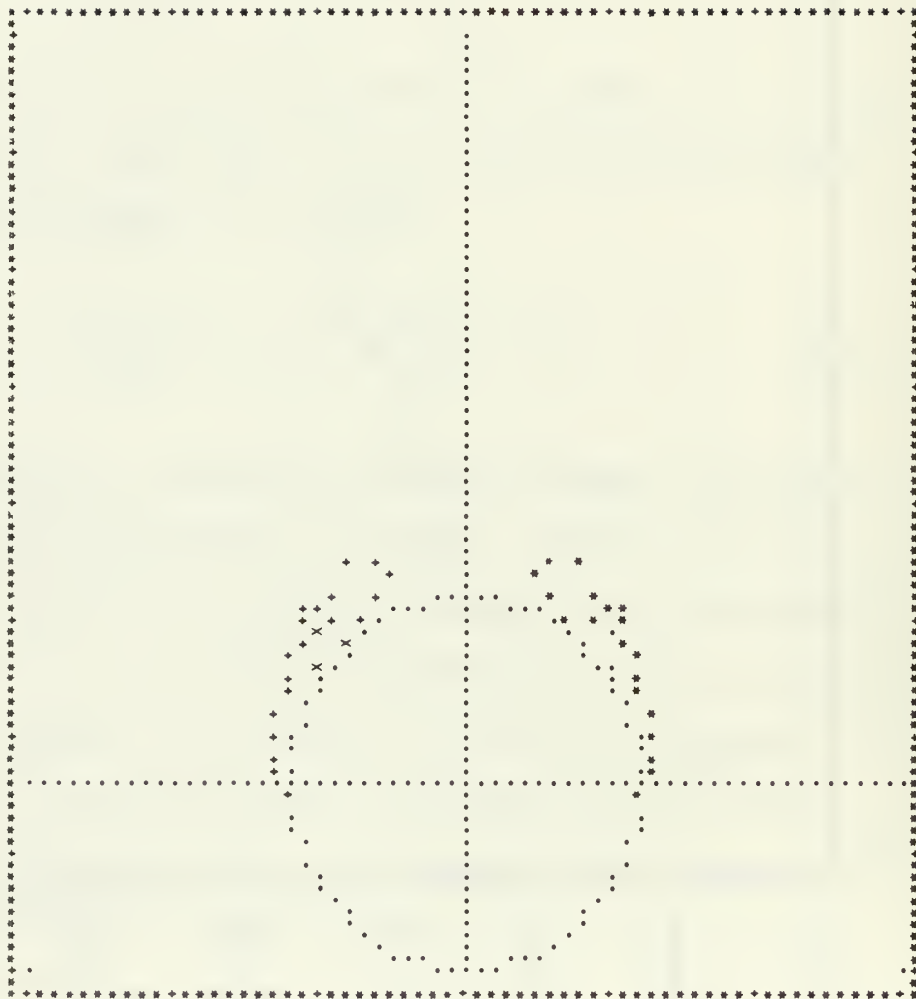
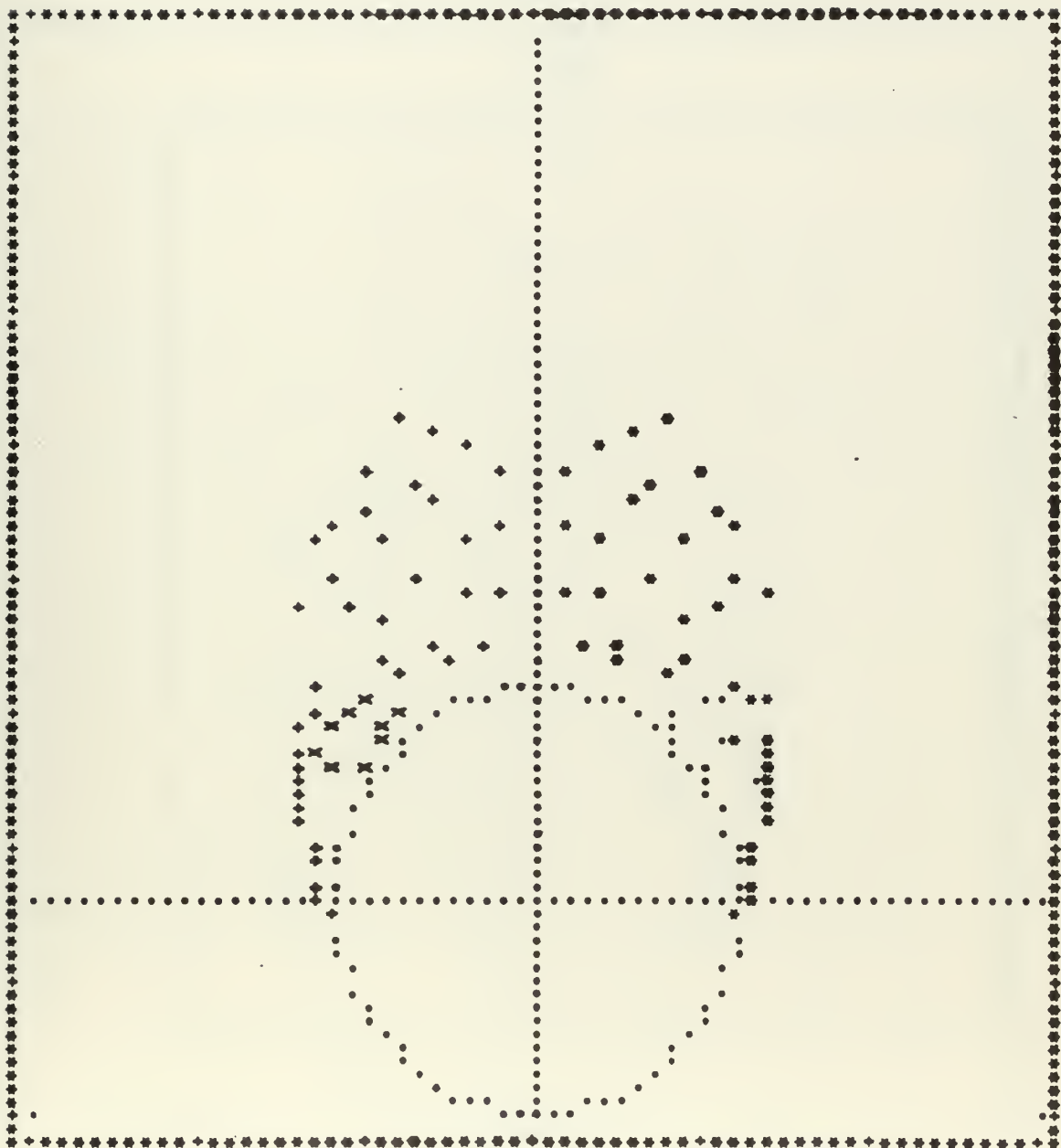


Figure 17  
Wake development corresponding  
to  $\frac{U_0 t}{c} = 4.6$  in Figure 15.



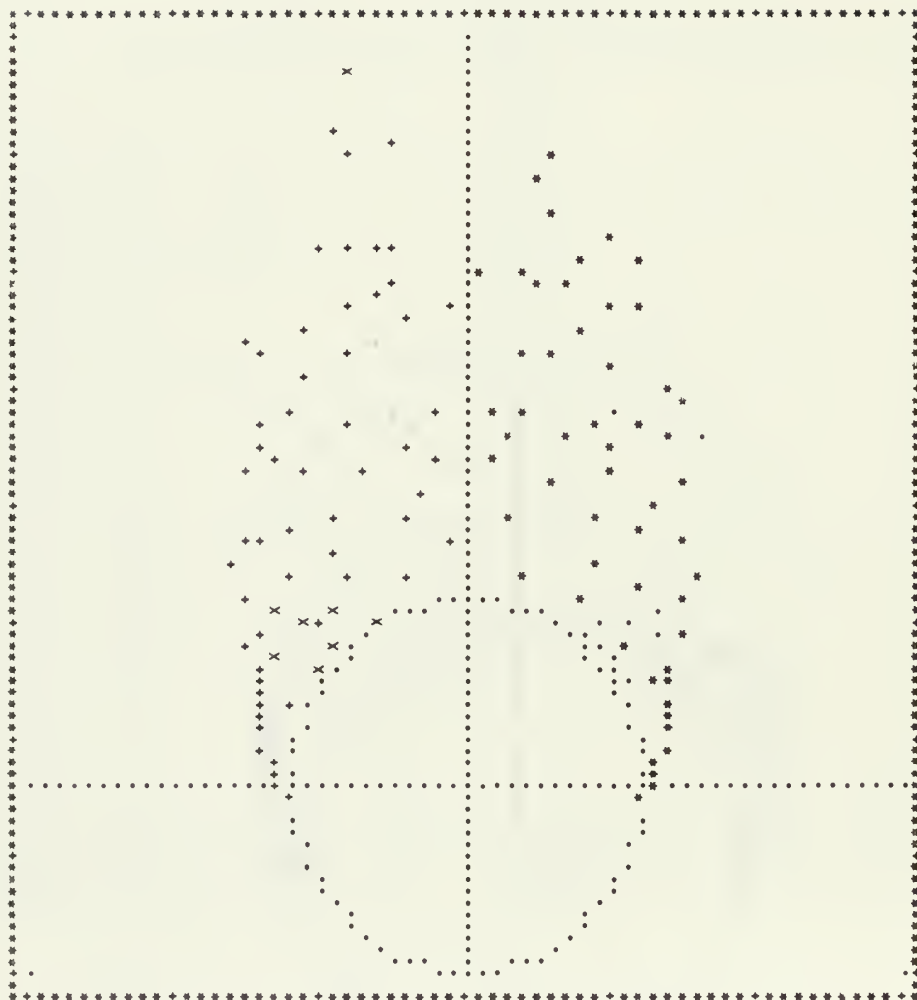
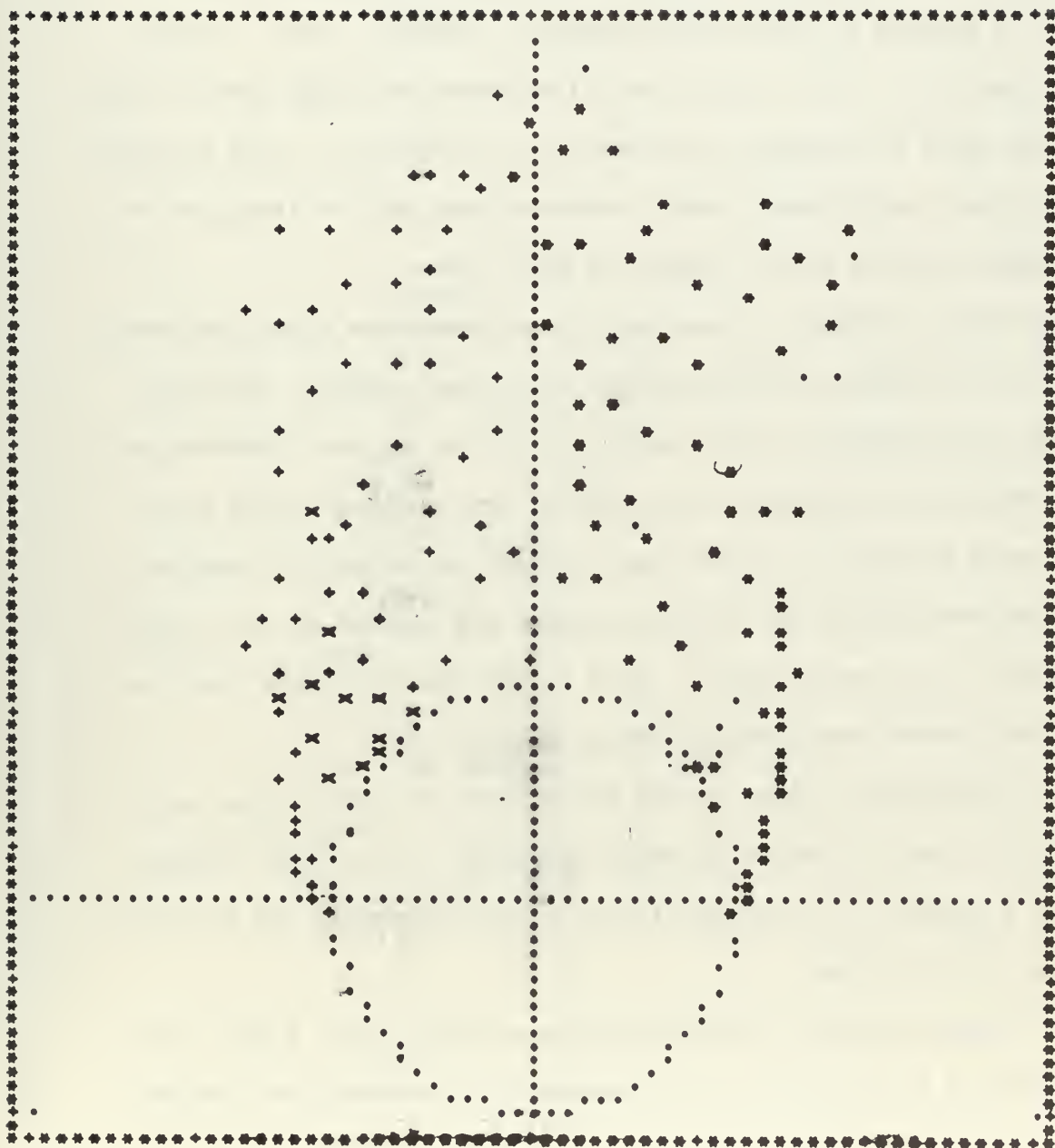


Figure 18  
Wake development corresponding  
to  $\frac{U}{c} = 7.4$  in Figure 15.

Figure 19  
Wake development corresponding  
to  $\frac{U_c t}{C} = 9.3$  in Figure 15.



about  $\pm 55$  degrees from the positive x-axis on the cylinder's surface; hence, these are the assumed angles for the model. Instead of placing them on the surface, however, the model was generally programmed to place them at about 0.01c. This still leaves the problem of placing the primary nascent vortices; to the author's knowledge, no truly satisfactory method does exist. The drag curves, and flow patterns shown in the figures of this subsection were all generated using arbitrarily selected placement locations. The maximum velocity found on cylinder's surface in these birth areas was, however, used to compute the strength from (51). For all the birth areas, the sign given to the resultant value of strength is as depicted in Figure 14. This sign convention comes from boundary layer considerations and the direction of the maximum velocity in the respective birth area.

In order to prevent the extremely high convective velocities that can occur if and when two vortices get too close together, the model provides for coalescence and cancellation of the vortices depending on their comparative strengths. The vortices are combined if the algebraic sum is not zero, in which case they are cancelled, by creating a new vortex having that sum for its strength and located at the "center of gravity" of the two vortices. With a great many vortices this procedure can consume much computer execution time.

As in the case of Model A, any future user of this program would of necessity have to have an intimate knowledge of its inner workings. Appendix A contains a brief description of the parameters and the major sections of the program.

This model was used to test a great many ideas using a great many runs. Figures 15 through 19 are presented to illustrate the kind and



type of output the model will generate. The program included with this thesis generated these figures. The primary vortices are injected into the stream at points whose angles from the positive x-axis are  $\pm 95$  degrees, and are located  $0.045c$  from the cylinder's surface.

#### IV. DISCUSSION OF RESULTS AND CONCLUSIONS

The primary result of this study is that reasonably representative drag coefficient curves can be generated using the two mathematical models developed. This is particularly true in the case of Model B, where the curves can be generated for both symmetric and asymmetric wake development. Figures 15 through 19 show the drag curve and wake development for an asymmetric wake case, while Figures 20 through 24 show the symmetric wake case. The assumptions involved only the placement locations of the nascent vortices and the coalescence distance used to prevent abnormally high velocities if two nascent vortices come too close together. The symmetric wake case was generated by making the same assumptions for placement location as in the asymmetric case, however, the coalescence distance was increased. Where this distance was  $0.06c$  for asymmetry, in the symmetric case it was  $0.08c$ . These values were arbitrarily selected.

In the case of Model B, the curve in Figure 15 was generated by assuming asymmetric generation of vorticity and assuming the vortex sheet is cut, freeing the core, when  $\left| \dot{\Gamma}_n \right|$  reached its first post-peak minimum. The amount of asymmetry and the time of sheet cutting is loosely based on the results of Sarpkaya's experimental work [24].

Aside from the above results, numerous computer runs were made in an effort to develop a method by which the separation characteristics could be analytically described. Though these attempts were not entirely successful, some information was gained about the character of the vortex sheet origin and the requirements necessary to produce a reasonably realistic drag curve and wake structure. Of the two models,

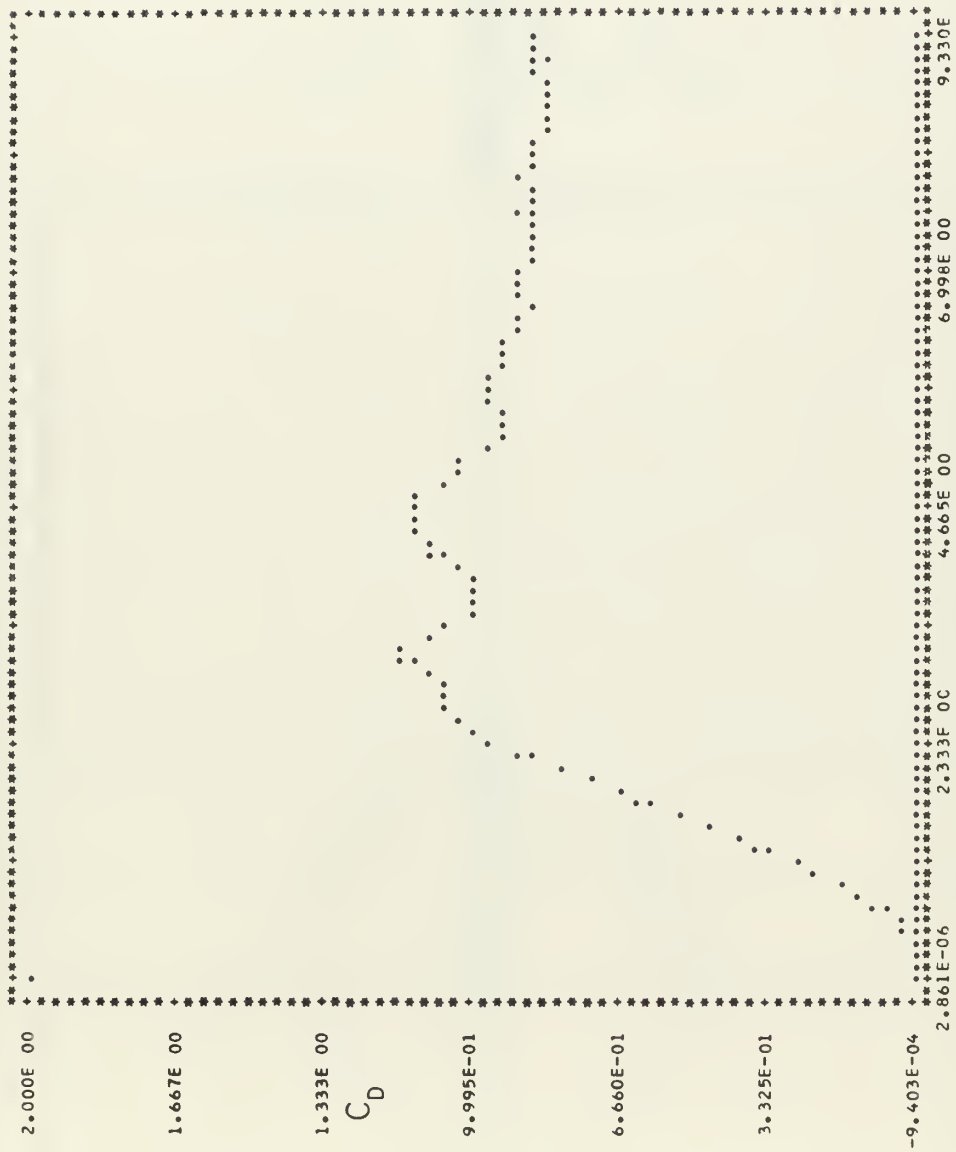


Figure 20  
 Drag coefficient curve generated  
 by Model B for a symmetric case.

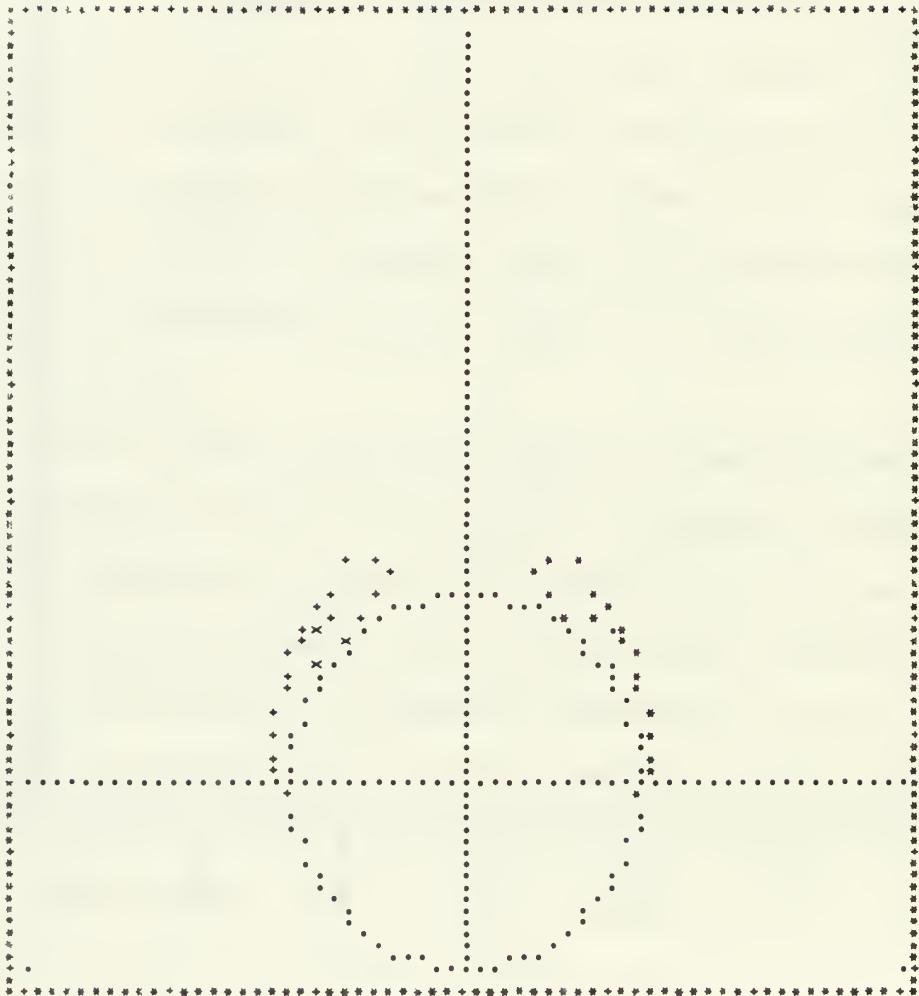


Figure 21  
Wake development corresponding  
to  $\frac{U_{\infty}^*}{C} = 1.8$  in Figure 20.

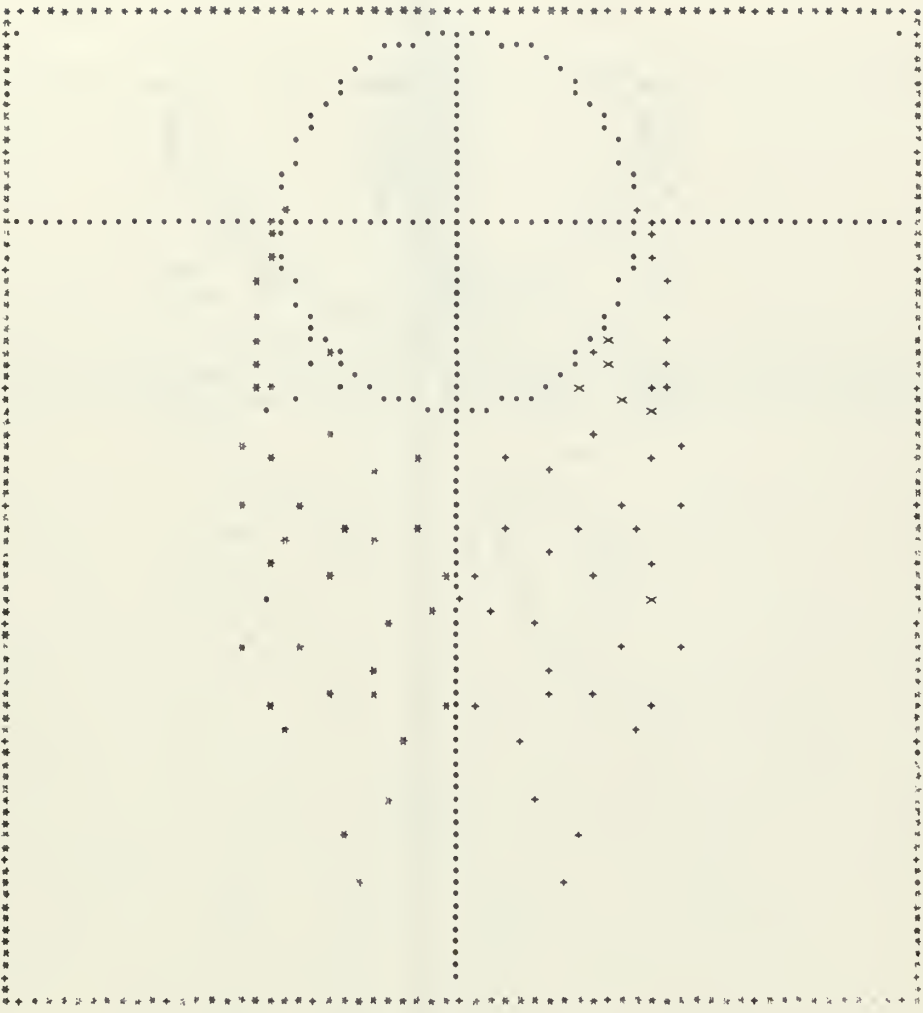


Figure 23  
Wake development corresponding  
to  $U_c^+ = 7.4$  in Figure 20.

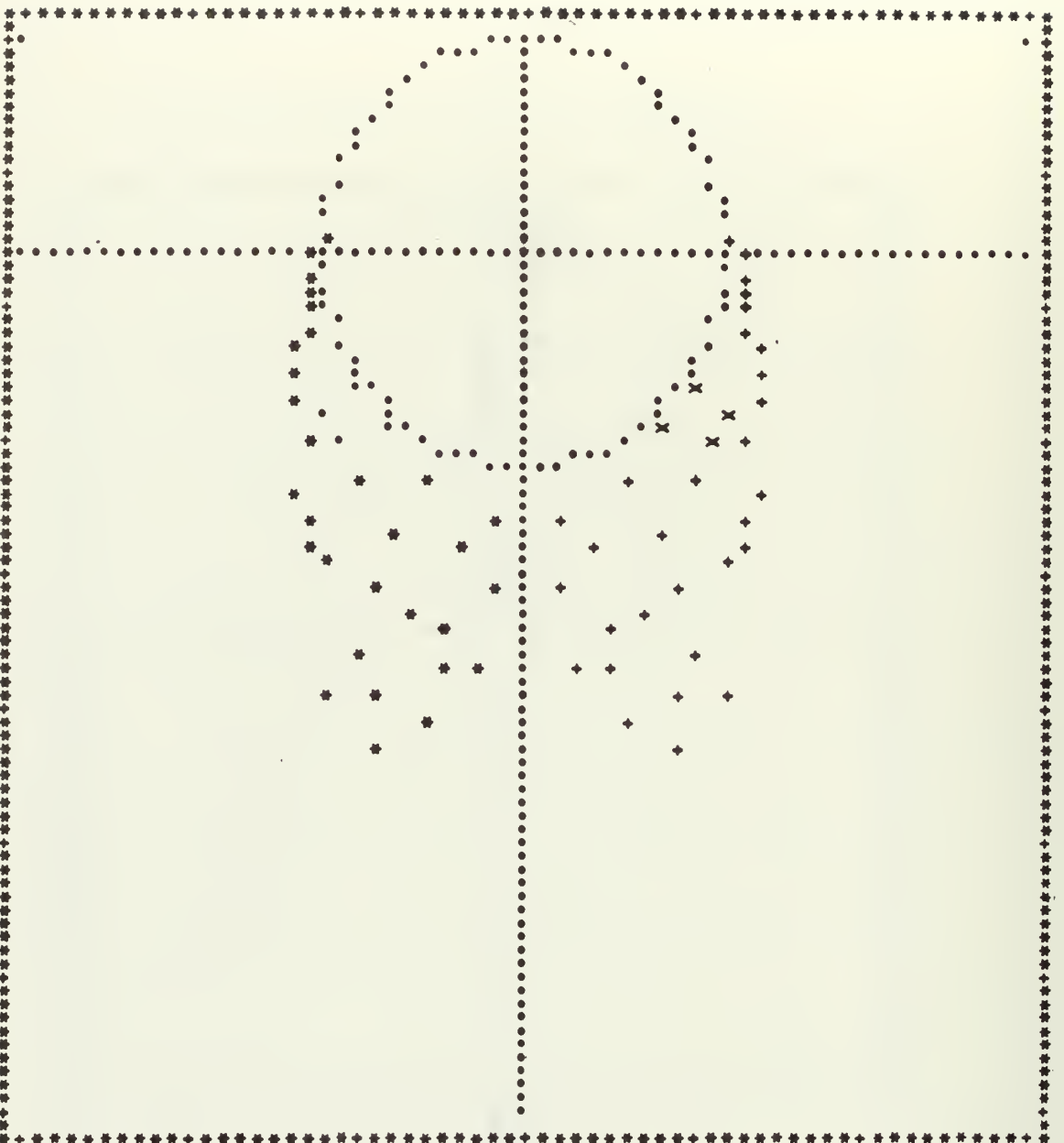
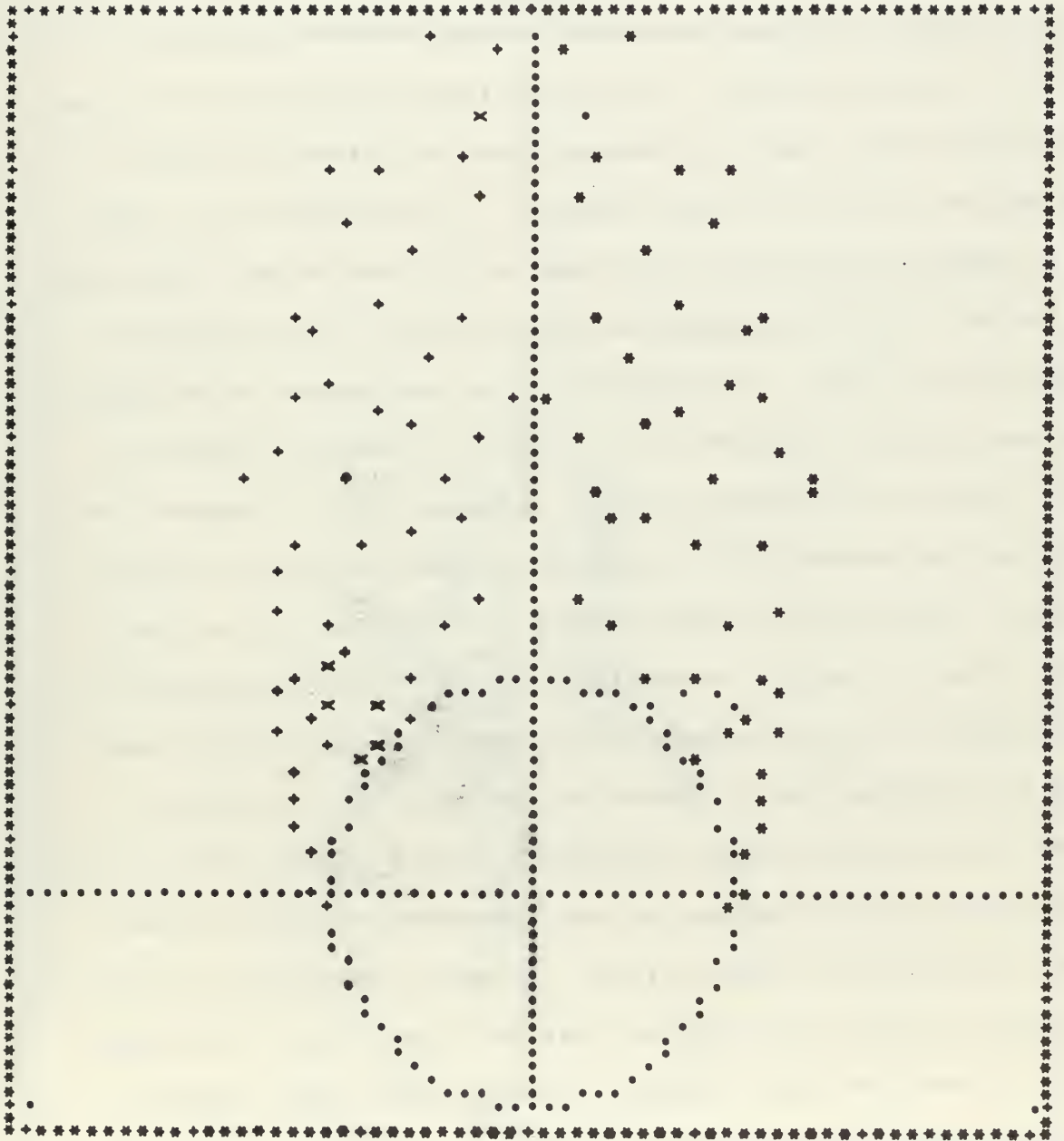


Figure 22  
Wake development corresponding  
to  $\frac{U_0 t}{c} = 4.6$  in Figure 20.



Figure 24  
Wake development corresponding  
to  $\frac{U_{\infty} L}{c} = 9.3$  in Figure 20.

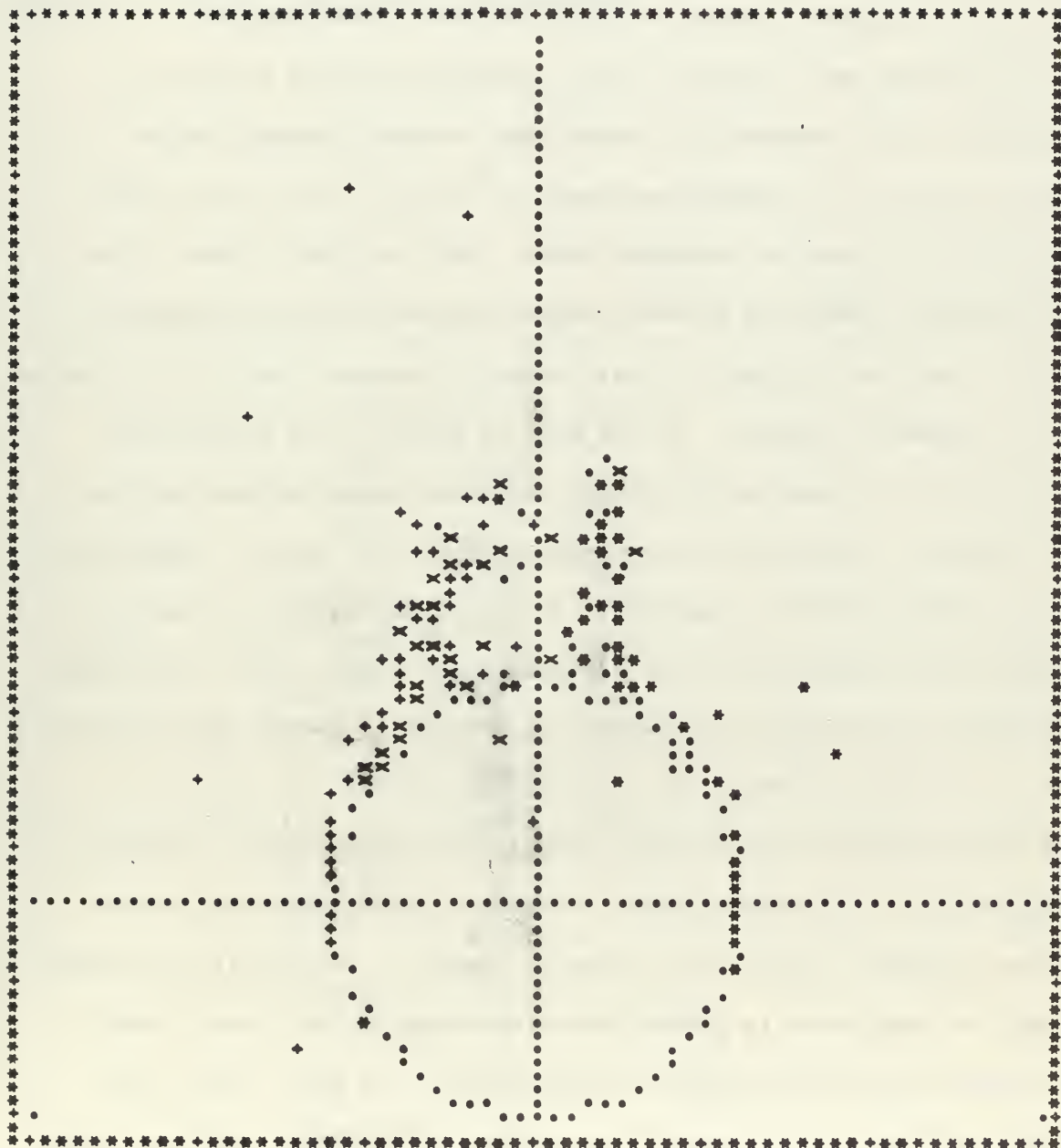


Model B was the most illuminating since the concept of a string of small strength vortices is more nearly like nature than is the concept upon which Model A is based. As a result, Model B was utilized more extensively in this study. It is for this reason then, that the majority of the remaining remarks in this section will be concerned with results from this model.

Of the various factors that go into the final description of the wake and computation of a drag curve, it was found that the location at which the nascent vortices are placed in Model B is by far the most critical parameter involved. Of the two items which determine the location of the vortex, angle and distance from the cylinder's surface, it appears that the latter is more important. It was observed that there was a tendency for the primary vortices to "hug" the surface (Figure 25), all the way to the rear stagnation point, if their initial placement distance was too small. "Too small" in this case appears to mean less than about  $0.03c$ . In Figure 25, the nascent vortices were placed at  $0.01c$  away from the cylinder's surface, at angles of  $\pm 95$  degrees. Increasing or decreasing  $\left| \Gamma_n \right|$  did not seem to have much effect on this tendency. Changing the secondary vortex birth location, for a fixed primary location, did not prevent this "hugging," nor did it appreciably change the roll-up tendency of the primary vortices if they were being shed reasonably well. Though the resulting wake formation in Figure 25 is not that desired for Reynolds numbers less than about  $2 \times 10^5$ , there is a striking resemblance to real flow patterns evident in the super critical Reynolds number region. By making approximately 50 computer runs in which only the birth location of the primary vortices was varied, it was found that a distance of about  $0.045c$  and an angle of about  $\pm 95$  degrees from the rear stagnation point, produced the most

Figure 25

Wake development showing "hugging"  
due to vortex placement distance  
being too close to cylinder's  
surface.



reasonable flow patterns and drag curve; Figures 15 through 19. This shedding angle is comparable with the observed angle of separation of about 98 degrees (measured in the same manner). The distance from the cylinder's surface however, is about twice the value predicted by the Blasius series solution of the boundary layer equations. It is suggested, therefore, that any future work in this area might well begin with a comprehensive study of the boundary layer transition region. A consideration of these regions above flat plates could be the starting point since the added problem of body curvature is not present.

It does not seem possible, after studying the works of many investigators, that Thompson [13] could have produced asymmetry with equations that are in themselves symmetric, were it not for the very real problem of computer round-off error. The fact that Figure 15 exhibits asymmetry would be of deep concern had Abernathy and Kronauer [10] not found that strings of small strength vortices would in fact roll-up in an asymmetric manner. In the case of Model B, the predominate errors are due to assuming Eulerian propagation approximations and not from round-off. The Eulerian approximations are, of course, symmetric, so it is assumed that the asymmetry is in fact due to the interactions Abernathy and Kronauer observed. Interestingly enough, when using Model B asymmetry was not always produced, which leads to another conclusion; there is a critical combination of separation points and spacing distance between sheets to cause the necessary interaction that forms the Kármán street. On the other hand, reasonable drag coefficient curves could be generated without any asymmetry present. The overall conclusion is that the drag curve is predominately influenced by the rate of vorticity creation and its subsequent diffusion into the wake. This then, points right back to the over-riding problem of boundary layer separation.

Since Model A feeds large vortex cores rather than creating vortex sheets, it would appear this model is better suited for describing the flow at Reynolds numbers less than about 50. By increasing the angles of the sheet origin, the drag curve peak can be increased to almost any desired value. In order to make the model applicable to the higher Reynolds number range, it will be necessary to find some scientifically based method of shedding these cores. The stability criterion of von Kármán and others may provide the answers.



## APPENDIX A

### A. DESCRIPTION OF COMPUTER PROGRAM FOR MODEL A

The complete program for this model includes a primary or main program with seven subroutines that accompany it. There is one other subroutine that is called that is not part of the listing included with this thesis. The subroutine is PLOTP and is called from the resident subroutine library of the Naval Postgraduate School Computing Center. The subroutine is used to produce printer plots, such as Figures 15 through 19, instead of using the CALCOMP continuous line plotters as output, so it is not critical to the actual program calculations. The curve plotting subroutines or procedures of other systems could be easily substituted for this one.

At the beginning of the main program and each subroutine is a short series of comment cards that indicate the purpose of the program and generally the parameters used therein. In general, the same notation, in FORTRAN format, is used in the program as was used to develop the equations in Section III(c); for example  $K_1$  in equation (43) is coded as K1, or  $\bar{Z}_1$  is coded as Z1B. Each computational section of the main program is preceded by comment cards indicating what computations that section is performing.

Since there is no on-line function for extracting the imaginary part of a double precision complex number in the IBM version of FORTRAN IV, EQUIVALENCE statements had to be used to recover these values.

It is assumed that the reader already has a working knowledge of FORTRAN coding techniques so that a definition list of the various parameter names used in the program will be sufficient guide for future use.



The need for understanding the program is brought about by the fact that in order to study vortex sheet cutting procedures, the logic of the coding will have to be changed each time a different procedure is used. The section of this thesis entitled Computer Output, contains several pages of output that are to be used as trial run checks for a new program deck punched from the program listing.

The type specification and precision of the following parameters is clearly indicated in the first few statements of the program, so there is no need for repeating it here. All arrays are stored in vector form, i.e., the values of the array elements are stored one column following another, going from left to right in the array.

If a parameter is not found in the following list (equation parameters described above are not included) but found in the program, then it is a dummy parameter used for intermediate operations only and therefore has no special significance as compared to those listed.

#### B. DEFINITION OF PARAMETERS

AA(144)	Vector containing the partitioned matrix elements.
AC(12)	Vector containing the partitioned elements of the right hand side of equation (45). First six elements contain the real parts, the second six the imaginary parts.
AG(12)	Vector containing the partitioned elements of the unknowns in equation (45).
CDCL(400)	Vector containing the lift and drag coefficient values for each time step.
CV(20)	Vector containing the free vortex velocities; corresponds to ZF(20) and GF(20).
DG1(401)	Contains $\dot{\Gamma}_1$ for each time step.
DG2(401)	Contains $\dot{\Gamma}_2$ for each time step.

DG1MAX DG2MAX DG1MIN DG2MIN	Contains the values of the maximum and minimum $\dot{\Gamma}_1$ and $\dot{\Gamma}_2$ for a run; used to determine when to cut the vortex sheets.
DT	Contains value of $\Delta t$ ; time step size.
DUDT	$\dot{U}$
EG	A tolerance value, usually $1.0 \times 10^{-12}$ .
EGS	EG squared.
GF(20)	Vector containing the values of the strengths ( $\Gamma_m$ ) of the free vortex cores; corresponds to the position vector ZF(20).
GG1	Value of $\Gamma_1$ during a time step.
GG2	Value of $\Gamma_2$ during a time step.
IT	Counter value for the pass number through the program. $1 \leq IT \leq NIT$
INNB	If bottom vortex is shed during a time step, this parameter equals 0, if vortex is not shed, it equals 1. It is used to determine whether a new vortex should be started from bottom sheet.
INNT	Has same indication as INNB, but applies to the top vortex and sheet.
NCHDT	Indicates the pass at which the value of DT is changed to prevent instabilities in the solution.
NFV	Counter used to indicate the number of free vortices existing. $NFV \leq 20$
NFVT	Contains the maximum value of NFV during any run. If $NFVT > 20$ , the DIMENSION statement must be changed as indicated in the program.
NIT	Contains the maximum value of IT during any run. If $NIT > 400$ , the DIMENSION statement must be changed as indicated in the program.
NKER(2)	Vector containing the matrix singularity determination from subroutine INVERT. NKER(1) applies to equation (42) while NKER(2) applies to equation (45).
NPL	Indicates number of passes through program between wake development plots.

NPRT	Indicates number of passes through program between status printouts.
PI	$\pi$
PI2	$\pi^2$
T(401)	Contains value of total elapsed $\frac{U_{\infty} t}{c}$ for each time step.
ZA(36)	Vector containing the values of the elements in the coefficient matrix of equation (45).
ZAA(4)	Same as ZA(36), but applies to equation (42).
ZC(6)	Vector containing the elements of the column matrix on the right hand side of equation (45).
ZCC(2)	Same as ZC(6), but applies to equation (42).
ZCP(100)	Contains the circle circumference points and scaling points used for plotting purposes.
ZF(20)	Contains the free vortex positions during a time step; corresponds to the vector GF(20) on a one for one basis.
ZG(6)	Contains the values of the unknowns in equation (45).
ZGG(2)	Same as ZG(6), but applies to equation (42).

## APPENDIX B

### A. DESCRIPTION OF COMPUTER PROGRAM FOR MODEL B

This program is much shorter from a coding standpoint than is Model

A. There is only one subroutine besides the plotting routine, PLOTP, needed for operation of the program, and it is included in the listing. The general comments previously made for Model A, apply equally well here. The only major difference, besides the concepts upon which the two are based, is that this program is written using single precision arithmetic rather than double precision as in the case of Model A.

### B. DEFINITION OF PARAMETERS

AVN(4)	Values, in degrees, of the nascent vortex placement angles actually used in the calculations. AVN(1) applies to birth area 1; AVN(2) applies to birth area 2, etc.
CDCL(100)	Same as Model A.
CLOCKR CLOCKS CLOCKT	} These parameters are used to determine the actual elapsed computer time for each pass and run; can be eliminated from the program without hurting its purpose.
CVV(400)	Contains the value velocities for each vortex during a time step. CVV(1) to CVV(100) Birth Area 1 CVV(101) to CVV(200) Birth Area 2 CVV(201) to CVV(300) Birth Area 3 CVV(301) to CVV(400) Birth Area 4
DTP	Same as DT in Model A
EG	Same as Model A
EGS	Same as Model A
GK(400)	Contains the value of the vortex strengths during a time step; corresponds to CVV(400) on a one for one basis.
IT	Same as Model A

ITIME(0)	An IBM on-line function used to make real time available to a FORTRAN IV program; can be eliminated without hurting the purpose of the program.
MPA	The value of nascent vortex placement distance as a function of RE as generated by formulas from Sarpkaya's paper [35]. Used for comparative purposes.
MP(4)	Contains the actual nascent vortex placement distance from the cylinder's surface used in the calculations. MP(1) corresponds to AVN(1) or NVM(1); MP(2) corresponds to AVN(2) or NVM(2); etc.
MS	Radius of the arc along which the search for maximum velocities is made; usually equal to 1.0.
MZD	Minimum distance two vortices can be from each other without being coalesced or cancelled.
NB	Total number of birth areas; usually equal to 4, but if only the primary nascent vortices are being studied, then NB=2.
NCAN	Counter indicating number of vortices cancelled during a run.
NCL	Counter indicating number of vortices coalesced during a run.
NIT	Same as Model A.
NP1	Indicates number of passes, times ten, between wake development plots.
NV	Counter indicating number of primary vortices generated in birth area 1 during a run. It is also equal to the number generated in birth area 2.
NVM(4)	Contains the values, in degrees, of the maximum velocity locations resulting from a search for same in the birth areas. NVM(1) corresponds to AVN(1); etc.
PI	$\pi$
RE	Reynolds number; used in conjunction with MPA.
TP(101)	Same as T(401) in Model A.
VELM(4)	Contains the values of maximum velocity found during the search for same in the birth areas. VELM(1) corresponds to NVM(1); etc.
ZCC(100)	Same as ZCP(100) in Model A.

ZCFP(51)      Contains the cylinder's circumferential locations from  
135 to 85 degrees (measured from the rear stagnation  
point).

ZCRP(61)      Contains the cylinder's circumferential locations from  
0 to 60 degrees (measured from the rear stagnation point).

ZF(400)        Contains the locations of the vortices during a time step.  
Corresponds to CVV(400) and GK(400).





[illegible]

NOTE: THE VORTEX SHEETS ARE CUT, FREEING THE CORES, WHEN  $\Delta S(D\text{-}GAMMA/DT)$  IS:  $TIP = 0.098$ ,  $BOTTOM = 0.917$

[illegible][illegible]

NOTE: THE VORTEX SHEETS ARE CUT, FREEING THE COPEES, WHEN  $\text{ABS}(D\text{-GAMMA}/DT)$  IS:  $\text{TOP} = 0.945$ ,  $\text{BOTTOM} = 0.954$

[illegible]

IT = 204 TIME = 9.370 DELTA TIME = 0.02000 CDCL = 1.200 -1.654

	CORE POSITION		TRUE CORE VELOCITY		D-W/DZ U	CORE STRENGTH	D-GAMMA DT	FEEDING SHEET ORIGIN (DEGPFS)
	X	Y	DX/DT	DY/DT				
UPPER FEEDING SHEET	0.711	0.774	0.1796	0.2014	-0.0263	0.020	-0.061	50.00
LOWER FEEDING SHEET	1.213	-0.559	0.0081	0.0340	0.0713	8.234	0.536	-50.00

NOTE: THE VORTEX SHEETS ARE CUT, FREEING THE CORES, WHEN ABS(D-GAMMA/DT) IS: TOP = 0.0 , BOTTOM = 0.730

FREE VORTEX CORES.

ORIGINATING FROM UPPER VORTEX SHEET

X	Y	U	V	STRENGTH	POSITION		CORE STRENGTH	D-GAMMA DT	FEEDING SHEET ORIGIN (DEGPFS)
					X	Y			
2.063	1.007	0.243	0.134	-7.727	0.0	0.0	0.0	0.0	0.0
EQUATION									
ZGG= (0.19398102132636370-01,0.0									
(-0.61231651162990520-01,0.0									
(0.1795639725761340,0.2014478242382351);									
(0.81049658827574290-02,0.3388639764213620-01);									
(10.22057158446897,-12.18040290419284);K19=									
(4.109098633912875,4.897033059289628);NKER=									
1,									

ORIGINATING FROM LOWER VORTEX SHEET

X	Y	U	V	STRENGTH	POSITION		CORE STRENGTH	D-GAMMA DT	FEEDING SHEET ORIGIN (DEGPFS)
					X	Y			
2.063	1.007	0.243	0.134	-7.727	0.0	0.0	0.0	0.0	0.0
EQUATION									
ZGG= (0.19398102132636370-01,0.0									
(-0.61231651162990520-01,0.0									
(0.1795639725761340,0.2014478242382351);									
(0.81049658827574290-02,0.3388639764213620-01);									
(10.22057158446897,-12.18040290419284);K19=									
(4.109098633912875,4.897033059289628);NKER=									
1,									

END

IT = 208 TIME = 9.450 DELTA TIME = 0.02000 CDCL = 1.239 -1.671

	CORE POSITION		TRUE CORE VELOCITY		D-W/DZ U	CORE STRENGTH	D-GAMMA DT	FEEDING SHEET ORIGIN (DEGPFS)
	X	Y	DX/DT	DY/DT				
UPPER FEEDING SHEET	0.728	0.793	0.2550	0.2835	0.0100	0.2058	-0.046	50.00
LOWER FEEDING SHEET	1.614	-0.557	0.0115	0.0328	0.0745	8.277	0.537	-50.00

NOTE: THE VORTEX SHEETS ARE CUT, FREEING THE CORES, WHEN ABS(D-GAMMA/DT) IS: TOP = 0.0 , BOTTOM = 0.730

FREE VORTEX CORES.

ORIGINATING FROM UPPER VORTEX SHEET

X	Y	U	V	STRENGTH	POSITION		CORE STRENGTH	D-GAMMA DT	FEEDING SHEET ORIGIN (DEGPFS)
					X	Y			
2.082	1.017	0.250	0.137	-7.727	0.0	0.0	0.0	0.0	0.0
EQUATION									
ZGG= (0.15243880856570030-01,0.0									
(-0.46132641808443010-01,0.0									
(0.2549713955197110,0.2834645103167961);									
(0.11533018884904830-01,0.32771416275103750-01);									
(10.16662932550766,-12.11611702324740);K19=									
(4.132724166121046,4.925188872175666);NKER=									
1,									

ORIGINATING FROM LOWER VORTEX SHEET

X	Y	U	V	STRENGTH	POSITION		CORE STRENGTH	D-GAMMA DT	FEEDING SHEET ORIGIN (DEGPFS)
					X	Y			
2.082	1.017	0.250	0.137	-7.727	0.0	0.0	0.0	0.0	0.0
EQUATION									
ZGG= (0.15243880856570030-01,0.0									
(-0.46132641808443010-01,0.0									
(0.2549713955197110,0.2834645103167961);									
(0.11533018884904830-01,0.32771416275103750-01);									
(10.16662932550766,-12.11611702324740);K19=									
(4.132724166121046,4.925188872175666);NKER=									
1,									

END

[illegible]

NOTE: THE VITEX SHEETS ARE CUT, FREEING THE CONES, WHEN ABS(D-GAMMA/DT) (S: TOP = 0.057, BOTTOM = 0.0

FREE VORTEX CORES.

[illegible][illegible]

NOTE: THE VORTEX SHEETS ARE CUT, FREEING THE CORES, WHEN  $\text{ABS}(D\text{-GAMMA}/DT)$  IS:  $\text{TOP} = 0.057$ ,  $\text{BOTTOM} = 0.0$

THE VCATX CRES.

ORIGINATING FROM LOWER VORTEX SHEET				ORIGINATING FROM UPPER VORTEX SHEET			
POSITION	IV	U	VELOCITY	POSITION	IV	U	VELOCITY
2.647	1.821	0.249	-7.727	4.216	2.610	1.471	-0.669
0.016	-0.851	0.177	8.550	1.003	-1.003	0.747	-0.612
CCUT	0.246157114	0.57087	0.0	0.257394651	1.8332510	-0.1000	1.26=
CCG=	0.4994270346	0.43000	0.0	0.207824252	2.32000	0.0	1.0
(-0.477663373642430)	(-0.016470063483497580)	(-0.14000000000000000)	(-0.37706532323232323)	(-0.6970065893937700)	(-0.03100000000000000)	(-0.03100000000000000)	(-0.03100000000000000)
(0.44333305217171717)	(0.00000000000000000)	(0.00000000000000000)	(0.44332692717171717)	(0.25333161737373737)	(0.00000000000000000)	(0.00000000000000000)	(0.00000000000000000)
(-0.11561534000000000)	(-0.13773346733522600)	(-0.13773346733522600)	(-5.126709810767235)	(-5.126709810767235)	(-5.126709810767235)	(-5.126709810767235)	(-5.126709810767235)

COMPUTER OUTPUT, MODEL B

INPUT 30625.000 ,TMAXP= 10.000000 ,NFOR= 2,NCOAL= 1,NTNAXI= 1,NOTP= 3  
 RENO

IT = 1 TP = 0.0 DTP = 0.09425 MPA = 0.01000 MZO = 0.06000  
 TIME STEP MULTIPLIER = 3

TRUE MAX-  
 VELOCITY  
 LOCATION  
 90  
 -90  
 0  
 0  
 \*\*FRONT, TOP \*\*  
 \*\*FRONT, BOTTOM\*\*  
 \*\*REAR, TOP \*\*  
 \*\*REAR, BOTTOM \*\*

THETA  
 USED IN  
 CALCULATIONS  
 95.00  
 -95.00  
 0.0  
 0.0

MAX. CROSS  
 & BACKFLOW  
 VELOCITIES  
 2.0000  
 2.0000  
 0.0  
 0.0

NASCENT VORTEX  
 PLACEMENT  
 DISTANCE (M)  
 0.045000  
 0.045000  
 0.0  
 0.0

COCL = 0.0 ZS1 = 0.0 ZS2 = 0.0

IT = 6 TP = 0.471 DTP = 0.09425 MPA = 0.01000 MZO = 0.06000  
 TIME STEP MULTIPLIER = 3

TRUE MAX-  
 VELOCITY  
 LOCATION  
 108  
 -108  
 0  
 0  
 \*\*FRONT, TOP \*\*  
 \*\*FRONT, BOTTOM\*\*  
 \*\*REAR, TOP \*\*  
 \*\*REAR, BOTTOM \*\*

THETA  
 USED IN  
 CALCULATIONS  
 95.00  
 -95.00  
 0.0  
 0.0

MAX. CROSS  
 & BACKFLOW  
 VELOCITIES  
 1.8096  
 1.8096  
 0.0  
 0.0

NASCENT VORTEX  
 PLACEMENT  
 DISTANCE (M)  
 0.045000  
 0.045000  
 0.0  
 0.0

COCL = 0.026 ZS1 = -0.368 ZS2 = -0.394 -0.000

VORTEX SHEETS

1. FRONT, TOP				2. FRONT, BOTTOM				3. REAR, TOP				4. REAR, BOTTOM			
POSITION	VELOCITY	GAMMA	#	POSITION	VELOCITY	GAMMA	#	POSITION	VELOCITY	GAMMA	#	POSITION	VELOCITY	GAMMA	#
0.46	1.15	-0.62	-0.1881	0.46	-0.96	1.15	0.62	0.1881	0.0	0.0	0.0	0.0	0.0	0.0	0.0
0.33	1.35	-0.40	-0.1621	0.33	-1.03	1.35	0.40	0.1621	0.0	0.0	0.0	0.0	0.0	0.0	0.0
0.19	1.42	-0.21	-0.1591	0.19	-1.06	1.42	0.21	0.1591	0.0	0.0	0.0	0.0	0.0	0.0	0.0
0.04	1.44	-0.04	-0.1571	0.04	-1.04	1.44	0.04	0.1571	0.0	0.0	0.0	0.0	0.0	0.0	0.0
-0.09	1.43	0.21	-0.1561	-0.09	-1.04	1.43	-0.21	0.1561	0.0	0.0	0.0	0.0	0.0	0.0	0.0

TOTAL NO. OF VORTEX PAIRS CANCELLED = 0. TOTAL NO. CF VORTEX PAIRS COALESCENCE = 0.

ELAPSED COMPUTING TIME FOR INTERATION = 1.01 SECONOS. TOTAL ELAPSED COMPUTING TIME = 0.07 MINUTES.



```

IT = 5C      TP = 4.618      DTP = 0.03425      MPA = 0.01000      W70 = 0.045000
TIME STEP MULTIPLIER = 3

      TRUE MAX. VELOCITY      THETA      MAX. CROSS      NASCENT VORTEX
      LOCATION      CALCULATIONS      LOCATION      PLACEMENT
      VELOCITIES      DISTANCE (M)

**FRONT, TOP      **      95.00      1.5700      0.045000
**FRONT, BOTTOM**      -95.00      1.5764      0.045000
**REAR, TOP      **      55.00      0.9023      0.045000
**REAR, BOTTOM **      -15.00      0.8848      0.045000

COCL = 1.096      -0.002      ZS1 = -0.582      0.007      ZS2 = -1.678      0.009

```

1. FRONT, TOP				2. FRONT, BOTTOM				3. REAR, TOP				3. REAR, BOTTOM				4. REAR, BOTTOM			
POSITION	VELOCITY	GAMMA #		POSITION	VELOCITY	GAMMA #		POSITION	VELOCITY	GAMMA #		POSITION	VELOCITY	GAMMA #		POSITION	VELOCITY	GAMMA #	
120	2.5	1	1	120	2.5	1	1	120	2.5	1	1	120	2.5	1	1	120	2.5	1	1
110	2.5	1	1	110	2.5	1	1	110	2.5	1	1	110	2.5	1	1	110	2.5	1	1
100	2.5	1	1	100	2.5	1	1	100	2.5	1	1	100	2.5	1	1	100	2.5	1	1
90	2.5	1	1	90	2.5	1	1	90	2.5	1	1	90	2.5	1	1	90	2.5	1	1
80	2.5	1	1	80	2.5	1	1	80	2.5	1	1	80	2.5	1	1	80	2.5	1	1
70	2.5	1	1	70	2.5	1	1	70	2.5	1	1	70	2.5	1	1	70	2.5	1	1
60	2.5	1	1	60	2.5	1	1	60	2.5	1	1	60	2.5	1	1	60	2.5	1	1
50	2.5	1	1	50	2.5	1	1	50	2.5	1	1	50	2.5	1	1	50	2.5	1	1
40	2.5	1	1	40	2.5	1	1	40	2.5	1	1	40	2.5	1	1	40	2.5	1	1
30	2.5	1	1	30	2.5	1	1	30	2.5	1	1	30	2.5	1	1	30	2.5	1	1
20	2.5	1	1	20	2.5	1	1	20	2.5	1	1	20	2.5	1	1	20	2.5	1	1
10	2.5	1	1	10	2.5	1	1	10	2.5	1	1	10	2.5	1	1	10	2.5	1	1
0	2.5	1	1	0	2.5	1	1	0	2.5	1	1	0	2.5	1	1	0	2.5	1	1
360	2.5	1	1	360	2.5	1	1	360	2.5	1	1	360	2.5	1	1	360	2.5	1	1
350	2.5	1	1	350	2.5	1	1	350	2.5	1	1	350	2.5	1	1	350	2.5	1	1
340	2.5	1	1	340	2.5	1	1	340	2.5	1	1	340	2.5	1	1	340	2.5	1	1
330	2.5	1	1	330	2.5	1	1	330	2.5	1	1	330	2.5	1	1	330	2.5	1	1
320	2.5	1	1	320	2.5	1	1	320	2.5	1	1	320	2.5	1	1	320	2.5	1	1
310	2.5	1	1	310	2.5	1	1	310	2.5	1	1	310	2.5	1	1	310	2.5	1	1
300	2.5	1	1	300	2.5	1	1	300	2.5	1	1	300	2.5	1	1	300	2.5	1	1
290	2.5	1	1	290	2.5	1	1	290	2.5	1	1	290	2.5	1	1	290	2.5	1	1
280	2.5	1	1	280	2.5	1	1	280	2.5	1	1	280	2.5	1	1	280	2.5	1	1
270	2.5	1	1	270	2.5	1	1	270	2.5	1	1	270	2.5	1	1	270	2.5	1	1
260	2.5	1	1	260	2.5	1	1	260	2.5	1	1	260	2.5	1	1	260	2.5	1	1
250	2.5	1	1	250	2.5	1	1	250	2.5	1	1	250	2.5	1	1	250	2.5	1	1
240	2.5	1	1	240	2.5	1	1	240	2.5	1	1	240	2.5	1	1	240	2.5	1	1
230	2.5	1	1	230	2.5	1	1	230	2.5	1	1	230	2.5	1	1	230	2.5	1	



UNIT =	75	TP = 6.974	DTP = 0.09425	MPA = 0.01000	MZD = 0.06000
		TIME STEP MULTIPLIER = 3			
		TRUE MAX. VELOCITY LOCATION	THETA USED IN CALCULATIONS	MAX. CROSS SECTIONAL VELOCITIES	NASCENT VORTEX PLACEMENT DISTANCE (M)
**FRONT, TOP **	114		95.00	1.5007	0.045000
**FRONT, BOTTOM **	-114		-95.00	1.5002	0.045000
**FRONT, TOP **	117		55.00	0.7877	0.045000
**REAR, BOTTOM **	-18		-55.00	0.9742	0.045000
EDCL = 1.014	0.044	ZS1 = -0.528	-0.010	ZS2 = -1.542	-0.034

CDCL =	1.014	0.044	ZS1 =	-0.528	-0.010	ZS2 =	-1.542	-0.054
--------	-------	-------	-------	--------	--------	-------	--------	--------

## VORTEX SHEETS

1. FRONT, TOP				2. FRONT, BOTTOM				3. REAR, TOP				4. REAR, BOTTOM			
POSITION	VELOCITY	GAMMA	GAMMA *	POSITION	VELOCITY	GAMMA	GAMMA *	POSITION	VELOCITY	GAMMA	GAMMA *	POSITION	VELOCITY	GAMMA	GAMMA *
52	0	10	0	52	0	10	0	52	0	10	0	52	0	10	0
53	0	10	0	53	0	10	0	53	0	10	0	53	0	10	0
54	0	10	0	54	0	10	0	54	0	10	0	54	0	10	0
55	0	10	0	55	0	10	0	55	0	10	0	55	0	10	0
56	0	10	0	56	0	10	0	56	0	10	0	56	0	10	0
57	0	10	0	57	0	10	0	57	0	10	0	57	0	10	0
58	0	10	0	58	0	10	0	58	0	10	0	58	0	10	0
59	0	10	0	59	0	10	0	59	0	10	0	59	0	10	0
60	0	10	0	60	0	10	0	60	0	10	0	60	0	10	0
61	0	10	0	61	0	10	0	61	0	10	0	61	0	10	0
62	0	10	0	62	0	10	0	62	0	10	0	62	0	10	0
63	0	10	0	63	0	10	0	63	0	10	0	63	0	10	0
64	0	10	0	64	0	10	0	64	0	10	0	64	0	10	0
65	0	10	0	65	0	10	0	65	0	10	0	65	0	10	0
66	0	10	0	66	0	10	0	66	0	10	0	66	0	10	0
67	0	10	0	67	0	10	0	67	0	10	0	67	0	10	0
68	0	10	0	68	0	10	0	68	0	10	0	68	0	10	0
69	0	10	0	69	0	10	0	69	0	10	0	69	0	10	0
70	0	10	0	70	0	10	0	70	0	10	0	70	0	10	0
71	0	10	0	71	0	10	0	71	0	10	0	71	0	10	0
72	0	10	0	72	0	10	0	72	0	10	0	72	0	10	0
73	0	10	0	73	0	10	0	73	0	10	0	73	0	10	0
74	0	10	0	74	0	10	0	74	0	10	0	74	0	10	0
75	0	10	0	75	0	10	0	75	0	10	0	75	0	10	0
76	0	10	0	76	0	10	0	76	0	10	0	76	0	10	0
77	0	10	0	77	0	10	0	77	0	10	0	77	0	10	0
78	0	10	0	78	0	10	0	78	0	10	0	78	0	10	0
79	0	10	0	79	0	10	0	79	0	10	0	79	0	10	0
80	0	10	0	80	0	10	0	80	0	10	0	80	0	10	0
81	0	10	0	81	0	10	0	81	0	10	0	81	0	10	0
82	0	10	0	82	0	10	0	82	0	10	0	82	0	10	0
83	0	10	0	83	0	10	0	83	0	10	0	83	0	10	0
84	0	10	0	84	0	10	0	84	0	10	0	84	0	10	0
85	0	10	0	85	0	10	0	85	0	10	0	85	0	10	0
86	0	10	0	86	0	10	0	86	0	10	0	86	0	10	0
87	0	10	0	87	0	10	0	87	0	10	0	87	0	10	0
88	0	10	0	88	0	10	0	88	0	10	0	88	0	10	0
89	0	10	0	89	0	10	0	89	0	10	0	89	0	10	0
90	0	10	0	90	0	10	0	90	0	10	0	90	0	10	0
91	0	10	0	91	0	10	0	91	0	10	0	91	0	10	0
92	0	10	0	92	0	10	0	92	0	10	0	92	0	10	0
93	0	10	0	93	0	10	0	93	0	10	0	93	0	10	0
94	0	10	0	94	0	10	0	94	0	10	0	94	0	10	0
95	0	10	0	95	0	10	0	95	0	10	0	95	0	10	0
96	0	10	0	96	0	10	0	96	0	10	0	96	0	10	0
97	0	10	0	97	0	10	0	97	0	10	0	97	0	10	0
98	0	10	0	98	0	10	0	98	0	10	0	98	0	10	0
99	0	10	0	99	0	10	0	99	0	10	0	99	0	10	0
100	0	10	0	100	0	10	0	100	0	10	0	100	0	10	0

VORTEX SHEETS																			
1. FRONT, TOP					2. FRONT, BOTTOM					3. REAR, TOP					4. REAR, BOTTOM				
POSITION	VELOCITY	GAMMA	POSITION	VELOCITY	GAMMA	POSITION	VELOCITY	GAMMA	POSITION	VELOCITY	GAMMA	POSITION	VELOCITY	GAMMA	POSITION	VELOCITY	GAMMA		
1.029	0.534	-0.0711	2.29	-0.28	-0.71	-0.04	0.2711	0.0	0.0	0.0	0.0	0.0	0.0	0.0	0.0	0.0	0.0		
1.322	0.230	-0.0809	2.61	-0.02	-0.49	-0.26	0.1621	0.0	0.0	0.0	0.0	0.0	0.0	0.0	0.0	0.0	0.0		
1.252	0.240	-0.0591	2.48	-0.87	-0.67	-0.01	0.1591	0.0	0.0	0.0	0.0	0.0	0.0	0.0	0.0	0.0	0.0		
1.146	0.823	-0.0157	1.15	-0.57	1.37	0.37	0.154	0.0	0.0	0.0	0.0	0.0	0.0	0.0	0.0	0.0	0.0		
1.110	0.283	-0.0156	1.38	-0.56	-0.09	-0.33	0.153	0.0	0.0	0.0	0.0	0.0	0.0	0.0	0.0	0.0	0.0		
1.100	0.126	-0.0132	1.22	-0.18	1.33	-0.42	0.152	0.0	0.0	0.0	0.0	0.0	0.0	0.0	0.0	0.0	0.0		
1.115	0.233	-0.0150	1.22	-0.46	-0.42	-0.02	0.150	0.0	0.0	0.0	0.0	0.0	0.0	0.0	0.0	0.0	0.0		
1.093	0.082	-0.0297	1.72	-0.59	-0.24	-0.10	0.297	0.0	0.0	0.0	0.0	0.0	0.0	0.0	0.0	0.0	0.0		
1.069	0.019	-0.0147	1.04	-0.22	-0.81	0.00	0.477	0.0	0.0	0.0	0.0	0.0	0.0	0.0	0.0	0.0	0.0		
1.224	0.027	-0.0147	1.04	-0.22	-0.81	0.00	0.477	0.0	0.0	0.0	0.0	0.0	0.0	0.0	0.0	0.0	0.0		
1.443	0.017	-0.0136	1.36	-0.06	-0.62	0.15	0.436	0.0	0.0	0.0	0.0	0.0	0.0	0.0	0.0	0.0	0.0		
1.181	0.038	-0.0145	1.60	-0.41	-0.25	0.09	0.145	0.0	0.0	0.0	0.0	0.0	0.0	0.0	0.0	0.0	0.0		
1.334	0.000	-0.0144	1.52	-0.11	-0.16	0.09	0.143	0.0	0.0	0.0	0.0	0.0	0.0	0.0	0.0	0.0	0.0		
1.346	0.000	-0.0143	1.79	-0.11	-0.32	0.01	0.142	0.0	0.0	0.0	0.0	0.0	0.0	0.0	0.0	0.0	0.0		
1.010	0.051	-0.0249	1.86	-0.55	-0.31	0.18	0.214	0.0	0.0	0.0	0.0	0.0	0.0	0.0	0.0	0.0	0.0		
1.010	0.000	-0.0249	1.86	-0.55	-0.31	0.18	0.214	0.0	0.0	0.0	0.0	0.0	0.0	0.0	0.0	0.0	0.0		
1.125	0.141	-0.0439	1.02	-0.20	-0.23	0.27	0.49	0.0	0.0	0.0	0.0	0.0	0.0	0.0	0.0	0.0	0.0		
1.077	0.000	-0.0439	1.81	-0.20	-0.23	0.27	0.49	0.0	0.0	0.0	0.0	0.0	0.0	0.0	0.0	0.0	0.0		
1.077	0.000	-0.0402	1.04	-0.13	0.08	0.39	0.271	0.0	0.0	0.0	0.0	0.0	0.0	0.0	0.0	0.0	0.0		
1.044	0.000	-0.0402	1.04	-0.13	0.08	0.39	0.271	0.0	0.0	0.0	0.0	0.0	0.0	0.0	0.0	0.0	0.0		
1.076	0.003	-0.0341	1.50	-0.05	0.00	0.19	0.266	0.0	0.0	0.0	0.0	0.0	0.0	0.0	0.0	0.0	0.0		
1.002	0.002	-0.0303	1.48	-0.36	-0.21	-0.23	0.262	0.0	0.0	0.0	0.0	0.0	0.0	0.0	0.0	0.0	0.0		
1.002	0.002	-0.0303	1.48	-0.36	-0.21	-0.23	0.262	0.0	0.0	0.0	0.0	0.0	0.0	0.0	0.0	0.0	0.0		
1.002	0.002	-0.0303	1.48	-0.36															

```

*****
THIS PROGRAM INTERJECTS VORTICIES (20 MAXIMUM) INTO THE WAKE USING
THE SINGLE FEEDING SHEET THEORY OF BRYSON (1964) WITH MODIFICATIONS
FOR ASYMMETRIC FEEDING AND WAKE FORMATION.
*****
DEFINITION OF PARAMETERS IN NAMELIST INPUT BLOCK.
*****
THETAT = ANGULAR POSITION OF ZT, DEGREES.
THETAB = ANGULAR POSITION OF ZB, DEGREES.
PCTADT = PERCENT OF CYLINDER RADIUS Z1 IS TO BE INITIALLY PLACED
        AWAY FROM CYLINDER.
PCTADB = PERCENT OF CYLINDER RADIUS Z2 IS TO BE INITIALLY PLACED
        AWAY FROM CYLINDER.
*****
IMPLICIT INTEGER(1,J,L,M,N,P,Q),REAL*8(A,B,D-H,O,R,T-Y),
CCOMPLEX*16(C,K,Z),REAL*4(S)
DIMENSION
CAG(12),ZGG(2),DUM(2,6),ZAA(4),ZCC(2),CV(20),AA(144),AC(12),
CDSIAX(4,4),DS2AX(12,12)
CCOMPLEX*8 CDCL(400),ZCP(100),ZZ8
REAL*4 T(401),DGI(401),DG2(401),XP(400),YP(401),
CPCTADT,PCTADB
REAL*8 PI,PI2
INTEGER*4 LL(144),MM(144),EG,EGS,NFV
COMMON /ALPHA/ZF(20),GF(20),Z2B,U,GG1,GG2
COMMON /BETA/Z1,Z1B,Z2,Z2B,K3,K4,K5,K6,K7,K8,K9,K10,K11,K12,K13,
CK14,K15,K16,K17,K18,K19,K20,ZT,ZTB,ZB,ZBB,PI,PI2
CK14,K15,K16,K17,K18,K19,K20,ZT,ZTB,ZB,ZBB,PI,PI2
EQUIVALENCE (ZC(1),ZCC(1),DUM(1,1)),(AA(1),DS1AA(1,1)),
C(AX(1),DS1AX(1,1),DS2AX(1,1))
*****
THE DIMENSIONS OF CV,ZF,AND GF MUST EQUAL NVFT. DIMENSIONS FOR OTHER
VARIABLE ARRAYS ARE:
        XP(NIT), CDCL(NIT), T(NIT+1), YP(NIT+1),
DG1(NIT+1), DG2(NIT+1).
*****
NVFT= 20
NIT= 400
NAMELIST/INPUT/THETAT,THETAB,PCTADT,PCTADB/OUTPUT/ZGG,ZG,K11,K19,
CNKER
READ (5,INPUT)
WRITE (6,INPUT)
CALL CANCEL (2)
*****
000000010
000000020
000000030
000000040
000000050
000000060
000000070
000000080
000000090
00000100
00000110
00000120
00000130
00000140
00000150
00000160
00000170
00000180
00000190
00000200
00000210
00000220
00000230
00000240
00000250
00000260
00000270
00000280
00000290
00000300
00000310
00000320
00000330
00000340
00000350
00000360
00000370
00000380
00000390
00000400
00000410
00000420
00000430
00000440

```



```

INT= 1
INNB= 1 2C
NCHDT= 4
NPRT= 4
NPL= 20
NFV= C
EG= 1.0D-12
EGS= EG*FG
PI= 3.141592653589793D0
PI2= 2.0D*PI
AT= THETAT*PI/180.0D0
ZT= DCMLPX(DCOS(AT),DSIN(AT))
ZTB= DCONJG(ZT)
AR= THETAB*PI/180.0D0
ZB= DCMLPX(DCOS(AB),DSIN(AB))
ZBB= DCONJG(ZB)
R= AT-PI/3.0D0
Z1= ZT+PCTADT*DCMLPX(DCOS(B),DSIN(B))
Z1B= DCONJG(Z1)
B= AP+PI/3.0D0
Z2= ZB+PCTADB*DCMLPX(DCOS(R),DSIN(R))
Z2B= DCONJG(Z2)

C
C CALCULATE CIRCUMFERENTIAL CIRCLE POINTS FOR PLOTTING PURPOSES.
C
NS= 72
S= 2.0*PI/NS
SA= C.0
DC 101 I= 1,NS
SA= SA+S
ZCP(I)= CMLPX(COS(SA),SIN(SA))
101 CONTINUE
ZCP(NS+1)= (-1.0, 2.5)
ZCP(NS+2)= (-1.0,-2.5)
ZCP(NS+3)= ( 4.0, 0.0)

C
C INITIALIZE ARRAYS.
C
DO 102 I= 1,NFVT
ZF(I)= 0.0D0
GF(I)= C.0D0
CV(I)= 0.0D0
102 CCNTINUE
DG1MAX= 0.0D0
DG2MAX= C.0D0
DG1MIN= 0.0D0
DG2MIN= 0.0D0
T(1)= 0.0

```

```

DT= 2.0D-2
C***** BEGINNING OF MAIN DO LOOP. *****
DO 131 IT= 1,NIT
U= 1.0D0
DUDT= 0.0D0
IF (IT.GT.NCHDT) DT= 0.05D0
143 K1= (ZT-Z1)*(ZT*Z1B-1.0D0)/(ZT-Z2)*(ZT*Z2B-1.0D0)
K2= (Z2*Z2B-1.0D0)/(ZT-Z2)*(ZT*Z2B-1.0D0)
K3= (ZB-Z2)*(ZB*Z2B-1.0D0)/(1.0D0-Z2*Z2B)
K4= (Z1*Z1B-1.0D0)/(ZB-Z1)*(ZB*Z1B-1.0D0)
K7= (0.0D0,1.0D0)*U*(1.0D0-(1.0D0/(ZT*ZT)))
K15= (0.0D0,1.0D0)*U*(1.0D0-(1.0D0/(ZB*ZB)))
CALL K1119 (ZT,K11)
CALL K1119 (ZB,K19)
C
C CALCULATE GROWING VORTEX CIRCULATION.
C
ZAA(1)= 1.0D0
ZAA(2)= -(K4*K3)
ZAA(3)= -(K1*K2)
ZAA(4)= 1.0D0
ZCC(1)= K1*(K7+(K11/PI2))
ZCC(2)= K3*(K15+(K19/PI2))
AC(1)= ZCC(1)
AC(3)= DUM(2,1)
AC(2)= ZCC(2)
AC(4)= DUM(2,2)
CALL MATCON (ZAA,2,AA)
CALL INVERT (4,EG,DS1AA,DS1AX,NKER(1),4)
CALL DMPRD (AX,AC,AG,4,4,1)
IF (DABS(AG(3)).LE.EG) AG(3)= 0.0D0
IF (DABS(AG(4)).LE.EG) AG(4)= 0.0D0
ZGG(1)= DCMPLEX(AG(1),AG(3))*PI2
ZGG(2)= DCMPLEX(AG(2),AG(4))*PI2
GG1= 1.05D0*ZGG(1)
GG2= ZGG(2)
K5= ((ZT*Z1B-1.0D0)/(1.0D0-Z1*Z1B))**2
K6= ((ZT-Z1)/(1.0D0-Z1*Z1B))**2
K8= (0.0D0,1.0D0)*DUDT*(1.0D0-(1.0D0/(ZT*ZT)))
K9= 1.0D0/(ZT-Z2)**2
K10= 1.0D0/(ZT*Z2B-1.0D0)**2
K12= K7+((GG2*K2+K11)/PI2)
K13= (ZB*Z2B-1.0D0)/(1.0D0-Z2*Z2B)**2
K14= (ZB-Z2)/(1.0D0-Z2*Z2B)**2
K16= (0.0D0,1.0D0)*DUDT*(1.0D0-(1.0D0/(ZB*ZB)))
K17= 1.0D0/(ZB-Z1)**2
K18= 1.0D0/(ZB*Z1B-1.0D0)**2
K20= K15+((GG1*K4+K19)/PI2)

```

C CALCULATION OF TIME DERIVATIVES.  
C

C CALL ZAARY

C CALCULATE ZC(I)  
C

DO 110 I=1,2  
IF (I.EQ.1) ZZ= ZT  
IF (I.EQ.2) ZZ= ZB

K= 0.000

IF (NEV) 109,109,103

103 DO 108 J= 1,NFV

ZS= 0.000

ZD= ZF(J)

IF ((CDABS(ZD) .LE. EG) .OR. (DABS(GF(J)).LE. EG)) GO TO 108

CALL DCVELP (ZD, CVV)

ZR= (ZZ-ZD)\*\*2

IF (CDABS(ZR)-EGS) 105,105,104

104 ZS= CVV/ZR

105 ZD= DCONJG (ZD)

ZR= (ZZ\*ZD-1.000)\*\*2

IF (CDABS(ZR)-EGS) 107,107,106

106 CVV= DCONJG(CVV)

ZS= ZS+CVV/ZR

107 K= K+GF(J)\*ZS

108 CONTINUE

109 IF (I.EQ.1) ZC(I)= K1\*((K/PI2)+K8)

IF (I.EQ.2) ZC(I)= K3\*((K/PI2)+K16)

110 CONTINUE

CALL DCVELP (Z1,ZC(3))

112 ZC(4)= DCONJG(ZC(3))

CALL DCVELP (Z2,ZC(5))

ZC(6)= DCONJG(ZC(5))

DO 135 I= 1,6

AC(I)= ZC(I)

AC(I+6)= DUM(2,I)

135 CONTINUE

CALL MATCON (ZA,6,AA)

CALL INVERT (12,EG,DS2AA,DS2AX,NKER(2),12)

CALL DMPRO (AX,AC,AG,12,12,1)

IF (DABS(AG(7)).LE. EG) AG(7)= 0.000

IF (DABS(AG(8)).LE. EG) AG(8)= 0.000

DO 136 I= 1,6

ZC(I)= DCMLPX(AG(I),AG(I+6))

136 CONTINUE

DG1(IT)= ZG(1)

DG2(IT)= ZG(2)

00001410  
00001420  
00001430  
00001440  
00001450  
00001460  
00001470  
00001480  
00001490  
00001500  
00001510  
00001520  
00001530  
00001540  
00001550  
00001560  
00001570  
00001580  
00001590  
00001600  
00001610  
00001620  
00001630  
00001640  
00001650  
00001660  
00001670  
00001680  
00001690  
00001700  
00001710  
00001720  
00001730  
00001740  
00001750  
00001760  
00001770  
00001780  
00001790  
00001800  
00001810  
00001820  
00001830  
00001840  
00001850  
00001860  
00001870  
00001880



```

C
C CALCULATE DRAG AND LIFT COEFFICIENTS.
C
113 K= PI2*DUDT
    ZS= 0.0D0
    IF (INNT.EQ.1) K= K+(0.0D0,1.0D0)*(DG1(IT)*(Z1-(1.0D0/Z1B))
C
    IF (INNB.EQ.1) K= K+(0.0D0,1.0D0)*(DG2(IT)*(Z2-(1.0D0/Z2B))
C
    IF (NFV) 117,117,115
115 DO 116 I=1,NFV
    IF ((CDABS(ZF(I)).LE.EG).OR.(DABS(GF(I)).LE.EG)) CV(I)= 0.0D0
    IF ((CDABS(ZF(I)).LE.EG).OR.(DABS(GF(I)).LE.EG)) GO TO 116
    CALL DCVELP (ZF(I),CVV)
    CV(I)= CVV
    ZS= ZS+ (0.0D0,1.0D0)*GF(I)*(CVV+DCONJG(CVV)/(DCONJG(ZF(I))**2))
116 CONTINUE
117 CCCL(IT)= K+ZS
C
C WRITE AND PLOT.
C
    IF (IT.LE.15) GO TO 141
    IF ((IT/NPRT)*NPRT-IT) 140,141,141
141 WRITE(6,2) IT,T(IT),DT,CCCL(IT),Z1,ZG(3),GC1,DG1(IT),
C
    THETAT,Z2,ZG(5),ZC(5),GG2,DG2(IT),THETAB,DG1MIN,DG2MIN
    IF (NFV) 119,119,118
118 J= NFV-1
    WRITE(6,3) (ZF(I),CV(I),GF(I),ZF(I+1),CV(I+1),GF(I+1),I=1,J,2)
119 WRITE(6,OUTPUT)
140 IF ((IT/NPL)*NPL-IT) 125,120,120
120 NPAIR= NS+3
    DO 121 I=1,NPAIR
    XP(I)= ZCP(I)
    YP(I)= AIMAG(ZCP(I))
121 CONTINUE
    N= 1
    CALL PLOTP (XP,YP,NPAIR,N)
    IF (NFV) 124,124,122
122 NPAIR= NFV
    DO 123 I= 1,NFV
    XP(I)= ZF(I)
    ZZ8= ZF(I)
    YP(I)= AIMAG(ZZ8)
123 CONTINUE
    N= 2
    CALL PLOTP (XP,YP,NPAIR,N)
124 NPAIR= 2
    ZZ8= Z1

```

00001890  
00001900  
00001910  
00001920  
00001930  
00001940  
00001950  
00001960  
00001970  
00001980  
00001990  
00002000  
00002010  
00002020  
00002030  
00002040  
00002050  
00002060  
00002070  
00002080  
00002090  
00002100  
00002110  
00002120  
00002130  
00002140  
00002150  
00002160  
00002170  
00002180  
00002190  
00002200  
00002210  
00002220  
00002230  
00002240  
00002250  
00002260  
00002270  
00002280  
00002290  
00002300  
00002310  
00002320  
00002330  
00002340  
00002350  
00002360

```

XP(1)= ZZ8
YP(1)= AIMAG(ZZ8)
ZZ8= Z2
XP(2)= ZZ8
YP(2)= AIMAG(ZZ8)
N= 3
WRITE (6,1)
CALL PLOTP (XP,YP,NPAIR,N)
WRITE (6,8) IT
WRITE (6,1)

C ADVANCE ALL PARAMETERS.
C
125 IF (NFV.GE.NFVT) GO TO 132
  I(IT+1)= I(IT)+DT
  IF (NFV) 137,137,126
126 DC 127 I= 1,NFV
  ZF(I)= ZF(I)+CV(I)*DT
127 CCONTINUE
137 C= ZG(1)
  CALL RUNKUT (Z1,ZT,DT,D,GG1,ZC(3),ZZ)
  Z1= ZZ
  Z1B= DCONJG(Z1)
  D= ZG(2)
  CALL RUNKUT (Z2,ZB,DT,D,GG2,ZC(5),ZZ)
  Z2= ZZ
  Z2B= DCONJG(Z2)

C CREATE FREE VORTS. IF APPROPRIATE.
C
  IF (IT.LE.NCHDT) GO TO 114
  B= (-ZG(1))
  IF (B.GT.DG1MAX) DG1MAX= B
  IF (B.EQ.DG1MAX) DG1MIN= B
  IF ((B.LT.DG1MAX).AND.(B.LT.DG1MIN)) DG1MIN= B
  GO TO 138
111 NFV= NFV+1
  INNT= 0
  ZF(NFV)= Z1
  GF(NFV)= GG1
  DG1MAX= 0.CD0
  DG1MIN= 0.CD0
  DT= 2.OD-2
  IF (NFV.GE.NFVT) GO TO 114
138 B= ZG(2)
  IF (B.GT.DG2MAX) DG2MAX= B
  IF (B.EQ.DG2MAX) DG2MIN= B

```

```

00002370
00002330
00002390
00002400
00002410
00002420
00002430
00002440
00002450
00002460
00002470
00002480
00002490
00002500
00002510
00002520
00002530
00002540
00002550
00002560
00002570
00002580
00002590
00002600
00002610
00002620
00002630
00002640
00002650
00002660
00002670
00002680
00002690
00002700
00002710
00002720
00002730
00002740
00002750
00002760
00002770
00002780
00002790
00002800
00002810
00002820
00002830
00002840

```

```

IF ((B.LT.DG2MAX).AND.(B.LT.DG2MIN)) DG2MIN= B
IF ((B.LT.DG2MAX).AND.(B.GT.DG2MIN)) GO TO 145
GO TO 114
145 NFV= NFV+1
INNB= 0
ZF(NFV)= Z2
GF(NFV)= GG2
DG2MAX= 0.0D0
DG2MIN= 0.0D0
DT= 2.0D-2
114 IF ((INNT.EQ.0).OR.(INNB.EQ.0)) NCHDT= IT+20
C INTRODUCE NEW GROWING VORTS. IF APPROPRIATE.
C
IF (INNT) 128,128,129
128 INNT= 1
AT= THE TAT*PI/180.0D0
ZT= DCMLPX(DCOS(AT),DSIN(AT))
ZTB= DCONJG(ZT)
B= AT-PI/3.0D0
Z1= ZT+PCTADT*DCMLPX(DCOS(B),DSIN(B))
Z1B= DCONJG(Z1)
129 IF (INNB) 130,130,131
130 INNB= 1
AB= THE TAB*PI/180.0D0
ZB= DCMLPX(DCOS(AB),DSIN(AB))
ZBB= DCONJG(ZB)
B= AB+PI/3.0D0
Z2= ZB+PCTADB*DCMLPX(DCOS(B),DSIN(B))
Z2B= DCONJG(Z2)
131 CONTINUE
C***** END OF MAIN DO LOOP *****
132 WRITE (6,1) IT= IT-1
IF (IT.GT.NIT) IT= IT-1
WRITE (6,7) (I,T(I),CDCL(I),DG1(I),DG2(I),I=1,IT)
DO 133 I= 1,IT
YP(I)= CDCL(I)
IF (ABS(YP(I)).GT.2.4) YP(I)= 0.0
133 CONTINUE
N= IT+1
YP(N)= 2.4
T(N)= 0.0
WRITE (6,1)
CALL PLOTP (T,YP,N,0)
WRITE (6,4)
DO 134 I= 1,IT
YP(I)= AIMAG(CDCL(I))
IF (ABS(YP(I)).GT.2.4) YP(I)= 0.0

```

```

00002850
00002860
00002870
00002880
00002890
00002900
00002910
00002920
00002930
00002940
00002950
00002960
00002970
00002980
00002990
00003000
00003010
00003020
00003030
00003040
00003050
00003060
00003070
00003080
00003090
00003100
00003110
00003120
00003130
00003140
00003150
00003160
00003170
00003180
00003190
00003200
00003210
00003220
00003230
00003240
00003250
00003260
00003270
00003280
00003290
00003300
00003310
00003320

```

```

134 CONTINUE
    WRITE (6,1) (T,YP,N,0)
    CALL PLOTP (T,YP,N,0)
    WRITE (6,5)
    DG1(N)=0.0
    DC I44 I=1,N
    DG1(I)=(-DG1(I))
    IF (ABS(DG1(I)).GT.4.0) DG1(I)=0.0
    IF (ABS(DG2(I)).GT.4.0) DG2(I)=0.0
144 CONTINUE
    CALL PLOTP (T,DG1,N,1)
    WRITE (6,1)
    DG2(N)=0.0
    CALL PLOTP (T,DG2,N,3)
    WRITE (6,6)
    RETURN
1 FCRMAT (1H1)
2 FCRMAT (///,3X,'IT = ',I4,4X,'TIME = ',F7.3,4X,'DELTA TIME = ',
CF9.5,
C4X,'CDCL =',2F7.3,
C//,T41,'CORE',T57,'TRUE CORE',T79,'DW/DZ',T95,'CORE',T106,'D-GAMMA'
C,T118,'FEEDING',T139,'POSITION',T57,'VELOCITY',T78,'VELOCITY',
CT93,'STRENGTH',T108,'DT',T116,'SHEET ORIGIN',T37,'X',T46,'Y',
CT54,'DX/DT',T63,'DY/DT',T77,'U',T86,'V',T118,'(DEGREES)',//,
C6X,'UPPER FEEDING SHEET',6X,2(F7.3,3X),4(F8.4,2X),1X,F7.3,4X,F8.3,
C4X,F7.2,/,
C6X,'LOWER FEEDING SHEET',6X,2(F7.3,3X),4(F8.4,2X),1X,F7.3,4X,F8.3,
C4X,F7.2,/,
CS,WHEN ABS(D-GAMMA/DT) IS: TOP = ,F8.3,/, BOTTOM = ,F8.3,///)00003610
3 FCRMAT (T8,'FREE VORTEX CORES',//,T19,'ORIGINATING FROM UPPER VORTEX SHEET',
CTEX SHEET',T85,'ORIGINATING FROM LOWER VORTEX SHEET',//,2(7X,'POSITION',
CTION',
C 15X,'VELOCITY',12X,'STRENGTH',8X),/,2(6X,'X',8X,'Y',11X,'U',8X)00003650
C,IV,27X),/,2(3X,2(F7.3,2X),4X,2(F7.3,2X),7X,F7.3,9X))
4 FCRMAT (///,3X,'DRAG COEFFICIENT VERSUS TIME',)
5 FCRMAT (///,3X,'LIFT COEFFICIENT VERSUS TIME',)
6 FCRMAT (///,3X,'D-GAMMA/DT VERSUS TIME: UPPER SHEET',//,3X,'NOTE: THE UPPER SHEET IS PLOTTED A
CT28,'LOWER SHEET',//,3X,'NOTE: THE LOWER SHEET IS PLOTTED A
CS THE NEGATIVE OF ITS TRUE VALUE',)
7 FCRMAT (///,T5,'PASS NO.',T13,'TIME',T29,'DRAG',T40,'LIFT',T51,
C,DG/DT',T63,'DG/DT',//,T51,'(TOP)',T62,'(BOTTOM)',//,
C(3X,I4,8X,3(F6.3,5X),2(F7.3,5X),60X))
8 FCRMAT (///,10X,'VORTEX POSITION PLOT FOR IT = ',I4)
    END

```

```

00003330
00003340
00003350
00003360
00003370
00003380
00003390
00003400
00003410
00003420
00003430
00003440
00003450
00003460
00003470
00003480
00003490
00003500
00003510
00003520
00003530
00003540
00003550
00003560
00003570
00003580
00003590
00003600
00003610
00003620
00003630
00003640
00003650
00003660
00003670
00003680
00003690
00003700
00003710
00003720
00003730
00003740
00003750
00003760

```



```

C*****SUBROUTINE DCVELP (Z,CV)*****00003770
C*****PURPOSE: TO CALCULATE THE FREE CONVECTIVE VELOCITY AT ANY POSITION,00003780
C*****ON OR OUTSIDE THE CYLINDER.00003790
C*****00003800
C*****00003810
C*****00003820
C*****00003830
C*****00003840
C*****00003850
C*****00003860
C*****00003870
C*****00003880
C*****00003890
C*****00003900
C*****00003910
C*****00003920
C*****00003930
C*****00003940
C*****00003950
C*****00003960
C*****00003970
C*****00003980
C*****00003990
C*****00004000
C*****00004010
C*****00004020
C*****00004030
C*****00004040
C*****00004050
C*****00004060
C*****00004070
C*****00004080
C*****00004090
C*****00004100
C*****00004110
C*****00004120
C*****00004130
C*****00004140
C*****00004150
C*****00004160
C*****00004170
C*****00004180
C*****00004190
C*****00004200
C*****00004210
C*****00004220

SUBROUTINE DCVELP (Z,CV)
PURPOSE: TO CALCULATE THE FREE CONVECTIVE VELOCITY AT ANY POSITION,
ON OR OUTSIDE THE CYLINDER.

PARAMETERS: Z = INPUT POSITION; COMPLEX*16
CV = OUTPUT LOCAL CONVECTIVE VELOCITY; COMPLEX*16

C*****
C*****IMPLICIT INTEGER(I,J,L,M,N,P,Q),REAL*8(A,B,D-H,O,R-Y),
C*****C*COMPLEX*16(C,K,Z)*****
C*****REAL*8 PI,PI2*****
C*****COMMON /ALPHA/ZF(20),GF(20),EG,EGS,NFV*****
C*****COMMON /BETA/Z1,Z18,Z2,Z2B,U,GG1,GG2*****
C*****PI= 3.141592653589793D0*****
C*****PI2= 2.000*PI*****
C*****K= 0.0D0*****
C*****IF (CDABS(Z)-EG) 114,114,101*****

C*****CALCULATION FOR FREE VORTS.*****
C*****
101 IF (NFV) 108,108,102
102 DO 107 I= 1,NFV
ZS= 0.0D0
IF ((CDABS(ZF(I)).LE.EG).OR.(DABS(GF(I)).LE.EG)) GO TO 107
ZR= Z-ZF(I)
IF (CDABS(ZR)-EG) 104,104,103
ZS= 1.0D0/ZR
103 ZS= 1.0D0/ZR
104 ZR= Z-(1.0D0/DCONJG(ZF(I)))
105 ZS= ZS-1.0D0/ZR
106 K= K+GF(I)*ZS
107 CONTINUE

C*****CALCULATION FOR GROWING VORTS.*****
C*****
108 DO 113 I= 1,2
IF (I.EQ.1) ZZ= Z1
IF (I.EQ.1) G= GG1
IF (I.EQ.2) ZZ= Z2
IF (I.EQ.2) G= GG2
ZS= 0.0D0
IF ((CDABS(ZZ).LE.EG).OR.(DABS(G).LE.EG)) GO TO 113
ZR= Z-ZZ
IF (CDABS(ZR)-EG) 110,110,109

```

```

109 ZS= 1. CDC/7R
110 ZR= Z-(1. CD0/DCCNJG(ZZ))
111 IF (CJABS(ZR)-EG) 112,112,111
112 ZS= ZS-(1. CD0/ZR)
113 K= K+G*ZS
      CONTINUE
      ZS= U*((1. OD0/(Z**2))-1. CD0)+(1. CD0)*K/PI2)
      CV= (-DCCNJG(ZS))
      GO TO 115
114 WRITE (6,1) Z
115 RETURN
1  FORMAT (1H1,3X,'***' ATTEMPT TO CALCULATE CONVECTIVE VELOCITY AT
      CENTER OF CYLINDER, ',',//,3X,'Z = ',2F23.16)
      END

```

```

00004230
00004240
00004250
00004260
00004270
00004280
00004290
00004300
00004310
00004320
00004330
00004340
00004350
00004360

```



```

C***** SUBROUTINE DMPRD (A,B,R,N,M,L) ***** 00004370
C***** ***** 00004380
C***** ***** 00004390
C***** ***** 00004400
C***** ***** 00004410
C***** ***** 00004420
C***** ***** 00004430
C***** ***** 00004440
C***** ***** 00004450
C***** ***** 00004460
C***** ***** 00004470
C***** ***** 00004480
C***** ***** 00004490
C***** ***** 00004500
C***** ***** 00004510
C***** ***** 00004520
C***** ***** 00004530
C***** ***** 00004540
C***** ***** 00004550
C***** ***** 00004560
C***** ***** 00004570
C***** ***** 00004580
C***** ***** 00004590
C***** ***** 00004600
C***** ***** 00004610
C***** ***** 00004620
C***** ***** 00004630
C***** ***** 00004640
C***** ***** 00004650
C***** ***** 00004660
C***** ***** 00004670
C***** ***** 00004680
C***** ***** 00004690

PURPOSE: TO MULTIPLY TWO COMPLEX*16 GENERAL MATRICES TOGETHER.

PARAMETERS: A = FIRST INPUT VECTOR.
             B = SECOND INPUT VECTOR.
             R = OUTPUT VECTOR.
             N = # ROWS IN MATRIX A, REAL*4
             M = # OF COLUMNS IN A AND ROWS IN B, INTEGER*4
             L = # OF COLUMNS IN B, INTEGER*4

FORMULA:
          |A||B|=|R|

C***** ***** 00004530
C***** ***** 00004540
C***** ***** 00004550
C***** ***** 00004560
C***** ***** 00004570
C***** ***** 00004580
C***** ***** 00004590
C***** ***** 00004600
C***** ***** 00004610
C***** ***** 00004620
C***** ***** 00004630
C***** ***** 00004640
C***** ***** 00004650
C***** ***** 00004660
C***** ***** 00004670
C***** ***** 00004680
C***** ***** 00004690

REAL*8
IR= 0
IK= -M
DO 10 K= 1,L
IK= IK+M
DO 10 J= 1,N
IR= IR+1
JI= J-N
IB= IK
R(IR)= 0.0D0
DO 10 I= 1,M
JI= JI+N
IB= IB+1
10 R(IR)= R(IR)+A(JI)*B(IB)
RETURN
END

```

```

C** SUBROUTINE INVERT(N,EP,A,X,KER,NACT)
C**
C** PUKPOSE: INVERT A REAL*8 DOURLLE DIMENSIONED ARRAY BY THE GAUSSIAN-
C** ELIMINATION WITH BACK SUBSTITUTION METHOD.
C**
C** PARAMETERS: N = ORDER OF MATRIX A.
C** EP = DIFFERENCE ERROR (1.0D-10 FOR DOUBLE PRECISION).
C** A = DOUBLE DIMENSION REAL*8 INPUT MATRIX.
C** X = INVERSE OF MATRIX A, OUTPUT, REAL*8.
C** KER = IF KER IS RETURNED EQUAL TO 2, MATRIX A IS
C** SINGULAR.
C** NACT = NUMERICAL VALUE OF N.
C**
C** IMPLICIT REAL*8(A-H,O-Z)
C** DIMENSION A(NACT,NACT),X(NACT,NACT)
C**
C** DO 1 I=1,N
C** DO 1 J=1,N
C** 1 X(I,J)=0.0D0
C** DO 2 K=1,N
C** 2 X(K,K)=1.0D0
C** DO 3 L=1,N
C** 3 KP=0
C** Z=0.0D0
C** DO 12 K=L,N
C** 11 IF(Z-DABS(A(K,L)))11,12,12
C** Z=DABS(A(K,L))
C** KP=K
C** DO 13 CONTINUE
C** 12 IF(L-KP)13,20,20
C** DO 14 J=L,N
C** 13 Z=A(L,J)
C** A(L,J)=A(KP,J)
C** A(KP,J)=Z
C** DO 15 J=1,N
C** 14 Z=X(L,J)
C** X(L,J)=X(KP,J)
C** X(KP,J)=Z
C** DO 20 IF(DABS(A(L,L))-EP)50,50,30
C** 20 IF(DABS(A(L,L))-EP)50,50,30
C** 30 IF(L=N)31,34,34
C** 31 LP1=L+1
C** DO 36 K=LP1,N
C** 32 IF(A(K,L))32,36,32
C** 32 RATIO=A(K,L)/A(L,L)
C** DO 33 J=LP1,N

```

```

33 A(K,J)=A(K,J)-RATIO*A(L,J)
35 DO 35 J=1,N
36 X(K,J)=X(K,J)-RATIO*X(L,J)
34 CONTINUE
40 DO 43 I=1,N
DO 43 J=1,N
S=0.000
IF(I1-N)41,43,43
I1P1=I1+1
41 DO 42 K=I1P1,N
S=S+A(I1,K)*X(K,J)
42 X(I1,J)={X(I1,J)-S)/A(I1,I1)
43 KER=1
GO TO 75
50 KER=2
75 CONTINUE
RETURN
END

```

```

00005160
00005170
00005180
00005190
00005200
00005210
00005220
00005230
00005240
00005250
00005260
00005270
00005280
00005290
00005300
00005310
00005320
00005330
00005340
00005350

```

```

SUBROUTINE K1119 (7,K)
      PURPOSE: TO CALCULATE THE CONSTANTS K11 AND K19.
      PARAMETERS: Z = INPUT, TOP OR BOTTOM FEEDING SHEET; COMPLEX*16
                  K = OUTPUT, K11 OR K19 DEPENDING ON Z; COMPLEX*16
      IMPLICIT INTEGER(I,J,L,M,N,P,Q),REAL*8(A,B,D,H,O,R-Y),
      COMPLEX*16(C,K,Z)
      COMMON /ALPHA/ZF(20),GF(20),EG,FGS,NFV
      K=0.0D0
      IF (NFV) 1C9,109,101
      IF (CDABS(Z)-EG) 108,108,102
      DO 1C7 I=1,NFV
        ZS=C.DC
        IF ((CDABS(ZF(I)).LE.EG).OR.(DABS(GF(I)).LE.EG)) GO TO 1C7
        ZF=Z-ZF(I)
        IF (CDABS(ZR)-EG) 104,104,103
        ZS=1.CDC/ZR
        ZR=Z-(1.CD0/DCONJG(ZF(I)))
        IF (CDABS(ZR)-EG) 106,106,105
        ZS=ZS-1.CD0/ZR
        K=K+GF(I)*ZS
      CONTINUE
      GO TO 109
      WRITE (6,1) Z
      RETURN
      I=CCENTER OF CYLINDER',//,3X,'ZB OR ZT = ',2F23.16)
      ATTEMPT TO CALCULATE K1119 FOR A ZB OR ZT AT
      1
      END

```

```

SUBROUTINE MATCON (B,N,G)
*****
PURPOSE: TO CONVERT A COMPLEX*16 MATRIX VECTOR INTO A REAL*8
PARTITIONED MATRIX VECTOR OF 2N ORDER, READY FOR INVERSION
USING SUBROUTINE INVERT.
IF |A| = |B| + I|C|, THEN:

$$|G| = \begin{Bmatrix} |B| & -|C| \\ |C| & |B| \end{Bmatrix}$$

PARAMETERS: A = INPUT VECTOR REPRESENTING A GENERAL SQUARE MATRIX.
              COMPLEX*16
              N = INPUT ORDER OF MATRIX A, INTEGER*4.
              G = OUTPUT VECTOR, REPRESENTS A SQUARE MATRIX. REAL*8
                MUST HAVE (2*N)**2 ELEMENTS.
*****
REAL*8 G(1),DUM(2,36)
COMPLEX*8 ZZ
COMPLEX*16 A(36),B(36)
EQUIVALENCE (A(1),DUM(1,1))
DO 105 I=1,36
  A(I)=B(I)
105 CONTINUE
NAE= N*N
CONVERT REAL PARTS.
M= 2*N*N+N
DO 102 I= 1,2
  DO 101 J= 1,NAE
    L= N*((J-1)/N)+(I-1)*M+J
    G(L)=A(J)
101 CONTINUE
102 CONTINUE
CONVERT IMAGINARY PARTS.
K= 2*N*(1-N)
M= 2*N*N-N
DO 104 I= 1,2

```

00005680  
00005690  
00005700  
00005710  
00005720  
00005730  
00005740  
00005750  
00005760  
00005770  
00005780  
00005790  
00005800  
00005810  
00005820  
00005830  
00005840  
00005850  
00005860  
00005870  
00005880  
00005890  
00005900  
00005910  
00005920  
00005930  
00005940  
00005950  
00005960  
00005970  
00005980  
00005990  
00006000  
00006010  
00006020  
00006030  
00006040  
00006050  
00006060  
00006070  
00006080  
00006090  
00006100  
00006110  
00006120  
00006130

```

103 J= 1,NAE
L= N*( (J-1)/N)+I*M+K+J
G(L)= DUM(2,J)*((-1.0DC)**(I+1))
104 CONTINUE
104 RETURN
END

```

```

00006140
00006150
00006160
00006170
00006180
00006190
00006200

```



[illegible]

\*\*\*\*\*  
 ATING  
 HE  
 REAL\*8  
 ON.  
 \*\*\*\*\*

\*\*\*\*\*



```
ZA(33) = 0.0D0  
ZA(34) = 0.0D0  
ZA(35) = 0.0D0  
ZA(36) = 1.0D0  
RETURN  
END
```

```
00006960  
00006970  
00006980  
00006990  
00007000  
00007010
```

[illegible]

```

EV= 1.0E-4
MPA=1.75/SQRT(RE)
MZD= 6.0*MPA
MS= 1.0
NB= 4
NIT= 100
NPI= 1
NV= 0
NCL= 0
NCAN= 0

```

```

C
C
C   CALCULATE CIRCUMFERENTIAL CIRCLE POINTS FOR PLOTTING PURPOSES.

```

```

      NS= 72
      S= 2.0*PI/NS
      A= 0.0
      DO 130 I= 1,NS
        A=A+S
        ZCC(I)= CMPLX(COS(A),SIN(A))
130  CONTINUE
      ZCC(NS+1)= (-1.0, 2.5)
      ZCC(NS+2)= (-1.0,-2.5)
      ZCC(NS+3)= ( 4.0, 0.0)

```

```

C
C
C   INITIALIZE ARRAYS.

```

```

      Z= (0.0,0.0)
      DO 1012 I= 1,NIT
        XP(I)= 0.0
        YP(I)= 0.0
        TP(I)= 0.0
        CDC(I)= Z
1012  CONTINUE

```

```

      N= 4*NIT
      DO 1011 I= 1,N
        ZF(I)= Z
        GK(I)= Z
1011  CONTINUE

```

```

C
C
C   POSITIONS ON CYLINDER, 60 TO 0 DEG. AND 135 TO 85 DEG., TOP ONLY
C   BOTTOM IS THE CONJUGATE OF THE TOP.

```

```

      DO 102 I=1,51
        A=(136-I)*PI/180.0
        ZCFP(I)= CMPLX(MS*COS(A),MS*SIN(A))
102  CONTINUE
      DO 136 I= 1,61
        A= (61-I)*PI/180.0

```

```

000000450
000000460
000000470
000000480
000000490
000000500
000000510
000000520
000000530
000000540
000000550
000000560
000000570
000000580
000000590
000000600
000000610
000000620
000000630
000000640
000000650
000000660
000000670
000000680
000000690
000000700
000000710
000000720
000000730
000000740
000000750
000000760
000000770
000000780
000000790
000000800
000000810
000000820
000000830
000000840
000000850
000000860
000000870
000000880
000000890
000000900
000000910
000000920

```







```

IF (NV.EQ.0) GO TO 106
DO 116 I=1,2
DO 117 J=1,61
IF (I.EQ.1) Z= ZCRP(J)
IF (I.EQ.2) Z= CONJG(ZCRP(J))
CALL CVELP(Z,0,0,CV)
UI= REAL(CV)
A= CABS(CV)
IF ((UI.LE.0.0).AND.(A.GT.VELM(I+2))) GO TO 118
GO TO 117
118 VELM(I+2)= A
IF (A.LE.EV) VELM(I+2)= 0.0
IF (A.GT.EV) NVM(I+2)= ((-1)**(I+1))*(61-J)
117 CONTINUE
116 CONTINUE
C CALCULATE NASCENT VORTEX PLACEMENT ANGLE TO BE USED IN FUTURE
C CALCULATIONS.
C
106 AVN(1)= 95.0
AVN(2)= -95.0
IF (VELM(3).GT.EV) AVN(3)= 55.0
IF (VELM(4).GT.EV) AVN(4)= -55.0
C CALCULATE VORTEX PLACEMENT DISTANCE (MP).
C
DO 122 I=1,NB
IF (VELM(I).LE.EV) GO TO 122
MP(I)= 0.045
122 CONTINUE
C
C LIFT AND DRAG COEFFICIENTS
C
ZS1= (0.0,0.0)
ZS2= ZS1
IF (NV.EQ.0) GO TO 110
DO 109 I=1,NB
K= 1+NIT*(I-1)
L= NV+NIT*(I-1)
DO 108 J= K,L
IF (ABS(GK(J)).LE.EG) GO TO 108
CV= CMPLX(-AIMAG(CVV(J)),REAL(CVV(J)))
ZS1= ZS1+GK(J)*CV
CV= CMPLX(-REAL(CVV(J)),AIMAG(CVV(J)))
CV= CV/CONJG(ZF(J)**2)
ZS2= ZS2+GK(J)*CMPLX(-AIMAG(CV),REAL(CV))
108 CONTINUE
109 CONTINUE

```

```

110 CCCL(IT)= ZS1-ZS2
WRITE (6,3)
WRITE (6,1) IT, TP(IT), DTP, MPA, MZD, NDTP, (NVM(I), AVN(I), VFLM(I), MP(I)
C I=1,NB), CCL(IT), ZS1, ZS2
IF (NV.EQ.0) GO TO 134
K= 2*NIT
L= 3*NIT
WRITE (6,2) (ZF(I), CVV(I), GK(I), ZF(I+NIT), CVV(I+NIT), GK(I+NIT),
CZF(I+K), CVV(I+K), GK(I+K), ZF(I+L), CVV(I+L), GK(I+L), I=1,NV)
IF (NCL.EQ.2) WRITE (6,5) NCL
CLOCKR= -CLOCKR+(ITIME(0)*.01)
CLOCKT= (-CLOCKR+ITIME(0)*.01)/60.0
WRITE (6,4) CLOCKR, CLOCKS
CLOCKR= ITIME(0)*.01

C
C
C PLT THE VORTICIES' LOCATIONS.
C
N= IT/10
IF ((N.EQ.NP1).OR.(IT.EQ.NIT)).OR.(TP(IT).GE.TMAXP) GO TO 131
GO TO 134
131 NPAIR= NS+3
DC 175 J= 1, NPAIR
XP(J)= REAL(ZCC(J))
YP(J)= AIMAG(ZCC(J))
175 CCNTINUE
N= 1
CALL PLOTP (XP, YP, NPAIR, N)
NPAIR= NV
DC 133 I= 1, NB
K= NIT*(I-1)
DC 132 J= 1, NV
XP(J)= REAL(ZF(K+J))
YP(J)= AIMAG(ZF(K+J))
132 CCNTINUE
N= 2
IF (I.EQ.NB) N= 3
IF (I.EQ.NB) WRITE(6,3)
CALL PLOTP (XP, YP, NPAIR, N)
133 CCNTINUE
NPI= NPI+1
WRITE (6,7) IT
IF ((IT.EQ.NIT).OR.(TP(IT).GE.TMAXP)) GO TO 1291

C
C
C ADVANCE ALL VORTICIES BY DT*(U+IV)
C
134 IF (NV.EQ.0) GO TO 161
DC 124 I= 1, NB
K= 1+NIT*(I-1)

```

```

00001890
00001900
00001910
00001920
00001930
00001940
00001950
00001960
00001970
00001980
00001990
00002000
00002010
00002020
00002030
00002040
00002050
00002060
00002070
00002080
00002090
00002100
00002110
00002120
00002130
00002140
00002150
00002160
00002170
00002180
00002190
00002200
00002210
00002220
00002230
00002240
00002250
00002260
00002270
00002280
00002290
00002300
00002310
00002320
00002330
00002340
00002350
00002360

```

```

00002370
00002380
00002390
00002400
00002410
00002420
00002430
00002440
00002450
00002460
00002470
00002480
00002490
00002500
00002510
00002520
00002530
00002540
00002550
00002560
00002570
00002580
00002590
00002600
00002610
00002620
00002630
00002640
00002650
00002660
00002670
00002680
00002690
00002700
00002710
00002720
00002730
00002740
00002750
00002760
00002770
00002780
00002790
00002800
00002810
00002820
00002830
00002840

L= NV+NIT*(I-1)
DO 123 J= K,L
IF (ABS(GK(J)).GT.EG) ZF(J)= ZF(J)+DTP*CVV(J)
123 CONTINUE
124 CONTINUE

C
C CREATE THE NASCENT VORTICITIES.
C

161 NV= IT
DO 127 I= 1,NB
K= NV+NIT*(I-1)
IF (I.GT.2) GO TO 170
GK(K)= (((-1)**I)* DTP*VELM(I)*VELM(I))/2.0
A= AVN(I)*PI/180.0
B= MP(I)+1.0
ZF(K)= CMPLX(B*COS(A),B*SIN(A))
GO TO 127
170 IF (VELM(I).LE.EV) GO TO 127
GK(K)= (((-1)**(I-1))*DTP*VELM(I)*VELM(I))/2.0
A= AVN(I)*PI/180.0
B= MP(I)+1.0
ZF(K)= CMPLX(B*COS(A),B*SIN(A))
127 CONTINUE
IF (NFOR.EQ.2) GO TO 171
N= NB/2
DO 172 I= 1,N
K= NV+NIT*2*(I-1)
L= K+NIT
GK(L)= -GK(K)
ZF(L)= CONJG(ZF(K))
172 CONTINUE
171 CONTINUE

C
C INDUCE NON-SYMMETRIC VORTEX SHEDDING.
C

IF (NNAXI.EQ.1) GO TO 163
N= TP(IT)
IF (N.NE.NTNAXI) GO TO 163
GK(NV+NIT)= 2.0*GK(NV+NIT)
163 TP(IT+1)= TP(IT)+DTP

COALESCENCE AND CANCELLATION OF VORTICIES WITHIN CLOSE PROXIMITY
TO EACH OTHER.

IF (NCOAL.EQ.1) GO TO 129
DO 144 I= 1,NB
K= 1+NIT*(I-1)
L= NV+NIT*(I-1)

```

```

CC 143 J=K,L LE.EG GO TO 143
IF (ABS(GK(J)).LE.EG) GO TO 143
DO 142 II=I,NB
NK=I+NIT*(II-1)
NL=NV+NIT*(II-1)
DO 141 JJ=NK,NL
((J,FQ,JJ).OR.(ABS(GK(JJ)).LE.EG)) GO TO 141
A=REAL(ZF(J))-ZF(JJ)
B=AIMAG(ZF(J))-ZF(JJ)
IF ((A*A+B*B).LE.(MZD*MZD)) GO TO 138
GO TO 141
138 G= GK(J)+GK(JJ)
IF (ABS(G).LE.EG) GO TO 139
Z=ZF(JJ)-ZF(J)
A=REAL(Z)
B=AIMAG(Z)
Z=ZF(J)
GP=ABS(GK(JJ))/((ABS(GK(J))+ABS(GK(JJ)))
ZF(J)=CMPLX(REAL(Z)+GP*A,AIMAG(Z)+GP*B)
NCL=NCL+1
GO TO 140
139 ZF(J)=(C,C,0.0)
NCAN=NCAN+1
140 ZF(JJ)=(0.0,0.0)
GK(JJ)=G
141 CCNTINUE
142 CCNTINUE
143 CCNTINUE
144 CCNTINUE
129 CCNTINUE
C***** END OF MAIN DO LOOP. *****
1291 IF (IT.GT.NIT) IT=IT-1
DO 135 I=1,IT
YP(I)=REAL(CDCL(I))
IF (ABS(YP(I)).GT.2.0) YP(I)=0.0
135 CCNTINUE
WRITE(6,3)
N=IT+1
YP(N)=2.0
TP(N)=C.0
CALL PLOTP (TP,YP,N,0)
WRITE(6,6) (TP(I),CDCL(I),I=1,IT)
RETURN
1 FORMAT (3X,'IT=',I4,I22,'TP=',F7.3,I42,'DTP=',F9.5,
CT62,'MPA=',F9.5,I80,'MZD=',F9.5,/,
CT22,'TIME STEP MULTIPLIER=',I2,/,
CT32,'TRUE MAX.',T48,'THETA',T62,'MAX. CROSS',T77,'NASCENT VORTEX',

```



```

C/, T32, 'VELOCITY', T47, 'USED IN', T62, '6 BACFLOW', T79, 'PLACEMENT',
C/, T32, 'LOCATION', T45, 'CALCULATIONS', T62, 'VELOCITIES', T77,
C, 'DISTANCE (M)', //,
C10X, '**FRONT, TOP', **/, 5X, I4, 10X, F7.2, 8X, F8.4, 9X, F9.6, //,
C10X, '**FRONT, BOTTOM', **/, 5X, I4, 10X, F7.2, 8X, F8.4, 9X, F9.6, //,
C10X, '**REAR, TOP', **/, 5X, I4, 10X, F7.2, 8X, F8.4, 9X, F9.6, //,
C10X, '**REAR, BOTTOM', **/, 5X, I4, 10X, F7.2, 8X, F8.4, 9X, F9.6, //,
C3X, CDCL = T62, 8X, ZSI = //, T9, 1, 2F8.3, //, 2, FRONT,
2 FORMAT (/, T75, 3, VORTEX, TOP, T108, 4, GAMMA, 1X, //,
C, BOTTOM, POSITION, 4X, VELOCITY, 3X, GAMMA, //,
C3(3X, POSITION, 4X, VELOCITY, 3X, GAMMA, 1X, //,
C, 1X, 2(F6.2, 1X), 2(F5.2, 1X), F6.3, 1, //,
C, 2(F6.2, 1X), 2(F5.2, 1X), F6.3, 1, //,
C, 2(F6.2, 1X), 2(F5.2, 1X), F6.3, 1, //,
3 FORMAT (1H1)
4 FORMAT (//, 3X, ELAPSED COMPUTING TIME FOR INTERACTION = , F8.2, SECONDS. ,
C, TOTAL ELAPSED COMPUTING TIME = , F8.2, MINUTES. ,)
5 FORMAT (//, 3X, TOTAL NO. OF VORTEX PAIRS CANCELLED = , 15, ., ,
C, TOTAL NO. OF VORTEX PAIRS COALESCENCED = , 15, ., ,
6 FORMAT (1H1, 5X, NORMALIZED TIME, 13X, DRAG COEF. , 8X, LIFT COEF. ,
C//, (7X, F8.4, 19X, F8.3, 11X, F8.3, 72X))
7 FORMAT (//, 10X, VORTEX POSITION PLOT FOR IT = , I4)
END

```

```

00003330
00003340
00003350
00003360
00003370
00003380
00003390
00003400
00003410
00003420
00003430
00003440
00003450
00003460
00003470
00003480
00003490
00003500
00003510
00003520
00003530
00003540
00003550
00003560
00003570
00003580

```

```

SUBROUTINE CVELP (Z,NC,NJ,ZCV)
PURPOSE: TO CALCULATE THE FREE CONVECTIVE VELOCITY AT ANY POSITION,
ON OR OUTSIDE THE CYLINDER.
PARAMETERS:
Z = NORMALIZED POSITION ON OR OUTSIDE CYLINDER FOR WHICH THE
VELOCITY IS DESIRED.
NB = NUMBER OF VORTEX BIRTH AREAS.
NV = MAXIMUM NO. OF NASCENT VORTICES SHED IN ONE OF THE BIRTH
AREAS. CALCULATED AS THOUGH NO COALESCENCE OR
CANCELLATION WERE BEING DONE. LE TO NIT/NB.
NC = 0, IF Z IS NOT A REAL VORTEX LOCATION.
1, IF Z IS A LOCATION FOR A REAL VORTEX.
NJ = 1, IF NC = 1, THEN THIS INDICATES THE J* POSITION IN THE
ZF (OR GK) ARRAY IN WHICH Z IS LOCATED.
ZCV = OUTPUT VELOCITY AT Z.
IMPLICIT REAL (A-H,O-Y), INTEGER (I-N), COMPLEX (Z)
COMMON /ALPHA/ZF(400),GK(400),EG,EGS,PI,NIT,NB,NV
A=REAL(Z)
B=AIMAG(Z)
IF ((A*A+B*B).LE.EGS) GO TO 105
ZS1=(1.C/(Z*Z))-CMPLX(1.0,0.0)
ZS2=(0.C,0.0)
ZS3=ZS2
IF ((NB.LE.0).OR.(NV.LE.0)) GO TO 104
DO 103 I=1,NB
K=1+NIT*(I-1)
L=NV+NIT*(I-1)
DO 102 J=K,L
IF (ABS(GK(J)).LE.EG) GO TO 102
IF ((J.EQ.NJ).AND.(NC.EQ.1)) GO TO 101
ZSU=Z-ZF(J)
A=REAL(ZSU)
B=AIMAG(ZSU)
IF ((A*A+B*B).LE.EGS) GO TO 101
ZS2=ZS2+(GK(J)/ZSU)
ZSU=Z-(1.C/CONJG(ZF(J)))
A=REAL(ZSU)
B=AIMAG(ZSU)
IF ((A*A+B*B).LE.EGS) GO TO 102
ZS3=ZS3+(GK(J)/ZSU)
101

```



```

102 CONTINUE
103 CONTINUE
104 ZS4= ZS2-ZS3
  ZC= CMPLX(-AIMAG(ZS4),REAL(ZS4))/(2.0*PI)
  ZS4= ZS1+ZC
  ZCV= CMPLX(-REAL(ZS4),AIMAG(ZS4))
  RETURN
105 WRITE (6,1) Z,NB,NV ,NJ,NC
  RETURN
1  FORMAT (1H1,3X,***** ATTEMPT TO CALCULATE A VELOCITY AT CENTER OF
  C CYLINDER. *****,//,3X,Z= ,2E15.8,3X,NB= ,I3,3X,NV= ,
  C14,3X,
  ,NJ= ,I4,3X,NC= ,I3,/,1H1)
  END
00004050
00004060
00004070
00004080
00004090
00004100
00004110
00004120
00004130
00004140
00004150
00004160
00004170

```

## LIST OF REFERENCES

1. Robertson, J. M., Hydrodynamics in Theory and Application, Prentice-Hall, 1965.
2. Schlichting, H., Boundary Layer Theory, translated by J. Kestin, 6th ed., McGraw-Hill, 1968.
3. Morkovin, M. V., "Flow About a Circular Cylinder - A Kaleidoscope of Challenging Fluid Phenomena," Proceedings ASME Symposium on Fully Separated Flows, p. 102-118, 1964.
4. Frederick, D., and Chang, T. S., Continuum Mechanics, Allyn and Bacon, 1965.
5. Kaplun, S., "Low Reynolds Number Flow Past a Circular Cylinder," Journal of Mathematics and Mechanics, Vol. 6, No. 5, p. 595, 1957.
6. Lamb, H., Hydrodynamics, 6th ed., Dover Publications, 1932.
7. Thom, A., "The Flow Past Circular Cylinders at Low Speeds," Proceedings of the Royal Society, London, Series A, Vol. 141, p. 651, 1933.
8. Kawaguti, M., "Numerical Solution of the Navier-Stokes Equations for the Flow Around a Circular Cylinder at Reynolds Number 40," Journal of the Physical Society of Japan, Vol. 8, p. 747, 1953.
9. Shair, F., Grove, A., Petersen, E., and Acrivos, A., "The Effect of Confining Walls on the Stability of the Steady Wake Behind a Circular Cylinder," Journal of Fluid Mechanics, Vol. 17, p. 546, 1963.
10. Abernathy, F., and Kronauer, R., "The Formation of Vortex Streets," Journal of Fluid Mechanics, Vol. 13, p. 1, 1962.
11. Fromm, J., and Harlow, F., "Numerical Solution of the Problem of Vortex Street Development," The Physics of Fluids, Vol. 6, p. 975, 1963.
12. Crandall, S., Engineering Analysis, McGraw-Hill, 1956.
13. Thompson, J., "Computer Experimentation With an Implicit Numerical Solution of the Navier-Stokes Equations for an Oscillating Body," AIAA Paper No. 69-185, 1969.
14. Wang, C., "The Flow Past a Circular Cylinder which is Started Impulsively From Rest," Journal of Applied Mechanics, ASME Paper No. 67-APM-31, 1967.

15. Ingham, D. B., "Note on the Numerical Solution for Unsteady Viscous Flow Past a Circular Cylinder," Journal of Fluid Mechanics, Vol. 31, p. 815, 1968.
16. Payne, R. B., "Calculations of Unsteady Viscous Flow Past a Circular Cylinder," Journal of Fluid Mechanics, Vol. 4, p. 81, 1957.
17. Taneda, S., "The Stability of Two-Dimensional Laminar Wakes at Low Reynolds Numbers," Journal of the Physical Society of Japan, Vol. 18, p. 288, 1963.
18. Tritton, D. J., "The Flow Past a Circular Cylinder at Low Reynolds Numbers," Journal of Fluid Mechanics, Vol. 6, p. 547, 1959.
19. Roshko, A., "On the Development of Turbulent Wakes from Vortex Streets," NACA TN 2913, March 1953.
20. Rosenhead, L., "Vortex Systems in Wakes," Advances in Applied Mechanics, Vol. 3, p. 185, Academic Press, 1953.
21. Wille, R., "Kármán Vortex," Advances in Applied Mechanics, Vol. 6, p. 273, Academic Press, 1960.
22. Apelt, C. J., "The Steady Flow of a Viscous Fluid past a Circular Cylinder at Reynolds Numbers 40 and 44," Rept. to Aeronautical Research Council, London, No. 20502, 1958.
23. Ujihara, B. H., "An Analytical Study of Separated Flow About a Circular Cylinder," North American Aviation, Space and Information Systems Division, SID 66-1805, NAS 2-3675, 23 Nov. 1966.
24. Sarpkaya, T., and Garrison, C. J., "Vortex Formation and Resistance in Unsteady Flow," Journal of Applied Mechanics, ASME Paper No. 62-WA-62, 1962.
25. Gerrard, J. H., "Numerical Computation of the Magnitude and Frequency of the Lift on a Circular Cylinder," Philosophical Transactions of the Royal Society of London, Series A, Vol. 261, p. 137, 1967.
26. Dennis S. C. R., and Shimshoni, M., "The Steady Flow of a Viscous Fluid Past a Circular Cylinder," Rept. to Aeronautical Research Council, London, No. 26104, 1964.
27. Bearman, P. W., "On Vortex Street Wakes," Journal of Fluid Mechanics, Vol. 28, p. 625, 1967.
28. Acher, J. A., and Dosanjh, D. S., "An Experimental Investigation of the Formation and Flow Characteristics of an Impulsively Generated Vortex Street," Transactions of the ASME, ASME Paper No. 68-FE-32, 1968.

29. Bryson, A. E., Jr., "Symmetric Vortex Separation on Circular Cylinders and Cones," Journal of Applied Mechanics, Vol. 26, No. 4, Transactions of the ASME, Vol. 81, Series E, Dec. 1959, p. 643.
30. Hanson, F. B., and Richardson, P. D., "The Near-Wake of a Circular Cylinder in Crossflow," ASME Paper No. 68-FE-5, 1968.
31. Schindel, L. H., "Separated Flow About Lifting Bodies," MIT Aerophysics Laboratory, Technical Report No. 80, 1963.
32. Koshko, A., "On the Drag and Shedding Frequency of Two-Dimensional Bluff Bodies," NACA TN 3169, 1954.
33. Sarpkaya, T., "Separated Flow About Lifting Bodies and Impulsive Flow About Cylinders," AIAA Journal, Vol. 4, p. 414, 1966.
34. Ward E. G., and Dalton, C., "Strictly Sinusoidal Flow Around a Stationary Cylinder," ASME Paper No. 69-FE-13, 1969.
35. Sarpkaya, T., "An Analytical Study of Separated Flow About Circular Cylinders," ASME Paper No. 68-FE-15, 1968.
36. Sarpkaya, T., "Lift, Drag, and Added-Mass Coefficients for a Circular Cylinder Immersed in a Time-Dependent Flow," Journal of Applied Mechanics, Vol. 30, No. 1, Transactions of the ASME, Vol. 85, Series E, March 1963, p. 13.
37. Friberg, E. G., "Measurement of Vortex Separation, Part I: Two-Dimensional Circular and Elliptic Bodies," MIT Aerophysics Laboratory Technical Report 114, 1965.
38. Milne-Thompson, Theoretical Hydrodynamics, 5th ed., The MacMillan Co., 1968.
39. Fox, L., An Introduction to Numerical Linear Algebra, 1st ed., Oxford University Press, 1965.
40. Nielsen, K. L., Methods in Numerical Analysis, 1st ed., The MacMillan Co., 1956.
41. Bellamy-Knight, P. G., "Analytical Study of Symmetrical Separated Flow About a Circular Cylinder," a Master's Thesis presented at the University of Manchester, Oct. 1967.
42. Fage, A., and Johansen, F. C., "The Structure of Vortex Sheets," Philosophical Magazine, Vol. 5, No. 28, 1928.
43. Edwards, R. H., "Leading Edge Separation From Delta Wings," Journal of the Aeronautical Sciences, Vol. 21, p. 134, 1954.
44. Rott, N., "Diffraction of a Weak Shock With Vortex Generation," Journal of Fluid Mechanics, Vol. 1, p. 111, 1956.

# INITIAL DISTRIBUTION LIST

	No. Copies
1. Defense Documentation Center Cameron Station Alexandria, Virginia 22314	20
2. Library, Code 0212 Naval Postgraduate School Monterey, California 93940	2
3. Naval Ship Systems Command, Code 2052 Via Code 31 Department of the Navy Washington, D. C. 20360	1
4. Professor T. Sarpkaya, Code 59 Department of Mechanical Engineering Naval Postgraduate School Monterey, California 93940	5
5. LT Martin D. Davis, USN 445 Crestview Road Southern Pines, North Carolina 28387	2





## DOCUMENT CONTROL DATA - R &amp; D

*Security classification of title, body of abstract and indexing annotation must be entered when the overall report is classified)*

1 ORIGINATING ACTIVITY (Corporate author)

Naval Postgraduate School  
Monterey, California 93940

2a. REPORT SECURITY CLASSIFICATION

Unclassified

2b. GROUP

3 REPORT TITLE

An Analytical Study of Separated Flow About a Circular Cylinder

4 DESCRIPTIVE NOTES (Type of report and inclusive dates)

Master's Thesis; December 1969

5 AUTHOR(S) (First name, middle initial, last name)

Martin Dorner Davis

6 REPORT DATE

December 1969

7a. TOTAL NO. OF PAGES

132

7b. NO. OF REFS

44

8a. CONTRACT OR GRANT NO

b. PROJECT NO

c.

d.

9a. ORIGINATOR'S REPORT NUMBER(S)

9b. OTHER REPORT NO(S) (Any other numbers that may be assigned this report)

10 DISTRIBUTION STATEMENT

This document has been approved for public release and sale, its distribution is unlimited.

11 SUPPLEMENTARY NOTES

12. SPONSORING MILITARY ACTIVITY

Naval Postgraduate School  
Monterey, California 93940

13. ABSTRACT

The problem of separated flow about a circular cylinder is studied analytically through the use of two potential flow models. Following a detailed review of the present state of knowledge, mathematical formulation of the models and appropriate computer programs are presented. These models are shown to be capable of simulating the asymmetric vortex shedding.

14	KEY WORDS	LINK A		LINK B		LINK C	
		ROLE	WT	ROLE	WT	ROLE	W
	Drag on circular cylinder						
	Vortex sheet						
	Vortex core						
	Forces on bluff bodies						
	Separated flow						
	Computer						
	Impulsively started flow						
	Shear layer development						







thesD1717

An analytical study of separated flow ab



3 2768 002 09612 5

DUDLEY KNOX LIBRARY